INTERLEAVED FREQUENCY DIVISION MULTIPLE ACCESS WITH MULTIPLE ANTENNAS AND BLOCK SPREADING FOR MOBILE BROADBAND COMMUNICATIONS

PNG KHIAM BOON
B.Eng. (1st Class Hons.), M. Eng., NUS

A THESIS SUBMITTED

FOR THE DEGREE OF DOCTOR OF PHILOSOPHY

DEPARTMENT OF
ELECTRICAL AND COMPUTER ENGINEERING

NATIONAL UNIVERSITY OF SINGAPORE

2013

DECLARATION

I hereby declare that this thesis is my original work and it has been written by me in its entirety. I have duly acknowledged all the sources of information which have been used in the thesis.

This thesis has also not been submitted for any degree in any university previously.

Png Khiam Boon

2 Jan 2013

Acknowledgements

I would like to express my deepest gratitude to my supervisor, Professor Ko Chi Chung, for his guidance and advice throughout the course of study. As a part-time student with a full-time job, I am especially grateful for his understanding when at times my progress was not as quick as one hopes. His timely support and constant encouragement are also deeply appreciated.

I would like to express my sincere thank to my co-supervisor, Dr Francois Chin, for his valuable guidance on my research work and his support and encouragement.

I also would like to thank Dr Peng Xiaoming for his guidance on my research work and his kind considerations when I have to take time off work for my study.

Next, I would like to thank the Agency for Science, Technology and Research (A*STAR) and the Institute for Infocomm Research (I^2R) for the study award offered to me and the organizations' support for my part-time study.

Last but not least, I wish to thank my parents for their support and encouragement throughout my study. I also wish to thank my wife for her support and understanding during this hectic period of my life.

Contents

Abstract

In this thesis, we study and propose enhancements to improve the performance of interleaved frequency division multiple access (IFDMA) in the uplink transmission of mobile broadband system. Our theoretical performance analysis of coded IFDMA system shows that receivers using maximum likelihood sequence estimation (MLSE) can maximize the available channel diversity if the required system design criteria are met. We formulate a generalized signal model for coded IFDMA system with different numerical configurations of transmit and receive antennas and proposed an iterative soft QRD-M algorithm for joint detection and decoding scheme of coded IFDMA systems based on the model. The proposed algorithm achieves similar diversity order as MLSE at a much lower complexity cost and its performance approaches the theoretical ideal lower bound within a few iterations. We also introduce a novel transmit diversity for IFDMA system. This antenna spreading diversity (ASD) can be used with a single receive antenna and be easily scaled up to work in systems with different number of numbers of transmit antennas. Moreover, we use block spreading (BS) with IFDMA to suppress inter-cell interference (ICI) while maintaining intra-cell orthogonality for low mobility users. The use of block spreading also allows more sub-carriers to be assigned to each user, thereby increasing the available frequency diversity for each user. To counter the loss of code orthogonality due to the presence of high mobility user in the system, we propose a novel scheme where the allocation of the users' operating sub-carriers and spreading codes is dependent on their mobility and a mobility-based multiple access interference (MAI) cancellation scheme is used at the receiver to

maintain system performance.

List of Tables

List of Figures

List Of Abbreviations

APP	*A Posterior Probability*
ASD	Antenna Spreading Diversity
ASIC	Application Specific Integrated Circuit
AWGN	Additive White Gaussian Noise
BER	Bit Error Rate
BS	Block Spreading
CDD	Cyclic Delay Diversity
CDMA	Code Division Multiple Access
DFT	Discrete Fourier Transform
FDE	Frequency Domain Equalizer
FDMA	Frequency Division Multiple Access
FEC	Forward Error Correcting
FFT	Fast Fourier Transform
FH	Frequency Hopping
FSTD	Frequency Switched Transmit Diversity
GMSK	Gaussian Minimum Shift Keying
GSM	Global System for Mobile Communications
ICI	Inter-Cell Interference
IFDMA	Interleaved Frequency Division Multiple Access
LAP	Linear Assignment Problem
LLR	Log Likelihood Ratio
LMMSE	Linear Minimum Mean Squared Error

MAI	Multiple Access Interference
MAP	Maximum *A Posteriori*
MFLB	Matched Filter Lower Bound
MIMO	Multiple-Inputs Multiple-Outputs
ML	Maximum Likelihood
MLSE	Maximum Likelihood Sequence Estimation
OCI	Out-of-Cell Interference
OFDM	Orthogonal Frequency Division Multiplexing
OFDMA	Orthogonal Frequency Division Multiple Access
PAPR	Peak-to-Average Power Ratio
PDF	Probability Density Function
QAM	Quadrature Amplitude Modulation
QAP	Quadratic Assignment Problem
QPSK	Quadrature Phase Shift Keying
QRD	Orthogonal Matrix Triangularization (QR) Decomposition
QS	Quasi-Synchronous
SC-FDMA	Single Carrier - Frequency Division Multiple Access
SFBC	Space Frequency Block Code
SIC	Successive Interference Cancellation
SINR	Signal-to-Interference and Noise Ratio
SISO	Soft-In Soft-Out
STBC	Space Time Block Code
TDMA	Time Division Multiple Access
VLSI	Very Large Scale Integration
ZF	Zero Forcing

Chapter 1

Introduction

Mobile cellular communications has become the pervasive technology for the 21st century. With the advent of social media, mobile gaming and video streaming services as well as the prevalent of the mobile computing devices such as smartphones and tablets, consumers are increasingly demanding higher data speed and greater coverage area. Along with more spectrum allocations, the evolution of the air interface, which forms the backbone of mobile wireless communications, is paramount to meet the growing demand. Correspondingly, new signal processing algorithms which can maximize the benefits of the new air interface need to be developed and implemented. We focus on the development of algorithms which leverage on the benefits of the emerging air interface considered for the uplink in future mobile cellular systems. Before introducing our proposed algorithms, we will provide a brief history of the evolution of the air interface in mobile cellular system in this chapter. In addition, our motivations and contributions in this thesis are also presented in this chapter.

1.1 Evolution of Air Interface of Mobile Cellular Systems

The first public mobile telephone system began operation in the United States of America (USA) in 1946 [1]. Mobile phones were assigned a single permanent channel for two-way communications via push-to-talk concepts [2]. Im-

provement was made to the system to support full-duplexing in the 1960s but the system remained impractical because of capacity constraints. For example, only twelve simultaneous calls could be supported over a 1,000 square miles area in New York City which had a market of ten million people in 1976 [1]. The cellular concept featuring frequency reuse, which helps to solve the capacity constraints, was demonstrated in 1968 at Bell Laboratories. Together with the invention of microprocessor, it paved the way for the deployment of the first commercial 1G cellular system, the Mobile Communication System L1, by the Nippon Telegraph and Telephone (NTT) [2]. This was followed by the deployment of European 1G systems in Scandinavia in 1981, in United Kingdom in 1982 and in France and Germany in 1985. The first commercial 1G cellular system arrived in the USA in 1983 [1].

The 1G cellular systems were all analog systems relying on frequency or amplitude modulation, which suffered from bandwidth inefficiency [2], for transmission. In the late 1980s, the maturity of very large scale integration (VLSI) and signal processing technology led to the digital revolution. The new digital 2G cellular system rode on the wave of the digital technology with the digital signal processors in application specific integrated circuits (ASICs) helping to miniaturize mobile phone sizes. The digital 2G systems also allowed, for the first time, the use of block and/or convolutional coding for error correction resulting in clearer voice transmissions and more reliable data transmission over fading channels. The 2G systems also introduced the use of digital modulations such as Gaussian minimum shift keying (GMSK) and quaternary phase shift keying (QPSK). Sophisticated multiple access technology like frequency division multiple access (FDMA), time division multiple access (TDMA) and code division multiple access (CDMA) also gained prominent usage in the digital 2G systems. Popular 2G systems include the TDMA/FDMA based Global System for Mobile Communications (GSM), which was first adopted by the European countries in 1991, and the CDMA based IS-95A standards, which gained

widespread deployment by 1996 [1]. At the beginning of this century, the 2G mobile cellular systems introduced packet switching [3] to allow for easier data transmission which became, and continues to be, a main feature in mobile cellular systems.

The next driver for upgrades in cellular system was the requirement for multimedia-level data rates and the push for greater data rates soon resulted in the deployment of the 3G cellular systems. In the 3G era, CDMA rose in prominence as it became the multiple access technology of choice for the two most popular 3G system standards: Wideband CDMA (W-CDMA) and CDMA2000. Compared to FDMA/TDMA, CDMA is more robust against multipath fading, provides greater coverage with fewer cell sites and enables better frequency reuse [4, 5]. 3G systems are also characterized by the usage of powerful turbo codes [6, 7] to improve performance and the usage of higher order of quadrature amplitude modulation (QAM) constellations such as the 16QAM and 64 QAM to support higher data rates. However, the use of these higher order modulations is usually restricted to short range transmission [2].

The 3rd Generation Partnership Project(3GPP) consortium officially commenced the standardization work on mobile cellular systems beyond 3G under the name of 3G Long Term Evolution (LTE) in 2006. In a departure from existing 3G systems, multiple access technologies based on orthogonal frequency division multiplexing (OFDM) air interface were chosen [8]. In the downlink, the popular orthogonal frequency division multiple access (OFDMA) is chosen while single carrier frequency division multiple access (SC-FDMA), which uses similar wireless air interface as OFDMA, is the chosen uplink multiple access technology [8]. Multiple antennas technology, which is regarded as the key technology to provide high capacity and data rates [2], was also incorporated in the 3G LTE systems.

1.2 Interleaved Frequency Division Multiple Access

SC-FDMA is the chosen uplink multiple access technology for 3G LTE and LTE-Advanced cellular system [8]. SC-FDMA uses similar wireless air interface as the popular OFDMA technology used in the downlink of the cellular systems. However, unlike OFDMA, SC-FDMA shifts the bulk of the processing complexity to the receiver at the base-station and has a lower peak-to-average power ratio (PAPR) which makes it a more attractive candidate for uplink transmission [9]. SC-FDMA facilitates the multiple access in the uplink through apportioning different sub-carriers to different users like in OFDMA. There are two approaches to the division of the sub-carriers to the users. The first is localized SC-FDMA (LFDMA) that assigns each mobile device a set of adjacent sub-carriers for its transmission. The second is distributed SC-FDMA, which is commonly realized as interleaved FDMA (IFDMA), that assigns a set of equidistantly distributed sub-carriers to each user [9]. Recently, a new sub-carrier assignment scheme known as block IFDMA (B-IFDMA) has emerged that assigns interleaved blocks of continuous sub-carriers to a single user [10, 11].

The use of frequency division multiple access preserves the users orthogonality in frequency-selective channels but exposes SC-FDMA to the problem of inter-cell interference (ICI) in the absence of cellular frequency reuse [12] [13] [14]. Solutions such as fractional frequency reuse reduce the spectrum availability at the cell edge [13], while solutions such as adaptive frequency reuse scheduling [12] [14] requires channel information which may not be readily available in the case of fast moving mobile devices. Moreover, the throughput performance of the SC-FDMA system, especially those using LFDMA, is also dependent on resource scheduling using accurate real-time channel information [9, 15].

1.3 Motivations and Scope

Previous performance analysis on IFDMA systems focused on the frequency domain [16, 17] with the assumption that the different sub-carriers assigned to a user experienced independent fading. Hence, it is difficult to establish quantitatively, the maximum channel diversity order achievable by IFDMA systems. Moreover, [16] only establishes an imprecise relationship between the number of sub-carriers assigned to a user and the diversity obtained by that user. We know from [15] that the frequency diversity gain, and hence the performance, in IFDMA systems is affected by the number of the sub-carriers assigned to a user relative to the total number of sub-carriers available in the system. The amount of frequency diversity gain determines the necessity and the usefulness of multi-user scheduling [15]. We seek to analyze the performance of IFDMA system in dense multipath environments [18] and establish the quantitative relationship between the number of sub-carriers assigned per user and the diversity order a user can achieve. Also, we like to determine the criteria required for coded IFDMA systems to achieve the maximum channel diversity order.

The simple frequency domain equalizer (FDE), though straightforward to design and implement, limit the diversity performance in the the receiver [19]. Maximum likelihood sequence estimation (MLSE) guarantees the diversity performance but is too complicated to be implemented, especially for the higher order of modulations and advanced error correcting code considered in future cellular system. We propose the use of an implementable iterative detection and decoding algorithm at the receiver to achieve the theoretical diversity performance of the MLSE. We also generalize the algorithm to use in IFDMA systems with multiple antennas employing either spatial multiplexing or transmit diversity schemes. The insights we gained from our theoretical analysis of IFDMA system also lead us to propose a novel transmit diversity scheme for coded IFDMA system. We compare the new scheme to existing schemes and demonstrate the effectiveness of the proposed scheme.

Next, we tackle the problem of FDMA systems' inability to reject ICI without the use of frequency reuse. We investigate the concept of two-layered spreading to reject out-of-cell interference (OCI) used in variable spreading factor(VSF)-orthogonal frequency/code division multiplexing (VSF-OFCDM) system [20, 21], which is a candidate for the 4G cellular system [2]. We extend the two-layered spreading concept to IFDMA and propose a block spread (BS)-IFDMA system. The performance of BS-IFDMA systems in time variant channels is analyzed and is found to be susceptible to the interferences caused by the presence of high mobility users. As support for high mobility users is crucial in future mobile system to cater for the "always-connected" experience, we propose a novel mobility-based MAI cancellation scheme to incorporate high mobility users into a BS-IFDMA system without degrading the system performance.

1.4 Contributions in Thesis

We have carried out a theoretical performance analysis of IFDMA systems and propose a number of algorithms to minimize the bit error rate (BER) performance of IFDMA systems. Specifically, we have proposed a generalized iterative detection and decoding algorithm based on QR decomposition and M-algorithm (QRD-M algorithm) for coded MIMO-IFDMA systems, which have similar diversity performance as MLSE. We also propose a new transmit antenna diversity scheme for coded IFDMA systems which can be decoded at the receiver using the proposed iterative soft QRD-M algorithm. The proposed transmit antenna diversity scheme can be used on its own or be combined with the cyclic delay diversity scheme to maximize the diversity performance of coded MIMO-IFDMA systems. In addition, we apply the concept of two-layered spreading to IFDMA systems and propose a mobility-based multiple access interference cancellation scheme to incorporate high mobility users in

the resulting BS-IFDMA systems.

We introduce a new generalized signal model for coded IFDMA systems with different numerical configurations of transmit and receive antennas. We analyze the theoretical upper bound of coded IFDMA system based on the new signal model and specify the design criteria for coded IFDMA systems to achieve the maximum channel diversity order regardless of the number of sub-carriers assigned per user. Moreover, we present a recursive calculation of log-likelihood ratio that enables the use of M-algorithm in a soft QRD-M APP detector to achieve the maximum diversity order at low complexity. We also propose a generalized iterative soft QRD-M algorithm for detection and decoding for coded MIMO-IFDMA system. The performance of the proposed algorithm approaches the ideal matched filter lower bound at high SNR and achieves a performance gain of up to 6 dB over linear MMSE detector.

The generalized signal model is used to design a novel transmit diversity named antenna spreading diversity scheme that has a guaranteed diversity gain factor equal to the number of transmit antennas used, if the receiver uses MLSE. We demonstrate through simulation that the proposed iterative soft QRD-M algorithm is able to match the diversity performance of MLSE for the proposed antenna spreading diversity scheme. We also analyze and compare the theoretical performance between the proposed antenna diversity scheme and the popular cyclic delay diversity scheme to show the benefits of the proposed scheme as well as to illustrate how the two schemes are complementary to each other. We specify the design criterion for the configuration of a combined transmit diversity scheme to suit the requirements of different systems and show the benefits of the combined diversity scheme through theoretical performance analysis and simulations.

We derive the multiple access interference (MAI) in BS-IFDMA system under time-varying channel and introduce a novel MAI cancellation scheme based on the users' mobilities. We formulate the total MAI in a system with

the proposed interference cancellation scheme to result in a quadratic assignment problem (QAP) to optimize the spreading code assignments for the users. Based on the characteristics of common spreading codes such as the Walsh-Hadamard and Orthogonal Gold codes, we devise a simplified search procedure in a branch-and-bound algorithm for solving the QAP. The simplified search procedure lowers the time taken to arrive at the solution by a factor which is equal to five times the spreading factor. We analyze the bit error rate (BER) performance of the proposed MAI cancellation scheme and show that with the cancellation scheme, the BER error floor due to the MAI caused by a high mobility user will always be lower than the theoretical BER. Conversely, without the cancellation scheme, the theoretical BER will always hit the error floor, limiting the system performance. We also show, through simulation, that the proposed MAI cancellation scheme coupled with the proposed optimized codes assignment enables up to half the total number of users in BS-IFDMA systems to be high mobility users while maintaining the system performance.

1.5 Thesis Organization

The thesis consists of five chapters. In this chapter, the evolution of the mobile cellular communications is briefly introduced to provide a general context to the investigations done on IFDMA system in the thesis. The motivations and contributions were also presented in this chapter. In Chapter 2, we introduce the generalized signal model for coded MIMO-IFDMA systems and present the proposed iterative soft QRD-M algorithm. We derive the theoretical BER performance of coded MIMO-IFDMA systems and formulate the criteria for maximizing the channel diversity in coded MIMO-IFDMA systems. In Chapter 3, we analyze the theoretical performance of the proposed transmit diversity scheme and demonstrate the ability of the proposed iterative soft QRD-M algorithm to match the theoretical performance through simulation. In Chapter 4,

we consider the use of block spreading in IFDMA systems and propose a novel multiple access interference cancellation scheme designed to incorporate high mobility users in BS-IFDMA systems. Lastly, Chapter 5 summarizes the research work in this thesis and provide suggestions for future work.

Chapter 2

Generalized Iterative Soft QRD-M Algorithm for IFDMA System

2.1 Introduction

Interleaved frequency division multiple access (IFDMA) scheme introduced in [22] is a promising candidate for the uplink transmission in next generation mobile wireless access system [16, 23–25]. IFDMA has also been formulated as either an orthogonal frequency division multiple access (OFDMA) scheme [26] with discrete fourier transform (DFT) precoding and equidistant frequency mapping [17, 24, 25, 27] or a code division multiple access (CDMA) scheme with specialized spreading codes [28, 29](i.e. frequency-domain orthogonal spreading codes, comb-spectrum codes). IFDMA is able to maintain perfect user orthogonality in frequency-selective channel [16, 29] like OFDMA. However, unlike OFDMA, IFDMA is a single-carrier (SC) scheme that guarantees low peak-to-average power ratio (PAPR) in the transmitted signals making it more suitable than OFDMA in uplink transmission [17, 24].

In this chapter, we introduce a new signal model in time domain using conventional MIMO matrix formulation for IFDMA systems, which provides a better insight of the inherent diversity attainable in the system. Instead of using the frequency domain signal model of IFDMA favored in [17, 24], we formulate the signal model of a IFDMA system in the time domain similar to [22]. In addition, we show that the IFDMA time domain signal model represented in matrix nota-

tions has the same form as a multiple-inputs multiple-outputs (MIMO) system. Using this model, the performance analysis on the bit error rate (BER) performance of coded IFDMA systems in a frequency-selective multipaths environment can be carried out. We also extend the signal model to form a generalized system signal model to describe coded IFDMA systems with different numerical configurations of transmit and receive antennas employing spatial multiplexing.

Previous performance analysis on IFDMA systems focused on the frequency domain [16, 17] with the assumption that the different sub-carriers assigned to a user experienced independent fading. Hence, it is difficult to establish quantitatively, the maximum channel diversity order achievable by IFDMA systems. Moreover, [16] only establishes an imprecise relationship between the number of sub-carriers assigned to a user and the diversity obtained by that user. Using our system model, we derive the upper bound on the BER of coded IFDMA system based on maximum likelihood sequence estimation (MLSE) in a frequency-selective channel. The BER performance analysis gives us quantitative insights on the relationship between the diversity order a user can achieve and the number of sub-carriers assigned to the user, as well as the criteria required for coded IFDMA systems to achieve the maximum channel diversity order.

Following the insights gained from the analysis, we design frequency hopping sequences that will enable all users within the system to achieve the maximum channel diversity order regardless of the number of sub-carriers assigned to each user. Alternatively, we can apply block spread technique [30] using the appropriate spreading factor to achieve the same diversity order. We shall compare the two techniques, discussing their respective advantages and disadvantages in terms of operational complexity as well as BER performance.

Various receiver structures have been proposed for uncoded IFDMA system, ranging from the simple frequency domain equalizer (FDE) [27] to the complex iterative block decision feedback equalizer (IB-DFE) [24, 31]. IB-DFE has significantly better performance than the simple feed forward FDE [24] and

is significantly less complex than the maximum likelihood (ML) detector especially when the number of sub-carriers assigned to a user is large. This makes IB-DFE [32] a promising receiver structure for high data-rate transmission. For coded IFDMA systems, *a posterior probability* (APP) detector based on the ML principle has been proposed for systems with small number of assigned sub-carriers per user [16, 22]. However, the complexity of the APP detector makes it prohibitive for usage in systems with large number of assigned sub-carriers per user. Our theoretical analysis shows that using MLSE in the receiver will maximize the diversity performance of IFDMA, but MLSE is computationally prohibitive except for the simplest forward error-correcting code (FEC) and modulations.

In this chapter, we propose a low-complexity APP detector, which is based on the M-algorithm and QR decomposition (QRD-M). The proposed APP detector provides a similar channel diversity order as that of MLSE. Moreover, we propose a iterative soft QRD-M algorithm for the detection and decoding of signals in IFDMA systems which improves the BER performance of coded IFDMA systems significantly. Unlike [24] which performs iterations within the detection process only, we formulate an iterative detect and decode algorithm that passes soft-decision statistics between a soft QRD-M detector and a soft-in soft-out (SISO) FEC code decoder that improves the BER performance of coded IFDMA systems, especially in dense multipaths environment. Simulation results show that a system using the proposed iterative algorithm approaches the hypothetical matched filter lower bound (MFLB) [16] at high SNR. The proposed iterative algorithm can also be generalized for coded MIMO-IFDMA systems with different numerical configurations of transmit and receive antennas. The proposed algorithm not only improves the BER performance of coded MIMO-IFDMA systems significantly, it also allows a base-station that serves asymmetrical mobile devices with different number of transmit antennas in the uplink to use a common hardware platform. The numerical evaluations also show that the pro-

posed algorithm is capable of achieving the maximum channel diversity order and outperforms the linear MMSE detector significantly. Specifically, the proposed algorithm approaches the hypothetical MFLB [16] with less than 0.5 dB degradation within 3 iterations and attains no less than 4 dB performance gain when compared to linear MMSE detection.

The rest of the chapter is organized as follows: In Section 2.2, we formulate the signal model for coded MIMO-IFDMA systems in time invariant channel. In Section 2.5, we describe the proposed generalized iterative soft QRD-M algorithm for the detection and decoding for coded IFDMA system in details. Next, we derive in Section 2.3, the upper bound on the BER performance that illustrates the maximum diversity order achievable in coded IFDMA systems. In Section 2.4, we establish the design criteria of FH-IFDMA and BS-IFDMA system to achieve the maximum diversity order in the channel and evaluate the relative strength and weakness of each scheme. Numerical examples are given in Section 2.6 to compare simulated performance with the derived theoretical bounds. Lastly, in Section 2.7, we summarize our observations and contributions.

2.2 System Signal Model

2.2.1 IFDMA Signal Model

In this thesis, we shall formulate the IFDMA system signal model in the time domain [33, 34] rather than the conventional frequency domain signal model used in [17, 24]. Moreover, unlike [22], we use matrix notations to cast the signal model in the form of conventional MIMO system. The developed signal model may be less intuitive but provides a better insight of the inherent diversity available in the system which is a key concern of this thesis.

Let S be the number of symbols transmitted per user in one block that constitutes a single IFDMA symbol (or equivalently the number of sub-carriers as-

signed to each user in the frequency domain) and G be the repetition factor [22] that determines the maximum possible number of orthogonal users in the system. For simplicity, we consider the case where all the users have the same S and G here, as the extension to the variable case is straightforward. Note that if all the users have the same S and G, the orthogonality between the users at the receiver is guaranteed as long as the number of users in the system does not exceed G. For maximum system capacity, we assume that the number of allocated users, $K = G$. As in [17], we consider quasi-synchronous (QS) uplink transmissions where the relative delay among all users are limited to a few chips duration using adaptive transmit timing control to align the time differences among different users [35]. The delays are upper bounded by τ_d and we consider a prefix length $N_{CP} = \lceil \frac{\tau_d + \tau_c}{T_c} \rceil$ where τ_c is the maximum delay spread of all the users' channel and T_c is chip duration.

We define the block of transmitted symbols by the k^{th} user as

$$\mathbf{x}_k = \begin{bmatrix} x_{k,0} & x_{k,1} & \dots & x_{k,S-1} \end{bmatrix}^T \tag{2.1}$$

where $\{\cdot\}^T$ represents the matrix transpose. For IFDMA transmission, the block is repeated G times and multiplied by a user-defined phase vector. The $N \times 1$ vector representing the transmitted sequence is given by

$$\mathbf{s}_k \;\; = \;\; \mathbf{E}_k \hat{\mathbf{x}}_k \tag{2.2}$$

where $\mathbf{E}_k$ is a $N \times N$ matrix, given by:

$$\mathbf{E}_k = \frac{1}{\sqrt{G}} \text{diag} \left\{ \begin{array}{ccccc} 1 & \dots & e^{j\frac{2\pi nk}{N}} & \dots & e^{j\frac{2\pi(N-1)k}{N}} \end{array} \right\} \tag{2.3}$$

and $\hat{\mathbf{x}}_k$ is a $N \times 1$ vector, given by:

$$\hat{\mathbf{x}}_k = \begin{bmatrix} \mathbf{x}_k^T & \mathbf{x}_k^T & \dots & \mathbf{x}_k^T \end{bmatrix}^T \tag{2.4}$$

i.e. $\hat{\mathbf{x}}_k$ is G repetitions of $\mathbf{x}_k$ and $N = SG$.

Before the transmission of the sequence $\mathbf{s}_k$ a cyclic prefix [36] of length N_{CP} is appended to the sequence. Since N_{CP} is designed so that it is larger than the combination of the maximum channel delay spread and the maximum tolerable difference between arrivals of different users' signal, the $N \times 1$ vector representing received sequence with proper synchronization can be written as:

$$\mathbf{r} = \sum_{k=1}^{K} \hat{\mathbf{h}}_k \mathbf{s}_k + \boldsymbol{\eta} \tag{2.5}$$

where $\boldsymbol{\eta}$ is a $N \times 1$ vector of additive white gaussian noise (AWGN) components with variance σ^2 and $\hat{\mathbf{h}}_k$ is a $N \times N$ circulant matrix with the first column being the channel impulse response of the k^{th} user given by,

$$\hat{\mathbf{h}}_k(:,1) = \begin{bmatrix} h_{k,0} & \dots & h_{k,P-1} & 0 & \dots & 0 \end{bmatrix}^T \tag{2.6}$$

where P is the number of resolvable channel paths. Note that $h_{k,p}$ can be zero since not all signals arrive at the receiver at the same time.

At the base-station receiver, the separation of the users' signals is usually preceded by a N-points Fast Fourier Transform (FFT) as the focus is on FDE [17, 24, 27, 37] using the architecture as shown in Figure 2.1(a). However, we propose a time domain user-separation operation using a new receiver architecture shown in Figure 2.1(b). The mathematical equivalence to the separation process in Figure 2.1(b) to obtain the signal for the k^{th} user is to pre-multiply $\mathbf{r}$ with the S-by-N matrix

$$\mathbf{U}_k = \frac{1}{\sqrt{G}} \begin{bmatrix} \widetilde{\mathbf{U}}_k & e^{-j\frac{2\pi k}{G}} \widetilde{\mathbf{U}}_k & \dots & e^{-j\frac{2\pi(G-1)k}{G}} \widetilde{\mathbf{U}}_k \end{bmatrix} \tag{2.7}$$

where $\widetilde{\mathbf{U}}_k = \text{diag} \begin{Bmatrix} 1 & e^{-j\frac{2\pi k}{N}} & \dots & e^{-j\frac{2\pi(S-1)k}{N}} \end{Bmatrix}$ is a $S \times S$ matrix.

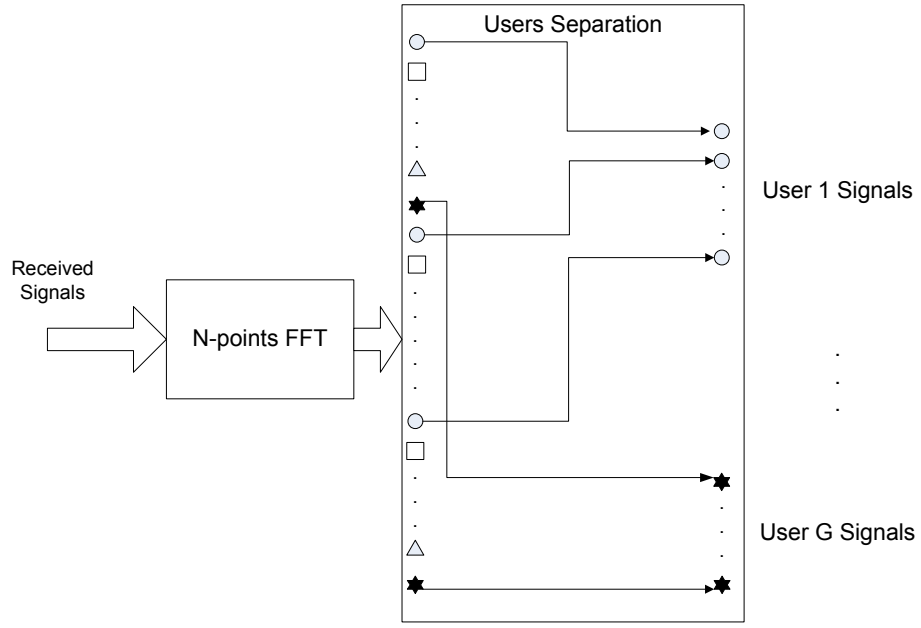

(a) Frequency Domain User-Separation

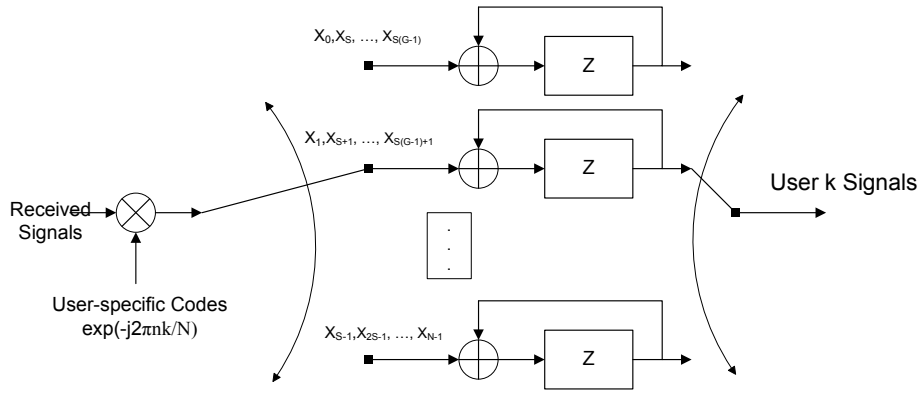

(b) Time Domain User-Separation

Figure 2.1: Frequency and Time Domain User-Separation

The $S \times 1$ vector representing the k^{th} user received signal is hence,

$$\begin{aligned} \mathbf{r}_k &= \mathbf{U}_k \mathbf{r} \\ &= \mathbf{U}_k \sum_{m=1}^{K} \hat{\mathbf{h}}_m \mathbf{s}_m + \mathbf{U}_k \boldsymbol{\eta} \\ &= \mathbf{U}_k \hat{\mathbf{h}}_k \mathbf{s}_k + \sum_{\substack{m=1 \\ m \neq k}}^{K} \mathbf{U}_k \hat{\mathbf{h}}_m \mathbf{s}_m + \boldsymbol{\eta}' \end{aligned} \tag{2.8}$$

We can rewrite

$$\mathbf{U}_k \hat{\mathbf{h}}_m \mathbf{s}_m = \mathbf{U}_k \hat{\mathbf{h}}_m \hat{\mathbf{E}}_m \hat{\mathbf{x}}_m \tag{2.9}$$

where $\hat{\mathbf{E}}_m$ is a $N \times N$ matrix given by,

$$\hat{\mathbf{E}}_m = \frac{1}{\sqrt{G}} \begin{bmatrix} \widetilde{\mathbf{U}}_m^* & \mathbf{0}_S & \dots & \mathbf{0}_S \\ \mathbf{0}_S & e^{j\frac{2\pi m}{G}} \widetilde{\mathbf{U}}_m^* & \dots & \mathbf{0}_S \\ \vdots & \vdots & \ddots & \vdots \\ \mathbf{0}_S & \mathbf{0}_S & \dots & e^{j\frac{2\pi (G-1)m}{G}} \widetilde{\mathbf{U}}_m^* \end{bmatrix} \tag{2.10}$$

and $\widetilde{\mathbf{U}}_m^*$ is the conjugate matrix of $\widetilde{\mathbf{U}}_m$ and $\mathbf{0}_S$ is a S-by-S zero matrix. Rewriting

$$\hat{\mathbf{h}}_m = \begin{bmatrix} \widetilde{\mathbf{h}}_m^{(0)} & \widetilde{\mathbf{h}}_m^{(G-1)} & \dots & \widetilde{\mathbf{h}}_m^{(1)} \\ \widetilde{\mathbf{h}}_m^{(1)} & \widetilde{\mathbf{h}}_m^{(0)} & \dots & \widetilde{\mathbf{h}}_m^{(2)} \\ \vdots & \vdots & \ddots & \vdots \\ \widetilde{\mathbf{h}}_m^{(G-1)} & \widetilde{\mathbf{h}}_m^{(G-2)} & \dots & \widetilde{\mathbf{h}}_m^{(0)} \end{bmatrix}, \tag{2.11}$$

where $\widetilde{\mathbf{h}}_m^{(i)}$ is a $S \times S$ matrix for $i = 0, \dots, G-1$, we then get

$$\mathbf{U}_k \hat{\mathbf{h}}_m \mathbf{s}_m = \frac{1}{G} \widetilde{\mathbf{U}}_k \mathbf{S}_{k,m} \widetilde{\mathbf{U}}_m^* \mathbf{x}_m \tag{2.12}$$

where

$$\mathbf{S}_{k,m} = \sum_{\gamma=0}^{G-1} e^{-j\frac{2\pi\gamma k}{G}} \widetilde{\mathbf{h}}_m^{(\gamma)} \left(\sum_{i=0}^{G-1} e^{-j\frac{2\pi i(k-m)}{G}} \right) \tag{2.13}$$

is a $S \times S$ matrix. Since

$$\sum_{i=0}^{G-1} e^{-j\frac{2\pi i(k-m)}{G}} = \begin{cases} 0 & m \neq k \\ G & m = k \end{cases}, \tag{2.14}$$

$$\mathbf{U}_k \hat{\mathbf{h}}_m \mathbf{s}_m = \begin{cases} 0 & m \neq k \\ \widetilde{\mathbf{U}}_k \left(\sum_{\gamma=0}^{G-1} e^{-j\frac{2\pi\gamma k}{G}} \widetilde{\mathbf{h}}_k^{(\gamma)} \right) \widetilde{\mathbf{U}}_k^* \mathbf{x}_k & m = k \end{cases} \tag{2.15}$$

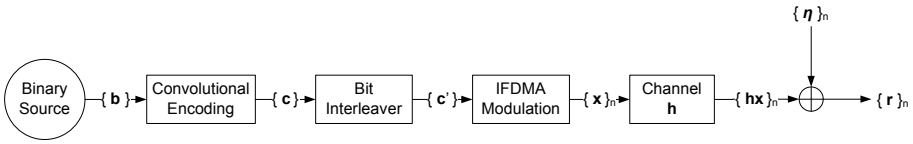

Figure 2.2: Equivalent Single-User System Model for coded IFDMA System

Thus, we can simplify (2.8) to:

$$\begin{aligned} \mathbf{r}_k &= \mathbf{U}_k\hat{\mathbf{h}}_k\mathbf{s}_k + \sum_{\substack{m=1 \\ m\neq k}}^{K} \mathbf{U}_k\hat{\mathbf{h}}_m\mathbf{s}_m + \boldsymbol{\eta}' \\ &= \mathbf{U}_k\hat{\mathbf{h}}_k\mathbf{s}_k + \boldsymbol{\eta}' \\ &= \mathbf{h}_k\mathbf{x}_k + \boldsymbol{\eta}' \end{aligned} \tag{2.16}$$

The variance of noise components in $\boldsymbol{\eta}'$ remains as σ^2 and the matrix, $\mathbf{h}_k$, is a $S \times S$ circulant matrix with

$$\mathbf{h}_k(:,1) = \begin{bmatrix} \sum_{\gamma=0}^{G-1} h_{k,\gamma S} e^{-j\frac{2\pi\gamma k}{G}} \\ \vdots \\ e^{-j\frac{2\pi l k}{N}} \sum_{\gamma=0}^{G-1} h_{k,\gamma S+l} e^{-j\frac{2\pi\gamma k}{G}} \\ \vdots \\ e^{-j\frac{2\pi(S-1)k}{N}} \sum_{\gamma=0}^{G-1} h_{k,\gamma S+S-1} e^{-j\frac{2\pi\gamma k}{G}} \end{bmatrix} \tag{2.17}$$

From (2.16) we see that the orthogonality among users can be maintained at the receiver despite the frequency selective channel. Note that at the receiver, only $\mathbf{h}_k$ need to be estimated for signal detection. Since $\mathbf{h}_k$ is a $S \times S$ circulant matrix, channel estimation can be performed at the base-station by transmitting a pilot with good auto-correlation property [38].

As an illustrative example, we consider the received signal of the first user in a channel where $P = 4$ and the number of sub-carriers assigned to the user, S, varies between 2 and 4. The total number of sub-carriers in the system N is fixed at 8, giving the corresponding number of users in the system, G to be 4 and 2 respectively. The $\hat{\mathbf{h}}_0$ is a 8×8 circulant matrix, which is independent on

S, is written as:

$$\hat{\mathbf{h}}_0 = \begin{bmatrix} h_{0,0} & 0 & 0 & 0 & 0 & h_{0,3} & h_{0,2} & h_{0,1} \\ h_{0,1} & h_{0,0} & 0 & 0 & 0 & 0 & h_{0,3} & h_{0,2} \\ h_{0,2} & h_{0,1} & h_{0,0} & 0 & 0 & 0 & 0 & h_{0,3} \\ h_{0,3} & h_{0,2} & h_{0,1} & h_{0,0} & 0 & 0 & 0 & 0 \\ 0 & h_{0,3} & h_{0,2} & h_{0,1} & h_{0,0} & 0 & 0 & 0 \\ 0 & 0 & h_{0,3} & h_{0,2} & h_{0,1} & h_{0,0} & 0 & 0 \\ 0 & 0 & 0 & h_{0,3} & h_{0,2} & h_{0,1} & h_{0,0} & 0 \\ 0 & 0 & 0 & 0 & h_{0,3} & h_{0,2} & h_{0,1} & h_{0,0} \end{bmatrix} \tag{2.18}$$

For the case of $S = 2$, $G = 4$,

$$\begin{aligned} \widetilde{\mathbf{h}}_0^{(0)} &= \begin{bmatrix} h_{0,0} & 0 \\ h_{0,1} & 0 \end{bmatrix}, \quad \widetilde{\mathbf{h}}_0^{(1)} = \begin{bmatrix} h_{0,2} & h_{0,1} \\ h_{0,3} & h_{1,2} \end{bmatrix}, \\ \widetilde{\mathbf{h}}_0^{(2)} &= \begin{bmatrix} 0 & h_{0,3} \\ 0 & 0 \end{bmatrix}, \quad \widetilde{\mathbf{h}}_0^{(3)} = \begin{bmatrix} 0 & 0 \\ 0 & 0 \end{bmatrix}. \end{aligned} \tag{2.19}$$

and

$$\mathbf{h}_0 = \begin{bmatrix} h_{0,0} + h_{0,2} & h_{0,1} + h_{0,3} \\ h_{0,1} + h_{0,3} & h_{0,0} + h_{0,2} \end{bmatrix} \tag{2.20}$$

For the case of $S = 4$, $G = 2$,

$$\begin{aligned} \widetilde{\mathbf{h}}_0^{(0)} &= \begin{bmatrix} h_{0,0} & 0 & 0 & 0 \\ h_{0,1} & h_{0,0} & 0 & 0 \\ h_{0,2} & h_{0,1} & h_{0,0} & 0 \\ h_{0,3} & h_{0,2} & h_{0,1} & h_{0,0} \end{bmatrix}, \\ \widetilde{\mathbf{h}}_0^{(1)} &= \begin{bmatrix} 0 & h_{0,3} & h_{0,2} & h_{0,1} \\ 0 & 0 & h_{0,3} & h_{0,2} \\ 0 & 0 & 0 & h_{0,3} \\ 0 & 0 & 0 & 0 \end{bmatrix}. \end{aligned} \tag{2.21}$$

and

$$\mathbf{h}_0 = \begin{bmatrix} h_{0,0} & h_{0,3} & h_{0,2} & h_{0,1} \\ h_{0,1} & h_{0,0} & h_{0,3} & h_{0,2} \\ h_{0,2} & h_{0,1} & h_{0,0} & h_{0,3} \\ h_{0,3} & h_{0,2} & h_{0,1} & h_{0,0} \end{bmatrix} \tag{2.22}$$

We can use (2.16) to represent a user's signals within a coded IFDMA system with an equivalent single-user model illustrated in Figure 2.2. Note that for notation simplicity, the user index k has been omitted in Figure 2.2 since the users are processed individually. Figure 2.2 shows the transmission of a block of convolutional coded information bits that spans several IFDMA symbols duration. The information bits stream $\mathbf{b}$ is encoded using a convolutional encoder to form the coded bit stream $\mathbf{c}$. The coded bit stream is then interleaved to form $\mathbf{c}'$. The interleaved bit stream is mapped to the constellation chosen and modulated for IFDMA transmission where $\{\mathbf{x}\}_n$ refers to the group of symbols transmitted by the user within the n^{th} IFDMA symbol.

The time domain signal model we derived has a couple of theoretical and practical advantages. Firstly, the signal model provides an insight to the diversity performance of IFDMA systems by inspecting the number of independent random variables in (2.17). Secondly, the signal model can be readily expanded into a general framework to represent IFDMA systems with multiple transmit and receive antennas as will be shown in the next section.

2.2.2 General Signal Model for MIMO-IFDMA

In this section, we will expand and generalize the signal model introduced in Section 2.2.1 for MIMO-IFDMA systems with different numerical configurations of transmit and receive antennas. Let the number of receive antennas in the base-station be A_R and the number of transmit antennas at the k^{th} mobile transmitter be $A_T(k)$. Thus the received signal at the a_R^{th} receive antenna can be

modified from (2.5) to form:

$$\mathbf{r}_{a_R} = \sum_{k=0}^{K-1} \sum_{a_T=0}^{A_T(k)-1} \hat{\mathbf{h}}_{a_T,a_R,k} \mathbf{s}_{a_T,k} + \boldsymbol{\eta}_{a_R} \tag{2.23}$$

where $\boldsymbol{\eta}_{a_R}$ is the vector of AWGN at the a_R^{th} receive antenna, $\mathbf{s}_{a_T,k}$ is the transmitted signal of the k^{th} user from the a_T^{th} transmit antenna and $\hat{\mathbf{h}}_{a_T,a_R,k}$ is a $N \times N$ circulant matrix with the first column given by:

$$\hat{\mathbf{h}}_{a_T,a_R,k}(:,1) = \begin{bmatrix} h_{a_T,a_R,k,0} & \dots & h_{a_T,a_R,k,P-1} & 0 & \dots & 0 \end{bmatrix}^T \tag{2.24}$$

which is the channel impulse response between the a_T^{th} transmit antenna of the k^{th} user and the a_R^{th} receive antenna at the base-station. The k^{th} user received signal at the a_R^{th} receive antenna can thus be written as:

$$\begin{aligned} \mathbf{r}_{a_R,k} &= \mathbf{U}_k \mathbf{r}_{a_R} \\ &= \mathbf{U}_k \sum_{m=1}^{K} \sum_{a_T=1}^{A_T} \hat{\mathbf{h}}_{a_T,a_R,m} \mathbf{s}_{a_T,m} + \mathbf{U}_k \boldsymbol{\eta}_{a_R} \\ &= \sum_{a_T=0}^{A_T(k)-1} \mathbf{U}_k \hat{\mathbf{h}}_{a_T,a_R,k} \mathbf{s}_{a_T,k} + \sum_{\substack{m=0 \\ m \neq k}}^{K-1} \sum_{a_T=0}^{A_T(k)-1} \mathbf{U}_k \hat{\mathbf{h}}_{a_T,a_R,m} \mathbf{s}_{a_T,m} + \mathbf{U}_k \boldsymbol{\eta}_{a_R} \\ &= \sum_{a_T=0}^{A_T(k)-1} \mathbf{h}_{a_T,a_R,k} \mathbf{x}_{a_T,k} + \boldsymbol{\eta}'_{a_R,k} \end{aligned} \tag{2.25}$$

where $\mathbf{h}_{a_T,a_R,k}$, is a circulant matrix with the first column given by

$$\mathbf{h}_{a_T,a_R,k}(:,1) = \begin{bmatrix} \sum_{\gamma=0}^{G-1} h_{a_T,a_R,k,\gamma S} e^{-j\frac{2\pi\gamma k}{G}} \\ \vdots \\ e^{-j\frac{2\pi l k}{N}} \sum_{\gamma=0}^{G-1} h_{a_T,a_R,k,\gamma S+l} e^{-j\frac{2\pi\gamma k}{G}} \\ \vdots \\ e^{-j\frac{2\pi(S-1)k}{N}} \sum_{\gamma=0}^{G-1} h_{a_T,a_R,k,\gamma S+S-1} e^{-j\frac{2\pi\gamma k}{G}} \end{bmatrix} \tag{2.26}$$

as $\mathbf{U}_k \hat{\mathbf{h}}_{a_T,a_R,m} \mathbf{s}_{a_T,m} = 0$ for $m \neq k$ as shown in (2.15). For $S \geq P$, $\mathbf{h}_{a_T,a_R,k}(:$

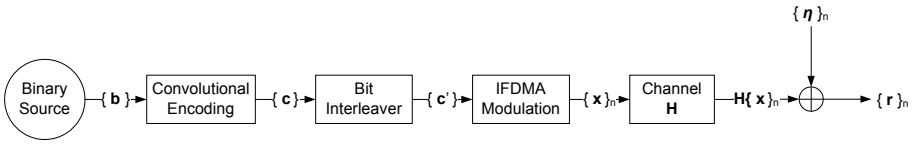

Figure 2.3: Equivalent Single-User System Model for coded MIMO-IFDMA

$, 1)$ is just a truncated version of $\hat{\mathbf{h}}_{a_T,a_R,k}(:,1)$, removing the excess zeros. For $S < P$, the different random variables in $\hat{\mathbf{h}}_{a_T,a_R,k}(:,1)$ are combined to form a smaller set of random variables. We can replace the summation over a_T in (2.25) by concatenating $\mathbf{h}_{a_T,a_R,k}$ horizontally and $\mathbf{x}_{a_T,k}$ vertically to write

$$\begin{aligned}\mathbf{r}_{a_R,k} &= \left[\begin{array}{ccc} \mathbf{h}_{0,a_R,k} & \dots & \mathbf{h}_{A_T(k)-1,a_R,k} \end{array}\right] \left[\begin{array}{c} \mathbf{x}_{0,k} \\ \vdots \\ \mathbf{x}_{A_T(k)-1,k} \end{array}\right] + \boldsymbol{\eta}'_{a_R,k} \\ &= \left[\begin{array}{ccc} \mathbf{h}_{0,a_R,k} & \dots & \mathbf{h}_{A_T(k)-1,a_R,k} \end{array}\right] \mathbf{x}_k + \boldsymbol{\eta}'_{a_R,k} \end{aligned} \tag{2.27}$$

Concatenating the received vector vertically for the different receive antennas gives

$$\mathbf{r}_k = \mathbf{H}_k \mathbf{x}_k + \boldsymbol{\eta}'_k \tag{2.28}$$

where $\mathbf{r}_k = \left[\begin{array}{ccc} \mathbf{r}_{0,k}^{\mathrm{T}} & \dots & \mathbf{r}_{A_R-1,k}^{\mathrm{T}} \end{array}\right]^{\mathrm{T}}$, $\boldsymbol{\eta}'_k = \left[\begin{array}{ccc} \boldsymbol{\eta}_{0,k}'^{\mathrm{T}} & \dots & \boldsymbol{\eta}_{A_R-1,k}'^{\mathrm{T}} \end{array}\right]^{\mathrm{T}}$ and

$$\mathbf{H}_k = \left[\begin{array}{ccc} \mathbf{h}_{0,0,k} & \dots & \mathbf{h}_{A_T(k)-1,0,k} \\ \vdots & \vdots & \vdots \\ \mathbf{h}_{0,A_R-1,k} & \dots & \mathbf{h}_{A_T(k)-1,A_R-1,k} \end{array}\right] \tag{2.29}$$

From (2.28), we note that systems with different number of transmit and receive antennas can be easily represented by making the appropriate modifications to $\mathbf{H}_k$ including single-antenna systems. Also, the structure of $\mathbf{H}_k$ provides us with an insight of the inherent diversity available in the system since the diversity available is limited by the number of independent random variables

within $\mathbf{H}_k$. The estimation of $\mathbf{H}_k$ can be performed by transmitting orthogonal pilots for the different antennas. The performance degradation due to the channel estimation inaccuracies can be limited by choosing sequences with good cross-correlation properties as pilots and frequent pilots transmission.

We can use (2.28) to represent a coded MIMO-IFDMA with a equivalent single-user model illustrated in Figure 2.2 like the model for the single antenna system. Note that for notation simplicity, user index k has been omitted in Figure 2.2 since users are processed individually.

2.3 Theoretical Performance Analysis

We use the signal model developed in Section 2.2 to analyze the theoretical performance of coded IFDMA systems. MLSE is considered at the receiver. We assume that the channel of each user has P channel taps and each channel tap is independent Rayleigh fading. Assuming accurate time and frequency synchronization [29] at the receiver, the users orthogonality can be maintained and IFDMA system can be viewed as a collection of parallel single user transmissions much like OFDMA system. Assuming that all the users have similar channel characteristic as a base-station usually serve users within a fixed area with similar environment, the system performance is equivalent to the single user performance. Thus we can derive the theoretical system performance by analyzing the individual user performance.

Observe that from (2.17), the relationship between P and S plays an important part in the determination of the statistical characteristic of $\mathbf{h}$. We will show that this determines the theoretical performance of the system. Therefore, we will analyze the theoretical performance with different relative values of P and S. More specifically, we consider two typical scenarios: (1) Large number of assigned sub-carriers per user (i.e. $S \geq P$)and (2) Small number of assigned sub-carriers per user (i.e. $S < P$).

2.3.1 Large number of assigned sub-carriers per user, $S \geq P$

In this section, we assume that the number of assigned sub-carriers per user, S, which is equivalent to the number of symbols transmitted per user per antenna, is larger than P, the number of channel paths. Using the signal model in Fig.2.2, we can derive an upper bound on the BER for the system using MLSE. In the following analysis, we will drop the user index k in our derivation for notation simplicity.

We consider two different coded bit sequences $\boldsymbol{c} = [c_0, c_1, ...]$ and $\tilde{\boldsymbol{c}} = [\tilde{c}_0, \tilde{c}_1, ...]$ arising from the input of two different information bit streams. The bit sequences $\boldsymbol{c}$ and $\tilde{\boldsymbol{c}}$ differ in d bits (i.e. the Hamming distance of $\boldsymbol{c}$ and $\tilde{\boldsymbol{c}}$ is d). Assume that the bit interleaver is well-designed so that these d bits are distributed across the entire sequence such that no two bits are grouped within one IFDMA symbol block, representing the optimal case which is fulfilled by most of the pairs of sequences. Let $\mathbf{y} = \{y_0, y_1, \ldots, y_{d-1}\}$ be the group of symbols from $\mathbf{x}$ such that $x_w \neq \tilde{x}_w$. Similarly, let $\tilde{\mathbf{y}}$ be the group of symbols from $\tilde{\mathbf{x}}$ that corresponds to $\mathbf{y}$. We denote the equivalent channel matrix for the i^{th} symbol as $\mathbf{h}_{a_T,a_R,i}$.

Consider the i^{th} pair of symbols from $\mathbf{y}$ and $\tilde{\mathbf{y}}$ being transmitted through the system. The square of the Euclidean distance between the pair of symbols, E_D is given as (from (2.16))

$$\begin{aligned} E_D^2 &= \left\| \mathbf{h}_i \begin{bmatrix} 0 \\ \vdots \\ y_i - \tilde{y}_i \\ \vdots \\ 0 \end{bmatrix} \right\| \\ &= \delta_i^2 \sum_{p=0}^{P-1} |h_{i,p}|^2 \end{aligned} \tag{2.30}$$

where δ_i is the distance between the i^{th} pair of symbols in the symbol constel-

lation and $h_{i,p}$ is the p^{th} entry of $\mathbf{h}_i(:,1)$. Therefore, the lower bound of the Euclidean distance between the i^{th} pair of symbols from $\mathbf{y}$ and $\tilde{\mathbf{y}}$ is,

$$D_i \geq \delta \sqrt{\sum_{p=0}^{P-1} |h_{i,p}|^2} \tag{2.31}$$

where δ is the minimum distance between two symbols in the symbol constellation. For example, if E_S is the symbol power, $\delta = \sqrt{2E_S}$ for QPSK constellation and $\delta = \sqrt{\frac{2}{5}E_S}$ for 16-QAM constellation. Note that if the interleaver cannot distribute the d bits so that each bit is within one IFDMA symbol block, the Euclidean distance may be lower than the bound in (2.31). Thus, the lower bound in (2.31) represents an optimal lower bound based on an ideal interleaver.

Thus, the square of the Euclidean distance between the two sequences, $\boldsymbol{c}$ and $\tilde{\boldsymbol{c}}$, is given by $\sum_{i=0}^{d-1} \delta_i^2 \sum_{p=0}^{P-1} |h_{i,p}|^2$ and the lower bound of the Euclidean distance between the sequences is given by $\delta\sqrt{\sum_{i=0}^{d-1} \sum_{p=0}^{P-1} |h_{i,p}|^2}$. Consequently, the pairwise error probability of deciding $\tilde{\boldsymbol{c}}$ is transmitted when $\boldsymbol{c}$ is actually transmitted conditional on the channel realization over which the symbols are transmitted is upper bounded as:

$$P_e\left\{\tilde{\boldsymbol{c}}|\boldsymbol{c} \cap \mathbf{h}\right\} \leq Q\left(\sqrt{\frac{\delta^2 \sum_{i=0}^{d-1} \sum_{p=0}^{P-1} |h_{i,p}|^2}{2N_0}}\right) \tag{2.32}$$

where N_0 is the noise spectral density. Evidently, the average pairwise error probability and the average BER is dependent on the distribution of $\alpha = \frac{\delta^2}{2N_0} \sum_{i=0}^{d-1} \sum_{p=0}^{P-1} |h_{i,p}|^2$. For simplicity, we assume that the channel variations during the transmission of the sequence $\boldsymbol{c}$ is negligible in slow-fading channel conditions. Hence we can write

$$\begin{aligned} \alpha_{S \geq P} &= \frac{\delta^2}{2N_0} \sum_{i=0}^{d-1} \sum_{p=0}^{P-1} |h_{i,p}|^2 \\ &= \frac{\delta^2 d}{2N_0} \sum_{p=0}^{P-1} |h_p|^2 \end{aligned} \tag{2.33}$$

Note that the second equality in (2.33) uses h_p to denote the p^{th} entry of $\mathbf{h}(:,1)$ which is the equivalent channel matrix between the transmit and receive antenna. Assume that h_p are independent circularly symmetric complex Gaussian random variables (i.e Rayleigh fading) with variance σ_p^2, where $\sum_{p=0}^{P-1}\sigma_p^2 = 1$. The summation $\sum_{p=0}^{P-1}|h_{i,p}|^2$ is then a summation of exponential random variables which has the probability density function (pdf) given by [39, 40]:

$$f(\xi) = \sum_{p=0}^{P-1} \frac{e^{-\frac{\xi}{\sigma_p^2}}}{\sigma_p^2 \prod_{i=0 i\neq p}^{P-1}\left(1-\frac{\sigma_p^2}{\sigma_i^2}\right)} \tag{2.34}$$

Using the Chernoff bound $Q(x) \leq \frac{1}{2}\exp(-x^2/2)$ and averaging over the random channels, the average pairwise error probability is upper bounded as:

$$\begin{aligned}
P_e\{\tilde{\boldsymbol{c}}|\boldsymbol{c}\} &= P_e(d) \\
&\leq \frac{1}{2}\int_0^\infty e^{\left(-\frac{\delta^2 d\xi}{4N_0}\right)} f(\xi)\,\mathrm{d}\xi \\
&= \frac{1}{2}\int_0^\infty e^{\left(-\frac{\delta^2 d\xi}{4N_0}\right)} \sum_{p=0}^{P-1} \frac{e^{-\frac{\xi}{\sigma_p^2}}}{\sigma_p^2 \prod_{i=0,i\neq p}^{P-1}\left(1-\frac{\sigma_p^2}{\sigma_i^2}\right)}\mathrm{d}\xi \\
&= \frac{1}{2}\sum_{p=0}^{P-1} \frac{\int_0^\infty e^{\left(-\frac{\delta^2 d\xi}{4N_0}\right)} e^{-\frac{\xi}{\sigma_p^2}}\mathrm{d}\xi}{\sigma_p^2 \prod_{i=0,i\neq p}^{P-1}\left(1-\frac{\sigma_p^2}{\sigma_i^2}\right)} \\
&= \frac{1}{2}\sum_{p=0}^{P-1} \frac{\int_0^\infty e^{-\xi\left(\frac{\delta^2 d\sigma_p^2+4N_0}{4\sigma_p^2 N_0}\right)}\mathrm{d}\xi}{\sigma_p^2 \prod_{i=0,i\neq p}^{P-1}\left(1-\frac{\sigma_p^2}{\sigma_i^2}\right)} \\
&= \frac{1}{2}\sum_{p=0}^{P-1} \frac{1}{\left(1+\frac{\delta^2 d\sigma_p^2}{4N_0}\right)\prod_{i=0,i\neq p}^{P-1}\left(1-\frac{\sigma_p^2}{\sigma_i^2}\right)}
\end{aligned} \tag{2.35}$$

For the special case of the channel having an uniform power delay profile (i.e. $\sigma_p^2 = \frac{1}{P}, p = 0,\ldots,P-1$), the pdf of α follows a chi-square distribution

with $2P$ degrees of freedom [41] given by

$$f_{S\geq P}(\alpha) = \frac{(2N_0P)^P \alpha^{P-1} e^{-\frac{2N_0P}{\delta^2 d}\alpha}}{(\delta^2 d)^P P!} \tag{2.36}$$

Performing a simple normalization to h_p, the upper bound on the conditional pairwise error probability can be rewritten as:

$$P_e\{\tilde{\boldsymbol{c}}|\boldsymbol{c}\cap\mathbf{h}\} \leq Q\left(\sqrt{\frac{\delta^2 d}{2PN_0}\sum_{i=0}^{P-1}\alpha_i^2}\right) \tag{2.37}$$

where α_i^2 are *i.i.d* exponential random variables with unity variance. Thus the summation of α_i^2 follows the Erlang distribution:

$$f(\xi) = \frac{1}{(P-1)}\xi^{P-1}e^{-\xi} \tag{2.38}$$

Thus, the average pairwise error probability can be upper bounded as:

$$\begin{aligned}
P_e\{\tilde{\boldsymbol{c}}|\boldsymbol{c}\} &= P_E(d) \\
&\leq \int_0^\infty \left(\frac{1}{\sqrt{2\pi}}\int_{\sqrt{\frac{\delta^2 d\xi}{2PN_0}}}^\infty e^{-\frac{t}{2}}\mathrm{d}t\right) f(\xi)\,\mathrm{d}\xi \\
&= \frac{1}{\sqrt{2\pi}}\int_0^\infty e^{-\frac{t}{2}} F\left(\frac{2PN_0}{\delta^2 d}t^2\right)\mathrm{d}t \\
&= \frac{1}{\sqrt{2\pi}}\int_0^\infty e^{-\frac{t}{2}}\left[\sum_{r=P}^\infty \frac{1}{r!}e^{-\frac{(1-\varepsilon)t^2}{2\varepsilon}}\left(\frac{1-\varepsilon}{\varepsilon}t^2\right)^r\right]\mathrm{d}t \\
&= \frac{\sqrt{\varepsilon}}{2}\sum_{r=P}^\infty \binom{2r}{r}\left(\frac{1-\varepsilon}{4}\right)^r \\
&\leq \frac{1}{2\sqrt{\varepsilon}}\binom{2P}{P}\left(\frac{1-\varepsilon}{4}\right)^P
\end{aligned} \tag{2.39}$$

where $\varepsilon = \frac{\delta^2 d}{\delta^2 d + 4PN_0}$.

Conventionally, the union bound on the BER for a convolutional code are derived from the transfer function using the assumption that the length of the error events are negligible compared to the length of the input sequence [42].

In [42], a tighter upper bound on the BER for terminated convolutional code is proposed. Given a weight enumerator, $W(B, D)$, for a terminated convolutional code defined as:

$$W(B, D) = \sum_{i} \sum_{j} c_{i,j} \cdot B^i D^j \tag{2.40}$$

where $c_{i,j}$ is the number of error events composed of a single error event with output Hamming distance j and input Hamming distance i, the upper bound on the BER can thus be written as:

$$BER \leq \frac{1}{L} \sum_{d=d_{free}}^{\infty} \sum_{i=1}^{L} i \cdot c_{i,d} P_E(d) \tag{2.41}$$

where L is the number of input bits and d_{free} is the minimum Hamming distance of the code. The weight enumerator, $W(B, D)$, can be derived from the modified trellis diagram in [42]. Combining (2.39) and (2.40),

$$BER \leq \frac{1}{2} \sum_{d=d_{free}}^{\infty} \sum_{i=1}^{L} \frac{i \cdot c_{i,d}}{4^P L \sqrt{\varepsilon}} \binom{2P}{P} \left(1 + \frac{\delta^2 d}{4PN_0}\right)^{-P} \tag{2.42}$$

Since δ^2 can be readily expressed as a linear function of the symbol power, E_S, the asymptotic BER $\approx (E_s/N_0)^{-P}$ indicating a diversity order of P for the case of the channel having an uniform power delay profile. In other words, IFDMA system can achieve the maximum diversity order for each user for $S \geq P$.

In Figure 2.4, we compare the upper bound on the BER based on the Chernoff bound and (2.41) for a channel with uniform power delay profile and a channel with an exponential decay power delay profile for different number of paths, P, with the number of sub-carriers assigned to a user, S, kept constant at 32. From Figure 2.4, the two power delay profiles have similar diversity performance trends with the uniform power delay profile serving as a worst-case performance scenario.

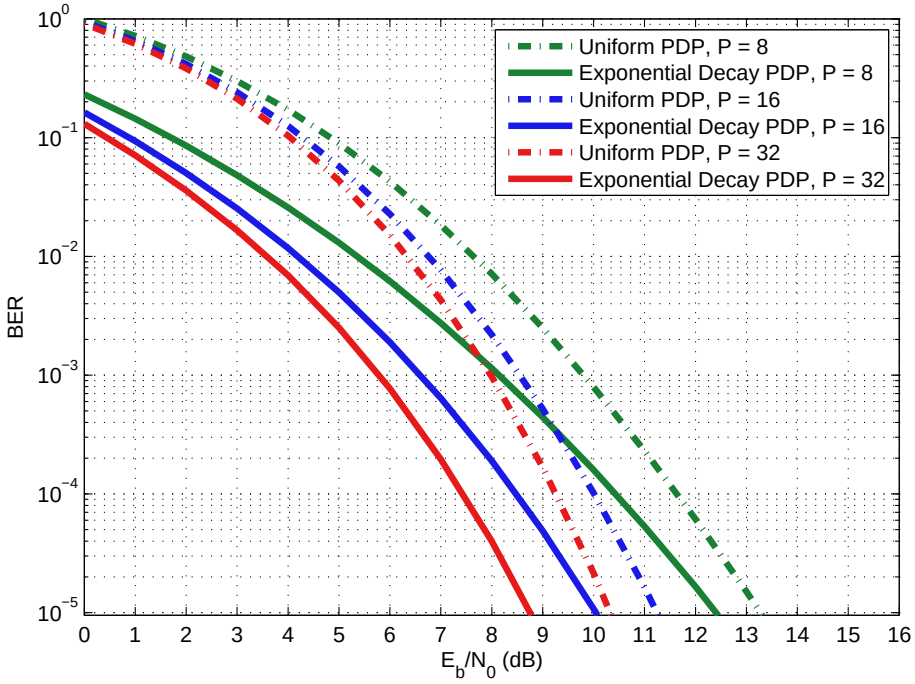

Figure 2.4: Theoretical Upper Bound for Exponential Decay vs Uniform Power Delay Profile for $S = 32$.

2.3.2 Small number of assigned sub-carriers per user, $S < P$

Next, we consider the case when $S < P$. Looking at the formulation of $\mathbf{h}_i$ with reference to (2.17), the variance of the independent circularly symmetric complex Gaussian random variables can be rewritten as $\sigma_l = \sum_{\gamma=0}^{G-1} \sigma_{\gamma S+l}, l = 0, \ldots, S-1$. For the case of channels with uniform power delay profile, the lower bound of the Euclidean distance between the i^{th} pair of symbols for $S < P$ (by replacing P by S in (2.31)), becomes,

$$D_i \geq \delta \sqrt{\sum_{p=0}^{S-1} |h_{i,p}|^2} \tag{2.43}$$

Following the derivation as above, the union bound on the BER can be written as:

$$BER \leq \frac{1}{2} \sum_{d=d_{free}}^{\infty} \sum_{i=1}^{L} \frac{i \cdot c_{i,d}}{4^S L \sqrt{\varepsilon}} \binom{2S}{S} \left(1 + \frac{\delta^2 d}{4SN_0}\right)^{-S} \tag{2.44}$$

In other words, the channel diversity is not fully exploited with the diversity

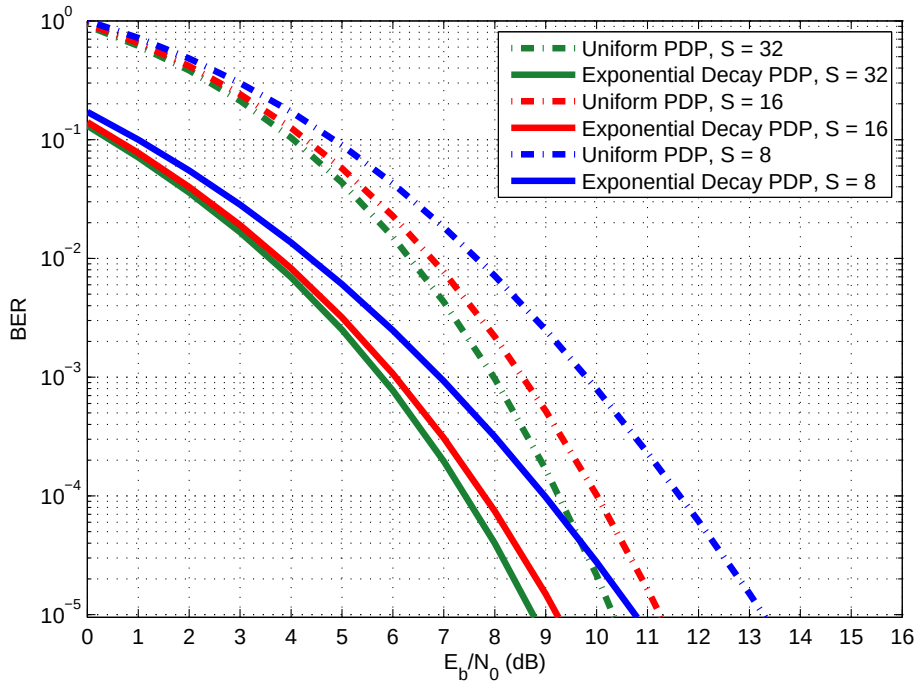

Figure 2.5: Theoretical Upper Bound for Exponential Decay vs Uniform Power Delay Profile for $P = 32$.

order for each user reduced by a factor of S/P. Studying (2.16) and following the derivations above, two elegant ways can be used to regain the diversity loss: frequency hopping (FH) and block spreading (BS). We derive the conditions for maximizing the diversity order for FH-IFDMA and BS-IFDMA in the next section using the insight gained from (2.16). Another alternative scheme to maximize the channel diversity order would be incorporating time division multiple access (TDMA) with IFDMA. However, this scheme has the problem of increasing receiver complexity as BS-IFDMA without the benefit of lowering inter-cell interference as we will discuss later.

In Figure 2.5, we compare the upper bound on the BER based on the Chernoff bound and (2.41) for a channel with uniform power delay profile and a channel with an exponential decay power delay profile for the number of paths, $P = 32$, and with different number of sub-carriers assigned to a user, S. Similar to Figure 2.4, Figure 2.5 shows that the two power delay profiles have similar diversity performance trends with the uniform power delay profile serving as a worst-case performance scenario.

2.3.3 MIMO-IFDMA

For the case of spatial multiplexing, the square of the Euclidean distance between the two received signals, E_D, is rewritten as (from (2.28))

$$\begin{aligned} E_D^2 &= \left\| \begin{bmatrix} \vdots & \ddots & \vdots & \ddots & \vdots \\ \mathbf{h}_{0,a_R,i} & \dots & \mathbf{h}_{a_T,a_R,i} & \dots & \mathbf{h}_{A_T-1,a_R,i} \\ \vdots & \ddots & \vdots & \ddots & \vdots \end{bmatrix} \begin{bmatrix} \vdots \\ y_i - \tilde{y}_i \\ \vdots \end{bmatrix} \right\| \\ &= \delta_i^2 \sum_{a_R=0}^{A_R-1} \sum_{p=0}^{P_D-1} |h_{a_T,a_R,i,p}|^2 \end{aligned} \tag{2.45}$$

where $P_D = \max(P, S)$, δ_i is the distance between the i^{th} pair of symbols in the symbol constellation and $h_{a_T,a_R,i,p}$ is the p^{th} entry of $\mathbf{h}_{a_T,a_R,i}(:,1)$. Therefore, the lower bound of the Euclidean distance between the i^{th} pair of symbols from $\mathbf{y}$ and $\tilde{\mathbf{y}}$ is $D_i \geq \delta\sqrt{\sum_{a_R=0}^{A_R-1}\sum_{p=0}^{P_D-1}|h_{a_T,a_R,i,p}|^2}$. Assuming the symbols in $\mathbf{y}$ and $\tilde{\mathbf{y}}$ are uniformly distributed across the different transmit antennas, the upper bound on the conditional pairwise error probability can be rewritten from (2.32) as:

$$P_e\left\{\tilde{\boldsymbol{c}}|\boldsymbol{c} \cap \mathbf{h}\right\} \leq Q\left(\sqrt{\frac{\delta^2 \sum_{i=0}^{d-1}\sum_{a_R=0}^{A_R-1}\sum_{p=0}^{P_D-1}|h_{a_T,a_R,i,p}|^2}{2N_0}}\right) \tag{2.46}$$

where $P_A = A_R \cdot A_T \cdot P_D$. Following the derivation in Section 2.3.1, the upper bound on the average pairwise error probability for a channel with uniform power delay profile is given by:

$$P_e\left\{\tilde{\boldsymbol{c}}|\boldsymbol{c}\right\} = P_e(d) \leq \frac{1}{2\sqrt{\varepsilon}}\binom{2P_A}{P_A}\left(\frac{1-\varepsilon}{4}\right)^{P_A} \tag{2.47}$$

where $\varepsilon = \frac{\delta^2 d}{\delta^2 d + 4P_D A_T N_0}$ and the union bound on the BER is written as:

$$BER \leq \frac{1}{2}\sum_{d=d_{free}}^{\infty}\sum_{i=1}^{L}\frac{i \cdot c_{i,d}}{4^{P_A}L\sqrt{\varepsilon}}\binom{2P_A}{P_A}\left(1+\frac{\delta^2 d}{4P_D A_T N_0}\right)^{-P_A} \tag{2.48}$$

2.4 Maximizing Channel Diversity Order

In this section, we derive the conditions for maximizing the diversity order for FH-IFDMA and BS-IFDMA for $S < P$ and compare their respective benefits and disadvantages.

2.4.1 FH-IFDMA System

Let $P \leq LS$, where $L > 1$ is an integer. The signal model provides us with an intuitive approach in designing the hopping sequence through observations about the random variables in (2.17). We can regain the diversity loss by ensuring that α follows a chi-square distribution with $2P$ degrees of freedom. As frequency hopping is equivalent to a user having different index for the IFDMA symbols transmitted within a packet, we maximize the diversity order by using an appropriate set of indices $\mathbf{u}(k) = \{u_0, u_1, ..., u_{L-1}\}$ for the k^{th} user. For channels with independent Rayleigh fading paths, it is akin to solving the set of conditional equations:

$$\sum_{\gamma=0}^{L-1} E\left[|h_{i,\gamma+g}|^2\right] e^{\frac{j2\pi\gamma}{G}(u_n-u_m)} = 0 \tag{2.49}$$

for $g = 0, 1, \ldots, S-1$ and $u_m, u_n \in \mathbf{u}(k)$. Since $E\left[|h_{i,\gamma+g}|^2\right] = 1$ for all g, we can satisfy the set of equations if $(u_m - u_n) = z\frac{G}{L}$, where z and $\frac{G}{L}$ are any integers. Since we can easily choose N so that $\frac{N}{P}$ and hence $\frac{G}{L}$ is an integer, the set of indices to maximize the diversity order for each user is simply given by $\mathbf{u}(k) = \left\{u_0, u_0 + \frac{G}{L}, ..., u_0 + \frac{G(L-1)}{L}\right\}$. Since each of the $\frac{G}{L}$ optimal frequency hopping patterns can be shared by L users, every user in the system can have his own distinct optimal hopping pattern and achieve the maximum diversity order of the channel. Using frequency hopping with the derived hopping sequence, the union bound on the BER reverts from (2.44) back to (2.42). Hence, the diversity order is P regardless of the value of S.

2.4.2 BS-IFDMA System

In BS-IFDMA systems, data at the transmitter within a single block of IFDMA symbols are spread across B blocks using orthogonal spreading codes as shown in Section 4.2. To maintain the same data rate for each user, the number of sub-carriers assigned to each user is increased by a factor of B. Hence, in BS-IFDMA systems, each user is differentiated by its IFDMA phase vector and its block spread code. Note that the reduction in number of orthogonal users in IFDMA is compensated by the assigning of these users in the block spread domain. At the receiver, the signals first undergo block despread to form B different sets of IFDMA received signals. Therefore, we can write the received signal of the k^{th} user in the b^{th} set similar to (2.16). The main difference is that the number of symbols within a block is increased from S to $B \cdot S$. Following the derivations above, all we need to do to maximize the channel diversity order is to chose B such that $B \cdot S \geq P$ or equivalently, $B \geq \frac{P}{S}$.

2.4.3 Comparison Between FH-IFDMA and BS-IFDMA

Both FH-IFDMA and BS-IFDMA are simple to implement at the transmitter. For FH-IFDMA, the frequency hopping can be realized by changing the user-specifc phase vector for different IFDMA symbol block. For BS-IFDMA, the spreading process can be easily implemented provided that binary spreading codes are used. However, at the receiver, the use of BS-IFDMA will result in a more complex implementation. Block spread increases the number of symbols transmitted per symbols from S to $B \cdot S$. For simple FDE in a single transmitter, single receiver system, this increase in complexity is negligible. For more complex detection schemes or in multiple antennas system, the increase can be significant especially if B is large. However, BS-IFDMA scheme does have the added advantage of lowering inter-cell interference [43] through the despreading process by incorporating a long cell-specific spreading code like in present

3G CDMA system. We know from [19] that the diversity order for MMSE FDE is dependent on the relative ratio between the number of diversity paths and the number of transmitted symbols per block. More specifically, we can improve the diversity order of the MMSE FDE by increasing the number of transmitted symbols per block. Block spreading allows the flexibility to do that without changing the maximum number of supported users or the data rate of each user. Thus, though both schemes have similar BER performances using our proposed detection and decoding scheme, BS-IFDMA performs better when a simple frequency domain equalizer is used at the receiver.

2.5 Iterative Soft QRD-M Algorithm

We describe the proposed iterative soft QRD-M algorithm for coded IFDMA system in this section. We derive the iterative detection and decoding algorithm used for coded IFDMA system using the system signal model in Section 2.2. Even though we consider the use of convolutional code in this thesis to show the effectiveness of the algorithm even with a non-capacity approaching code, the extension to other, capacity-approaching error-correcting codes such as turbo code and LDPC code is trivial. From Figure 2.2, we see that the convolutional code and the IFDMA modulation can be regarded as a serially concatenated scheme much like in turbo code [6, 7]. Thus, we can apply the principle of iterative decoding to the detection and decoding of the received signals [44, 45]. Reliability information is passed between the APP detector and the ECC decoder iteratively as shown in Figure 2.6. Note that since users are processed separately, we drop the user index k for notation simplicity. A conventional APP detector implementing the maximum *a posteriori* (MAP) algorithm has computational cost which increases exponentially with the number of symbols transmitted per block and the constellation size used [46]. Therefore, to keep the complexity of the detector to a practical level, a suboptimum APP detector

based on the principles of the M-algorithm [47] and QR decomposition [48] is used.

In each iteration, the QRD-M detector generates the soft decision metrics from the received complex data $\mathbf{r}$ and the soft *a priori* information supplied by the SISO ECC decoder. Subsequently, the SISO ECC decoder calculates a new set of soft *a priori* information for the APP detector in the next iteration based on the soft decision metrics from the detector. The process is repeated until the designed maximum number of iterations is reached.

2.5.1 QR Decomposition

Rewrite (2.16) for the n^{th} received IFDMA symbol as:

$$\{\mathbf{r}\}_n = \mathbf{H}\{\mathbf{x}\}_n + \{\boldsymbol{\eta}\}_n \tag{2.50}$$

Applying the principle of QR decomposition [48] to $\mathbf{H}$, i.e. $\mathbf{H} = \mathbf{QR}$, we can orthogonalize (2.50) by:

$$\begin{aligned} \{\mathbf{z}\}_n &= \mathbf{Q}^H\{\mathbf{r}\}_n \\ &= \mathbf{R}\{\mathbf{x}\}_n + \mathbf{Q}^H\{\boldsymbol{\eta}\}_n \\ &= \mathbf{R}\{\mathbf{x}\}_n + \{\boldsymbol{\xi}\}_n \end{aligned} \tag{2.51}$$

where $\{\cdot\}^H$ represents the Hermitian operation. Since $\mathbf{Q}$ is unitary, the variance of $\{\boldsymbol{\xi}\}_n$ is same as the $\{\boldsymbol{\eta}\}_n$. Note that no explicit knowledge of the number of transmit antennas is required after the orthogonalization.

Alternatively, we can apply the linear minimum mean squared error (LMMSE) criterion to the orthogonalization [49–51]. Defining

$$\underline{\mathbf{H}} = \begin{bmatrix} \mathbf{H} \\ \sigma\mathbf{I}_{A_T \cdot S} \end{bmatrix} \tag{2.52}$$

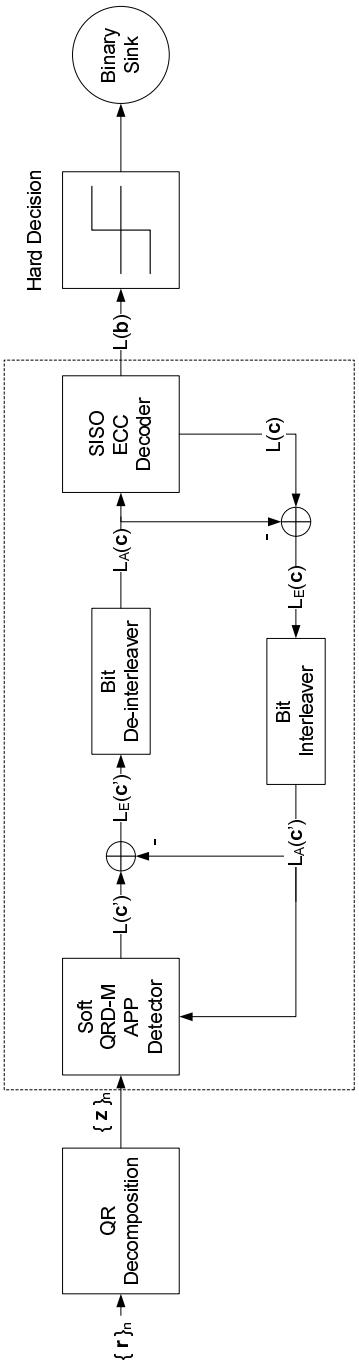

Figure 2.6: Iterative Soft QRD-M Algorithm for Detection and Decoding of coded IFDMA System.

where $\mathbf{I}_{A_T \cdot S}$ is an $A_T \cdot S \times A_T \cdot S$ identity matrix and σ is the standard deviation of the AWGN components in $\{\boldsymbol{\xi}\}_n$. Corresponding to the usual QR decomposition, we can write $\underline{\mathbf{H}} = \underline{\mathbf{Q}}\underline{\mathbf{R}}$ with $\underline{\mathbf{Q}} = \left[\mathbf{Q}_1^T \mathbf{Q}_2^T\right]^T$. Hence, applying the QR decomposition to $\underline{\mathbf{H}}$ gives

$$\begin{aligned} \underline{\mathbf{H}} &= \underline{\mathbf{Q}}\underline{\mathbf{R}} \\ &= \begin{bmatrix} \mathbf{Q}_1\underline{\mathbf{R}} \\ \mathbf{Q}_2\underline{\mathbf{R}} \end{bmatrix} \end{aligned} \tag{2.53}$$

If we apply the Hermitian of $\underline{\mathbf{Q}}$ to a zeros-padded received vector $\{\underline{\mathbf{r}}\}_n = \left[\{\mathbf{r}\}_n^T \ \mathbf{0}_{A_T \cdot S}^T\right]^T$, where $\mathbf{0}_{A_T \cdot S}$ is an all-zeros vector of size $A_T \cdot S$, we will get

$$\begin{aligned} \{\underline{\mathbf{z}}\}_n &= \underline{\mathbf{Q}}^H \{\underline{\mathbf{r}}\}_n \\ &= \underline{\mathbf{R}} \{\mathbf{x}\}_n - \sigma \mathbf{Q}_2^H \{\mathbf{x}\}_n + \mathbf{Q}_1^H \{\boldsymbol{\eta}\}_n \\ &= \underline{\mathbf{R}} \{\mathbf{x}\}_n + \boldsymbol{\xi}_n \end{aligned} \tag{2.54}$$

2.5.2 Soft QRD-M Algorithm

Since the data are independent and thus the entries in $\{\mathbf{x}\}_n$ are independent discrete random variables, we can approximate entries in $\boldsymbol{\xi}_n$ as AWGN components with variance σ^2. Assuming that the bits are independent after proper interleaving, the log-likelihood ratio (LLR) for i^{th} bit in the bit-streams $\mathbf{c}'$ in Figure 2.6 can be written as:

$$\begin{aligned} L(c_i') &= \ln \frac{\mathrm{P}\left(c_i' = 1 | \{\mathbf{r}\}_{0,\ldots,N_S-1}\right)}{\mathrm{P}\left(c_i' = 0 | \{\mathbf{r}\}_{0,\ldots,N_S-1}\right)} \\ &= \ln \frac{\sum_{\mathbf{c}' \in \mathbb{C}_{i,1}} \mathrm{P}\left(\{\mathbf{r}\}_{0,\ldots,N_S-1} | \mathbf{c}'\right) \mathrm{P}\left(\mathbf{c}'\right)}{\sum_{\mathbf{c}' \in \mathbb{C}_{i,0}} \mathrm{P}\left(\{\mathbf{r}\}_{0,\ldots,N_S-1} | \mathbf{c}'\right) \mathrm{P}\left(\mathbf{c}'\right)} \\ &= \ln \frac{\mathrm{P}\left(c_i' = 1\right)}{\mathrm{P}\left(c_i' = 0\right)} + \ln \frac{\sum_{\mathbf{c}' \in \mathbb{C}_{i,1}} \mathrm{P}\left(\{\mathbf{r}\}_{0,\ldots,N_S-1} | \mathbf{c}'\right) \prod_{j \neq i} \mathrm{P}\left(c_j'\right)}{\sum_{\mathbf{c}' \in \mathbb{C}_{i,0}} \mathrm{P}\left(\{\mathbf{r}\}_{0,\ldots,N_S-1} | \mathbf{c}'\right) \prod_{j \neq i} \mathrm{P}\left(c_j'\right)} \\ &= L_A(c_i') + L_E(c_i') \end{aligned} \tag{2.55}$$

where N_S is the total number of transmitted IFDMA symbol period and $\mathbb{C}_{i,b}$ is the set of vectors $\mathbf{c}$ with $c_i = b$, $b = 0, 1$. Note that only the extrinsic information, $L_E(\mathbf{c}')$, is passed to the SISO ECC decoder after de-interleaving as the *a priori* information, $L_A(\mathbf{c})$. Similarly, the LLR for i^{th} bit in the bit-streams $\mathbf{c}$ can be written as:

$$L(c_i) = L_A(c_i) + L_E(c_i) \tag{2.56}$$

where $L_E(\mathbf{c})$ is the extrinsic information supplied to the APP detector.

We can perform the calculation of the LLRs for the bits in different IFDMA symbol blocks separately. We denote the vector of coded bits mapped to the S symbols transmitted within a single IFDMA symbol block as $\tilde{\mathbf{c}}$. We can divide he transmitted bits into $\tilde{\mathbf{c}} = [\tilde{\mathbf{c}}_0\, \tilde{\mathbf{c}}_1 \ldots \tilde{\mathbf{c}}_{S-1}]$, where $\tilde{\mathbf{c}}_i$ is the group of bits that maps to the i^{th} complex symbol and $\tilde{\mathbf{c}}_i = [\tilde{c}_{i,0}\, \tilde{c}_{i,1} \ldots \tilde{c}_{i,j} \ldots \tilde{c}_{i,Q-1}]$ where Q is the number of bits mapped to each complex symbol. Since the bits are independent, the LLR of $\tilde{c}_{i,j}$ (where j is the index of the bits within a complex symbol) can be simplified from (2.55) to

$$L(\tilde{c}_{i,j}) = \ln \frac{\mathrm{P}\left(\tilde{c}_{i,j} = 1\right)}{\mathrm{P}\left(\tilde{c}_{i,j} = 0\right)} + \ln \frac{\sum_{\tilde{\mathbf{c}} \in \mathbb{C}_{i,j,1}} \mathrm{P}\left(\mathbf{r}|\tilde{\mathbf{c}}\right) \prod_{kl \neq ij} \mathrm{P}\left(\tilde{c}_{k,l}\right)}{\sum_{\tilde{\mathbf{c}} \in \mathbb{C}_{i,j,0}} \mathrm{P}\left(\mathbf{r}|\tilde{\mathbf{c}}\right) \prod_{kl \neq ij} \mathrm{P}\left(\tilde{c}_{k,l}\right)} \tag{2.57}$$

where $\mathbb{C}_{i,j,b}$ is the set of 2^{SQ-1} vectors of $\tilde{\mathbf{c}}$ with $\tilde{c}_{i,j} = b$, $b = 0, 1$.

The logarithm of summations expressions required in (2.57) are computationally complex. We simplify the calculation through two approaches: QR decomposition and application of the M-algorithm. By applying the QR orthogonalization through (2.51) or (2.54), (2.57) is rewritten as

$$L(\tilde{c}_{i,j}) = \ln \frac{\mathrm{P}\left(\tilde{c}_{i,j} = 1\right)}{\mathrm{P}\left(\tilde{c}_{i,j} = 0\right)} + \ln \frac{\sum_{\tilde{\mathbf{c}} \in \mathbb{C}_{i,j,1}} \mathrm{P}\left(\mathbf{z}|\tilde{\mathbf{c}}\right) \prod_{kl \neq ij} \mathrm{P}\left(\tilde{c}_{k,l}\right)}{\sum_{\tilde{\mathbf{c}} \in \mathbb{C}_{i,j,0}} \mathrm{P}\left(\mathbf{z}|\tilde{\mathbf{c}}\right) \prod_{kl \neq ij} \mathrm{P}\left(\tilde{c}_{k,l}\right)} \tag{2.58}$$

Note that the conditional probability in (2.58) can be written as product of

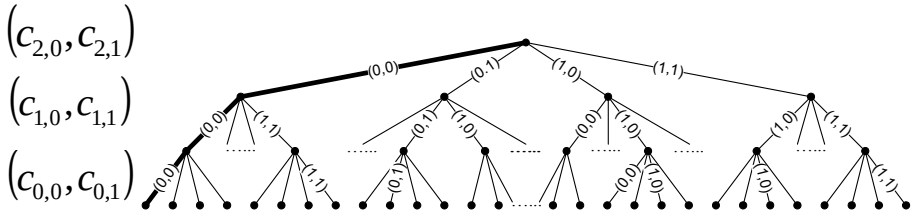

Figure 2.7: Decoding Tree for $S = 3$, $Q = 2$.

probabilities:

$$\begin{aligned} P\left(\mathbf{z}|\tilde{\mathbf{c}}\right) &= \prod_{i=0}^{S-1} P\left(z_i|\tilde{\mathbf{c}}\right) \\ &= \prod_{i=0}^{S-1} \frac{1}{\sigma\sqrt{2\pi}} \exp\left\{ -\frac{\left(z_i - \sum_{j=i}^{S-1} R_{i,j} x_{j|\tilde{\mathbf{c}}}\right)^2}{2\sigma^2} \right\} \end{aligned} \tag{2.59}$$

where z_i is the i^{th} complex symbol in the group of vectors, $\mathbf{z}$. $R_{i,j}$ is the element in the i^{th} row and j^{th} column of $\mathbf{R}$ and $x_{i|\tilde{\mathbf{c}}}$ is the i^{th} transmitted complex symbol given the bit vector $\tilde{\mathbf{c}}$. We can write the logarithm of the probability for a particular $\tilde{\mathbf{c}}$ as:

$$\begin{aligned} L_{\tilde{\mathbf{c}}}^{i,j} &= \ln\left[P\left(\mathbf{z}|\tilde{\mathbf{c}}\right) \prod_{kl \neq ij} P\left(\tilde{c}_{k,l}\right) \right] \\ &= \sum_{k=0}^{S-1} \sum_{l=0}^{Q-1} \ln P(\tilde{c}_{k,l}) - \ln P(\tilde{c}_{i,j}) \\ &\quad -\frac{1}{2\sigma^2} \sum_{k=0}^{S-1} \left(z_k - \sum_{l=k}^{S-1} R_{k,l} x_{l|\tilde{\mathbf{c}}} \right)^2 - \frac{S}{2} \ln(2\pi\sigma^2) \\ &= \sum_{k=0}^{S-1} \left[\sum_{l=0}^{Q-1} \ln P(\tilde{c}_{k,l}) - \frac{1}{2\sigma^2} \left(z_k - \sum_{l=k}^{S-1} R_{k,l} x_{l|\tilde{\mathbf{c}}} \right)^2 \right] \\ &\quad - \ln P(\tilde{c}_{i,j}) - \frac{S}{2} \ln(2\pi\sigma^2) \end{aligned} \tag{2.60}$$

Thus, the calculation of individual $L_{\tilde{\mathbf{c}}}^{i,j}$ is broken down into S stages through the application of QR decomposition. The value of $L_{\tilde{\mathbf{c}}}^{i,j}$ for a particular vector $\tilde{\mathbf{c}}$ is a summation of the branch metrics along a path that corresponds to the vector

in the tree structure shown in Figure 2.7. In Figure 2.7, the partial view of the decoding tree for an IFDMA system with $Q = 2$ (i.e. QPSK constellation) and $S = 3$ is shown with the path corresponding to the all-zeros vector highlighted. For the k^{th} stage, the branch metrics are $\ln\left[P\left(z_k|\tilde{c}_{k,0},\ldots,c_{S,Q-1}\right)P\left(\tilde{c}_{k,0}\right)\ldots P\left(\tilde{c}_{k,Q-1}\right)\right]$ starting from $k = S$ at the top of the tree to $k = 1$.

However, as can be seen from Figure 2.7, the number of diverging paths increases exponentially at each stage. QR decomposition does not, by itself, reduce the number of calculations required. To do so, we apply the M-algorithm, keeping only the largest M paths in each stage so that the number of paths to consider is limited to a manageable number regardless of the actual value of S or Q. To justify the application of the M-algorithm, we need to show that the approximations made are valid and appropriate. Rewriting (2.58) using $L_{\tilde{\mathbf{c}}}^{i,j}$, we get

$$L(\tilde{c}_{i,j}) = \ln\frac{\mathrm{P}\left(\tilde{c}_{i,j}=1\right)}{\mathrm{P}\left(\tilde{c}_{i,j}=0\right)} + \ln\frac{\sum_{\tilde{\mathbf{c}}\in\mathbb{C}_{i,j,1}}\exp\left(L_{\tilde{\mathbf{c}}}^{i,j}\right)}{\sum_{\tilde{\mathbf{c}}\in\mathbb{C}_{i,j,0}}\exp\left(L_{\tilde{\mathbf{c}}}^{i,j}\right)} \tag{2.61}$$

We enumerate the set of $L_{\tilde{\mathbf{c}}}^{i,j}$ for $\tilde{\mathbf{c}} \in \mathbb{C}_{i,j,b}$ as $L_{\tilde{\mathbf{c}}}^{i,j}(k)$, $k = 0,\ldots,SQ-1$, in descending magnitude. Hence, $\ln\left(\sum_{\tilde{\mathbf{c}}\in\mathbb{C}_{i,j,b}} e^{L_{\tilde{\mathbf{c}}}^{i,j}}\right) = \ln\left(\sum_{k=0}^{SQ-1} e^{L_{\tilde{\mathbf{c}}}^{i,j}(k)}\right)$. Denoting $\ln\left(\sum_{k=0}^{SQ-1} e^{L_{\tilde{\mathbf{c}}}^{i,j}(k)}\right)$ as Λ_{SQ-1}, we can write the summation of the logarithms recursively as:

$$\begin{aligned}
\Lambda_{SQ-1} &= \ln\left(\sum_{k=0}^{SQ-1} e^{L_{\tilde{\mathbf{c}}}^{i,j}(k)}\right) \\
&= \ln\left\{e^{L_{\tilde{\mathbf{c}}}^{i,j}(0)}\prod_{k=1}^{SQ-1}\left(1+\frac{e^{L_{\tilde{\mathbf{c}}}^{i,j}(k)}}{\sum_{l=0}^{k-1} e^{L_{\tilde{\mathbf{c}}}^{i,j}(l)}}\right)\right\} \\
&= L_{\tilde{\mathbf{c}}}^{i,j}(0) + \sum_{k=1}^{SQ-1}\ln\left(1+\frac{e^{L_{\tilde{\mathbf{c}}}^{i,j}(k)}}{e^{\Lambda_{k-1}}}\right) \\
&= \Lambda_{SQ-2} + \ln\left(1+e^{L_{\tilde{\mathbf{c}}}^{i,j}(SQ-1)-\Lambda_{SQ-2}}\right)
\end{aligned} \tag{2.62}$$

with $\Lambda_0 = L_{\tilde{\mathbf{c}}}^{i,j}(0)$. Since Λ_k is monotonically increasing and $L_{\tilde{\mathbf{c}}}^{i,j}(0) > \ldots > L_{\tilde{\mathbf{c}}}^{i,j}(SQ-1)$, the value of $\ln\left(1+e^{L_{\tilde{\mathbf{c}}}^{i,j}(k)-\Lambda_{k-1}}\right) \to 0$ as k increases. In other

words, we can approximate Λ_{SQ-1} by Λ_T, where $T < SQ - 1$, and the approximation error becomes smaller with increasing T. Note that for $T = 1$, the approximation above becomes the max-log approximation. Thus, to approximate the LLR of $\tilde{c}_{i,j}$, only the T largest values of $L^{i,j}_{\tilde{\mathbf{c}}}$ of the vectors in $\mathbb{C}_{i,j,1}$ and $\mathbb{C}_{i,j,0}$ need to be calculated.

Therefore the application of the M-algorithm is appropriate as it keeps the M ($M > T$) largest path metrics at each stage, allowing us to approximate $L(\tilde{c}_{i,j})$ for $i = 1, \ldots, S$, $j = 1, \ldots, Q$ with small loss of accuracy. Also, note that the bits $\tilde{c}_{k,0}, \ldots, \tilde{c}_{k,Q-1}$ only affect the path metrics calculation from the k^{th} stage to the 1^{st} stage. Hence, in the calculation of $L^{i,j}_{\tilde{\mathbf{c}}}$, we can reuse the path metrics from the S^{th} stage to the $(k+1)^{th}$ stage, further reducing the number of computations required. We will discuss more on the complexity of the algorithm when we look at the structure of $\mathbf{R}$ in Section 2.5.4.

The recursion derived in (2.62) allows the proposed algorithm to work exclusively in the log-domain, eliminating computationally complex operations like multiplications and exponential functions in the branch metric calculations unlike in [45], where the M-algorithm is applied directly to the calculation of the APP for each bit to limit the number of computations required. The process is repeated for each individual bit in [45] and is computationally much more expensive than the proposed solution as it requires more operations per bit and uses exponential functions and logarithm functions in the calculations. On the other hand, the proposed algorithm offers more accuracy and flexibility than the solution in [44] where max-log approximation is used directly for simplification to simplify the logarithm of a summation into logarithm of the maximum term and the LLR is calculated using only the M survivor paths determined by hard decision M-algorithm [52]. If for a particular considered bit, there does not exist a path within the M paths with the complementary bit, the corresponding bit is assumed to have high reliability and an arbitrary high LLR value is assigned [44]. Evidently, the degree of approximation of the proposed algorithm

can be adjusted to suit the system requirement.

2.5.3 SISO ECC Decoder

For the SISO ECC decoder, the Bahl-Cocke-Jelinek-Raviv (BCJR) algorithm [46] is used to compute the extrinsic information from the LLRs provided by the QRD-M APP detector. The BCJR is a form of MAP algorithm which takes into account the trellis structure of the convolutional code used. The APP of each individual coded bit is calculated recursively starting from the two ends of the trellis. Terminated convolutional code using a feed forward encoder is used with the information bits padded with '0's at the end so that the trellis terminates at the all-zeros state. The encoder is also reset to the all-zeros state before the encoding process. Various other algorithms can be used in combination with the soft QRD-M detector proposed above if different ECCs other than a convolutional code are used. For example, if a LDPC code is used in place of a convolutional code, the belief propagation algorithm can be used to generate the required soft extrinsic information.

2.5.4 Computational Complexity

There exists significant amount of potential computational savings in the proposed algorithm for mobile devices transmitting at a high data rate (i.e. a lot of assigned sub-carriers, $S >> P$). The savings are due to the special structure of the matrix $\mathbf{R}$ used in the soft QRD-M APP detector. For $S < 2P$, the matrix $\mathbf{R}$ is a conventional upper triangular matrix that allows us to compute the LLRs in stages as shown in Section 2.5.2. However, for $S \geq 2P$, the upper half of $\mathbf{R}$ will be punctured by zeros.

Notice that $\mathbf{h}$ is simply a circulant matrix. If we write $\mathbf{h} = [\mathbf{h}_0, \ldots, \mathbf{h}_{S-1}]$, $\mathbf{Q} = [\mathbf{q}_0, \ldots, \mathbf{q}_{S-1}]$ and $\mathbf{R} = [r_{i,j}]$, $i = 0, \ldots, S-1, j = 0, \ldots, S-1$, we can see that $|r_{0,0}| = |\mathbf{h}_0|$. If we let $r_{0,0} = |\mathbf{h}_0|$ and write $\mathbf{h}_i$ as the linear combinations

of $\mathbf{q}_i$, we get

$$\mathbf{h}_i = \sum_{j=0}^{i} r_{j,i}\mathbf{q}_j \tag{2.63}$$

or alternatively,

$$\mathbf{q}_i = \frac{1}{r_{i,i}}\left(\mathbf{h}_i - \sum_{j=0}^{i-1} r_{j,i}\mathbf{q}_j\right) \tag{2.64}$$

Therefore, for $j \geq i$, $r_{i,j} = \mathbf{q}_i^H \mathbf{h}_j = \frac{1}{r_{i,i}^*}\left(r_{0,0}^* r_{0,j-i} - \sum_{k=0}^{i-1} r_{k,i}^* r_{k,j}\right)$.

Solving for $i = j$, we get $|r_{i,i}|^2 = |r_{0,0}|^2 - \sum_{k=0}^{i-1} |r_{k,i}|^2$ and choose $r_{i,i} = \sqrt{|r_{0,0}|^2 - \sum_{k=0}^{i-1} |r_{k,i}|^2}$.

Note that the first row of $\mathbf{R}$ is actually the cyclic auto-correlation of $\mathbf{h}_0$ scaled down by $|\mathbf{h}_0|$. As such, $r_{0,i} = 0$ for $i = P+1, \ldots, S-P$, $S \geq 2P$. Hence, we see that the total number of non-zeros elements in $\mathbf{R}$ is capped at $2P-1$ instead of S. Therefore, the maximum number of calculations required for each stage in the QRD-M detector is determined by P rather than S. This represents a huge computational saving for very large $S >> P$. Note that the above derivation is applicable to both ZF and MMSE QRD.

2.5.5 Generalized Algorithm for MIMO-IFDMA

The proposed iterative soft QRD-M algorithm can be easily generalized for coded MIMO-IFDMA system. The generalized algorithm is applicable for different numerical configurations of transmit and receive antennas, assuming that the number of receive antennas, A_R, is more than or equal to, the number of transmit antennas, A_T. Notice that the equivalent signal model for the single antennas IFDMA system in Figure 2.2 and the one for MIMO-IFDMA system in Figure 2.3 are very similar. Instead of a circulant channel matrix $\mathbf{h}$ for the single antenna system, the MIMO system has a channel matrix $\mathbf{H}$ that is an amalgamation of different circulant matrices. The QR decomposition in (2.50

and 2.54) can also be applied to $\mathbf{H}$. The signal processing after the QR decomposition required no explicit knowledge of the number of transmit antennas used. Unlike [31], the proposed algorithm is dependent only on the product of A_T and S instead of the individual values of A_T and S. This gives the receiver more flexibility to share the common hardware platform for different numerical configurations of transmit antennas. For example, the same computational resources used to detect and decode a user's signal with $S = 32$ and $A_T = 1$ can be reused to detect and decode a user's signal with $S = 16$ and $A_T = 2$.

As we perform the calculation of the LLRs for the bits in different IFDMA symbol blocks separately, the probability calculation in (2.59) can be extended to the multiple antennas case by replacing S, the number of sub-carriers assigned to the user, to $A_T \cdot S$. In other words, instead of having S stages in the calculation of (2.60), there are $A_T \cdot S$ stages. Since, the M-algorithm is used repeatedly at each stage to limit the number of considered paths for the next stage regardless of the actual number of possible paths, the proposed algorithm makes no distinction between the decoding of signals in multiple antennas systems and in single antenna systems. Thus, the parameter that controls the operation of the proposed algorithm is the user's symbol transmission rate and not the transmit antenna configuration of the user.

2.6 Simulation Results

In this section, we provide the numerical examples and simulation results of our proposed algorithms. We compare the simulated performance of the proposed generalized iterative soft QRD-M algorithm with the derived theoretical upper bound to show that the proposed algorithm can achieve the maximum channel diversity order. We also use the performance of hypothetical MFLB [16] as an ideal lower bound to measure the performance of the proposed algorithm. The simulated performance of the proposed algorithm is shown to approach MFLB

Table 2.1: IFDMA Simulation System.

Centre Frequency		2.4 GHz
System Bandwidth		5 MHz
IFFT Size, N		256
Cyclic Prefix Length, N_{CP}		32
Modulated Symbol Constellation		QPSK
Forward Error Correcting Code	Type	Convolutional Code
	Code Rate	1/2
	Generator Polynomial	[5 7]
Channel Model	Power Delay Profile	Uniform
	Type of Fading Path	Slow Rayleigh Fading
	Antenna Correlation	Uncorrelated
Maximum Number of Iterations in Proposed Algorithm		3
Channel Estimation		Ideal
Minimum Number of Transmitted Packets		10000
Minimum Number of Received Packets with Decoding Error		50

at high SNR within a few iterations with negligible performance degradation at low BER. The simulation results will also show that the proposed algorithm has significant performance gain over conventional FDE with the gain increasing with the greater channel diversity order.

2.6.1 Simulation System

We consider a system with 5 MHz bandwidth and centre frequency of 2.4 GHz with $N = 256$. The designed cyclic prefix length, $N_{CP} = 32$ and all the users' signals are assumed to be synchronized to arrive within N_{CP}. The transmitters use a rate-1/2 terminated convolutional code with generator polynomial [5 7] [53] and QPSK constellation (i.e. $Q = 2$). We consider block transmission using a pseudo-random bit-interleaver with each block containing 254 information bits. Since the constraint length of the convolutional code used is 2, two '0' bits is padded to the information bitstream to terminate the trellis in the all-zeros state.

The channel is assumed to remain unchanged during one transmission block and varies independently for different transmission blocks. We assume each user has independent and identically distributed (i.i.d.) channel profile with in-

Table 2.2: Simulation System Configurations for Section 2.6.2 - Section 2.6.4.

System Parameters	Section		
	2.6.2	2.6.3	2.6.4
Type of QR Decomposition	ZF, MMSE QRD	MMSE QRD	
Number of Users	8		
Number of Sub-carriers per User, S	32		
Number of Channel Paths, P	32	16	8, 16, 32
Number of Paths to Keep in Each Stage, M	8	4, 8, 16	8

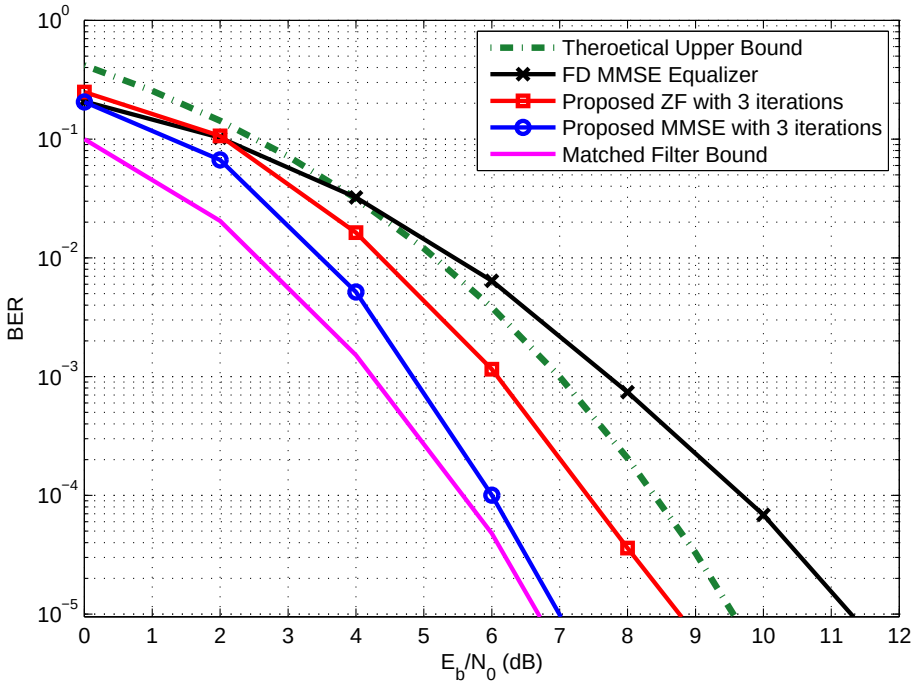

Figure 2.8: BER Performance Comparison for ZF QRD and MMSE QRD.

dependent Rayleigh fading paths and uniform power delay profile [18]. At the receiver, we assume prefect knowledge of the channel and the signals are synchronized in time and frequency at the receiver. For statistical accuracy, we make sure that at least 10000 transmission blocks are simulated and there is at least 50 received blocks with decoding errors. The simulation system configuration is summarized in Table 2.1. In Table 2.2, the simulation system configurations for Section 2.6.2 to Section 2.6.4 are summarized for easy reference.

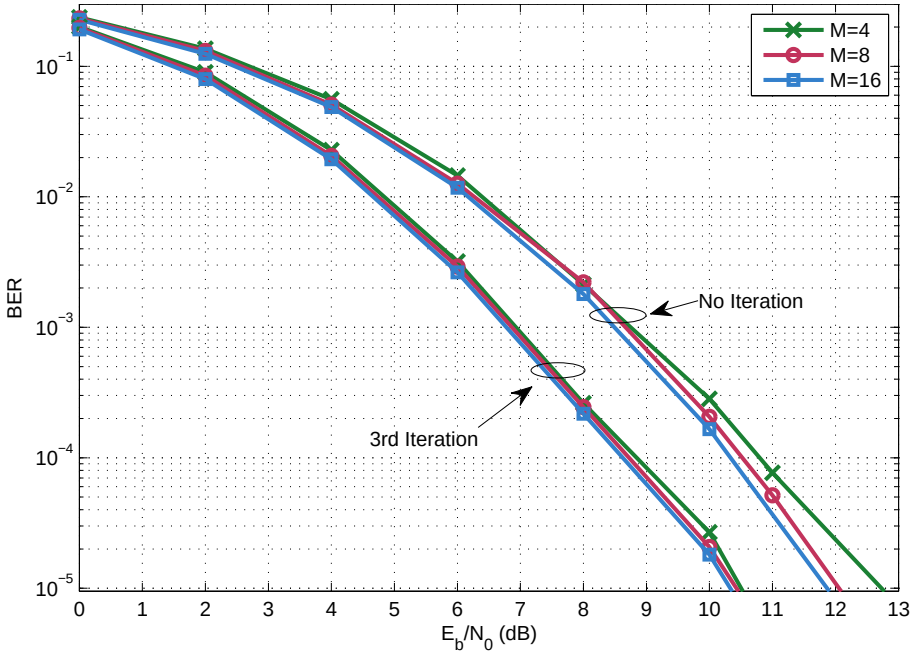

Figure 2.9: BER Performance Comparison for Varying M.

2.6.2 ZF versus MMSE QR Decomposition

In Figure 2.8, we compare the performance between using zero forcing (ZF) QRD 2.51 and LMMSE QRD 2.54. We consider a system with 8 users each with $S = 32$ assigned sub-carriers. The hypothetical ideal MFLB [16] and the derived theoretical upper bound are also plotted for reference. We also compare the BER performance of the proposed algorithm with that of MMSE FDE. The number of channel paths P is set to 32 in Figure 2.8. From Figure 2.8, it is obvious that the proposed algorithm, especially when MMSE QRD is used, outperforms MMSE FDE greatly with a performance gain of over 4 dB at BER = 10^{-5}. Moreover, the proposed algorithm using MMSE QRD approaches the MFB at high SNR with less than 0.5 dB performance gap at BER = 10^{-5}. Comparing the slope of the BER performance, we see that the proposed algorithm can achieve the same maximum channel diversity order as the theoretical MLSE upper bound unlike the MMSE FDE, whose diversity order is limited [19] as evident by the curve intercepting the MLSE upper bound. Since MMSE QRD outperforms the ZF QRD significantly, we will use MMSE QRD with the proposed algorithm for the rest of the simulations.

2.6.3 Effects of Varying Number of Paths to Keep in Each Stage

In Figure 2.9, we plot the simulated BER performance of a system using the proposed iterative QRD-M algorithm with $S = 32$, $P = 16$ for varying M, the number of paths to keep in each stage, from 4 to 16. For the case where no iteration is performed, the difference in performance is more pronounced. However, after 3 iterations, the performances are very close for the different M values. Thus using a small M would be enough to guarantee good performance which lowers the implementation complexity requirement. This is especially true when iterative detection and decoding is used as shown in Figure 2.9. Since there is minimal performance improvement when M is increased from 8 to 16 regardless of the employment of iterative detection and decoding, we will set $M = 8$ for the rest of the simulations.

2.6.4 Varying Number of Channel Paths

We consider a system with $S = 32$ and simulate the BER performances of the system under varying number of channel paths, P. From the performance curves in Figure 2.10 to Figure 2.12, we can see that the BER performance curves of the proposed algorithm are a parallel shift of the upper bound curve for all instances of P. Thus, the proposed algorithm tracks the increase in the channel diversity unlike the MMSE FDE whose performance curve shows a saturation of the diversity order as P increases.

From Figure 2.10 to Figure 2.12, we can also see that regardless of the value of P, the greatest performance gain occurs at the first iteration with subsequent iterations offering little or negligible gain. Thus a very small number of iterations is required for the system to realize the full performance gain the proposed algorithm can offer. Also, the nominal performance gain over MMSE FDE increases with increasing value of P, rising from 3.5 dB for $P = 8$ to 4.2 dB for

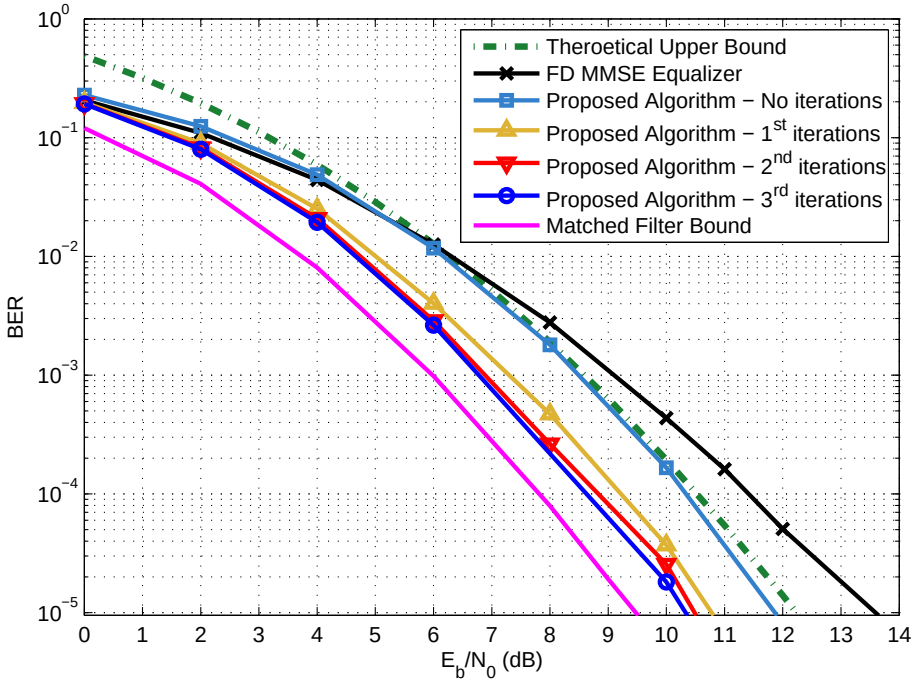

Figure 2.10: BER Performance for $P = 8$.

$P = 32$ at BER = 10^{-5}.

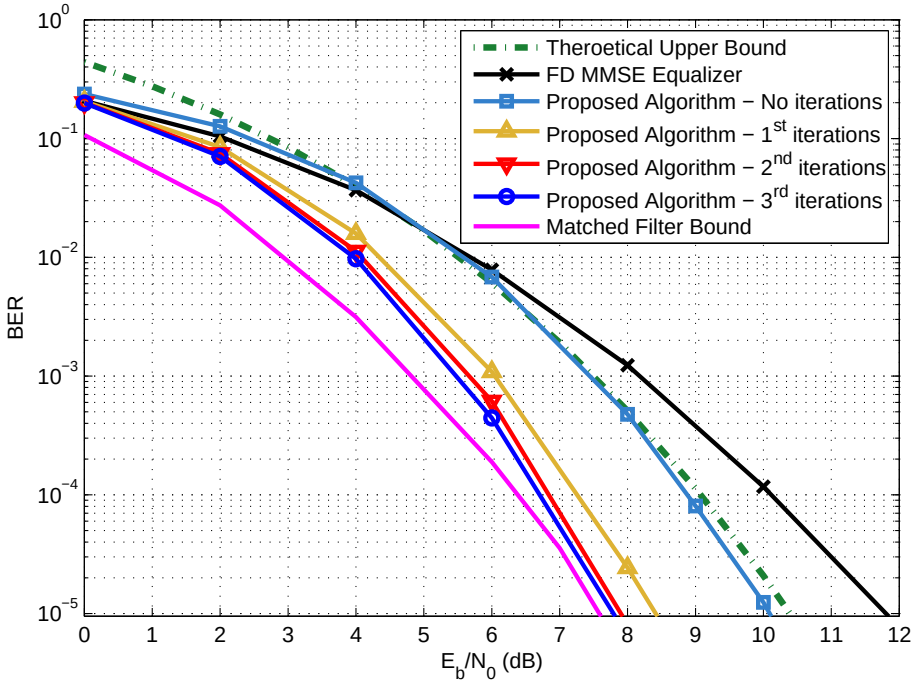

Figure 2.11: BER Performance for $P = 16$.

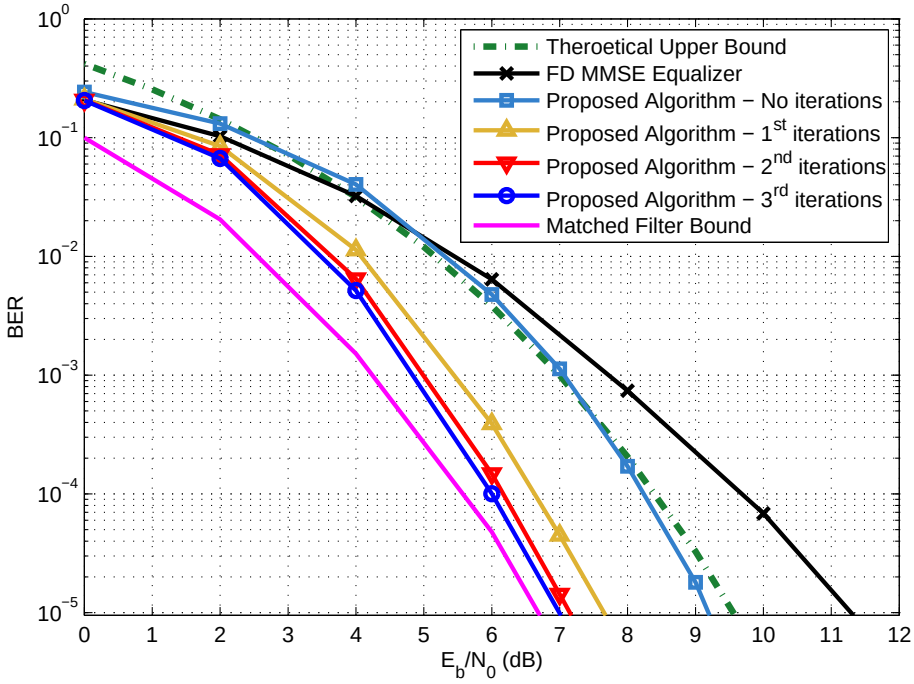

Figure 2.12: BER Performance for $P = 32$.

2.6.5 Multiple Receive Antennas System

Next, we investigate the case where the base-station are equipped with multiple receive antennas while mobile devices have only a single transmit antenna. We set $A_R = 2$, $S = 32$ and $P = 16$. We assume the channels of the different receive antennas are uncorrelated. The corresponding BER performance is shown in Figure 2.13. The most striking result in Figure 2.13 is the performance of MMSE FDE. Compared to the MMSE FDE performance in Figure 2.11, which has the same value of $P = 16$, there is an obvious increase in the diversity order as the receiver antennas are processed independently. Nevertheless, the maximum channel diversity order is only achieved by the proposed algorithm and the performance gain over MMSE FDE is still in excess of 3 dB at BER = 10^{-5} after performing three decoding iterations.

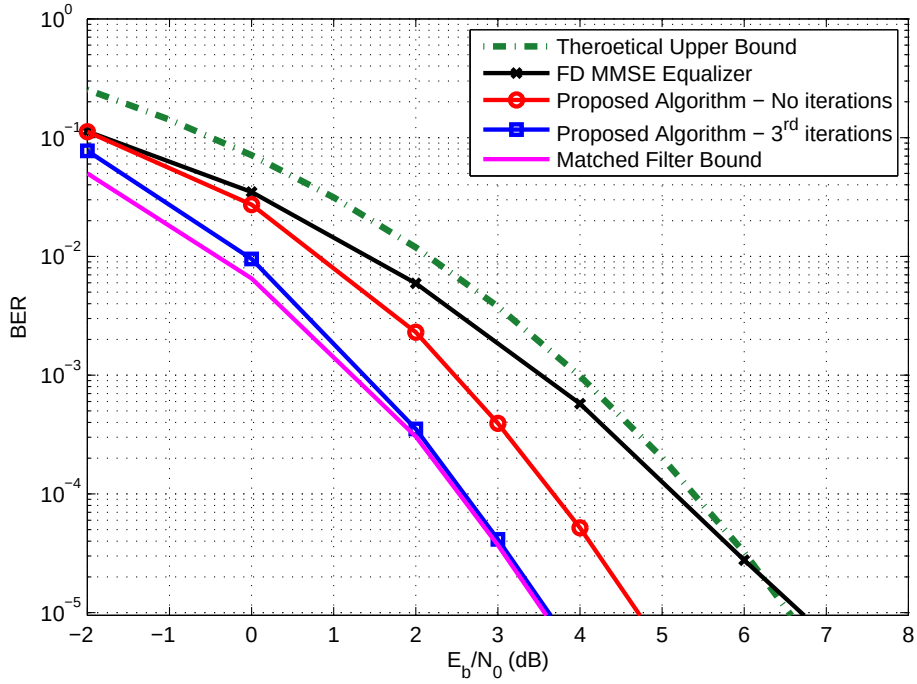

Figure 2.13: BER Performance Comparison for $A_T = 1, A_R = 2, P = 16$.

2.6.6 Spatial Multiplexing System with Multiple Transmit and Receive Antennas

We simulate the performance of the proposed algorithm in a two-transmit, two-receive antennas (i.e. $A_T = A_R = 2$) with S set at 16 and P set at 8. The channels of the different transmit and receive antennas are assumed to be uncorrelated. The BER performance is shown in Figure 2.14. Note that a linear MMSE equalizer is used in place of the MMSE FDE for the case of two transmit antennas. From Figure 2.14, we can see the greatest performance gain of the proposed algorithm over linear MMSE equalization. The performance gain at BER = 10^{-5} after three iterations is almost 6 dB and the performance of the proposed algorithm is only 0.25 dB worse than the MFB at the same BER.

We collate the simulation results of the proposed algorithm from the different numerical configurations of transmit and receive antennas from Figure 2.12, Figure 2.13 and Figure 2.14 that has the same data rate and total diversity order into Figure 2.15. For the sake of clarity, we only show the BER performance after three iterations. From Figure 2.15, we observe that the BER graphs are

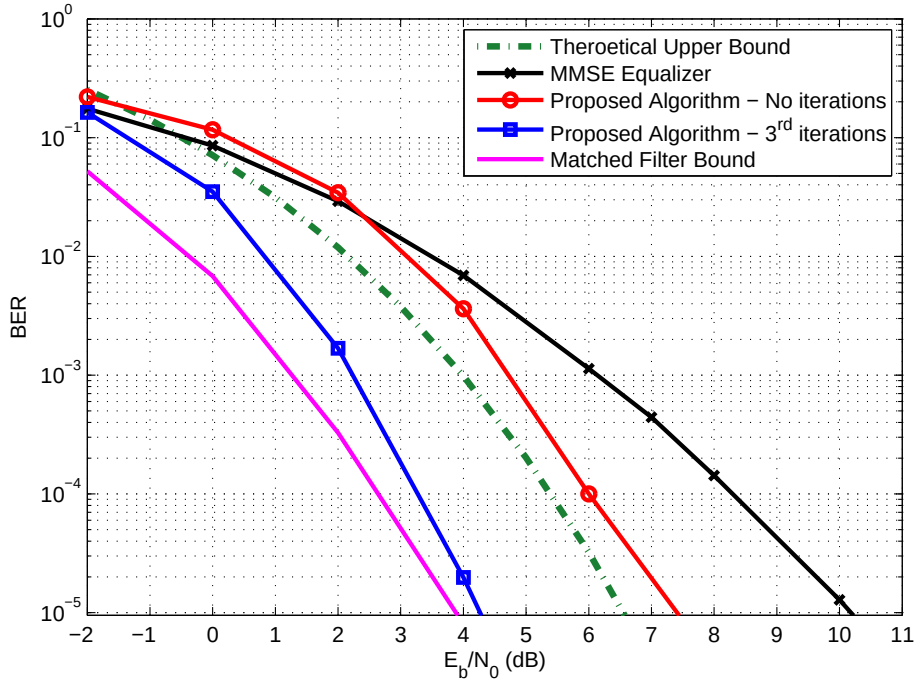

Figure 2.14: BER Performance Comparison for $A_T = 2, A_R = 2, P = 8$.

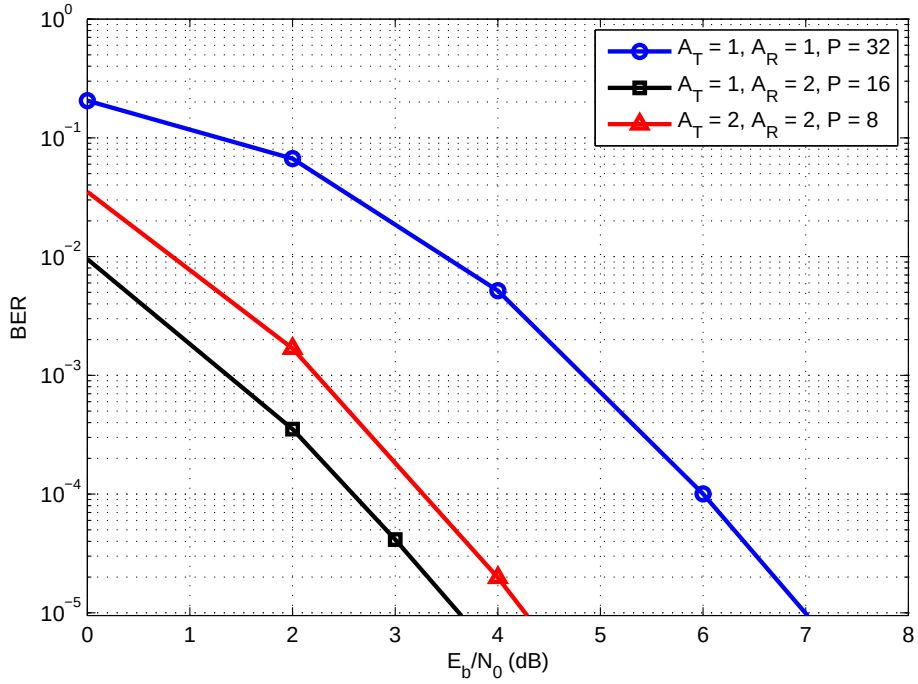

Figure 2.15: BER Performance with Total Diversity Order = 32.

simply parallel-shifted versions of each other. The two receive antennas accounting for the array gain of 3 dB over single receive antenna. This shows that the proposed algorithm performs equally well regardless of the number of antennas at the transmitter.

Table 2.3: Simulation System Configurations for FH-IFDMA and BS-IFDMA System.

System Parameters	FH-IFDMA	BS-IFDMA
Type of QR Decomposition	MMSE QRD	
Number of Users	32	
Block Spreading Factor, B	-	2, 4, 8
Number of Sub-carriers per User, S	8	16, 32, 64
Number of Channel Path, P	16	
Number of Paths to Keep in Each Stage, M	8	

2.6.7 Maximizing Diversity Performance with Frequency Hopping and Block Spreading

We investigate the ability of frequency hopping and block spreading to preserve the maximum diversity order for $S < P$. The simulation system configurations are summarized in Table 2.3. We simulate the performance for $S = 8$ using the hopping sequence design in Section 2.4.1. We also simulate the performance of a BS-IFDMA system with $B = 2$, which is the smallest B that meets the requirement in Section 2.4.2. In Figure 2.16 we compare the BER performances between the three systems: IFDMA, FH-IFDMA and BS-IFDMA using proposed detection and decoding scheme after three iterations for $P = 16$. The theoretical upper bound and the ideal matched filter lower bound for BS-IFDMA/FH-IFDMA is also plotted for reference. As observed from Figure 2.16, both FH-IFDMA and BS-IFDMA perform equally well in maintaining the maximum diversity order of 16 while IFDMA system is unable to do so.

We know from [19] that the diversity order for MMSE FDE is dependent on the relative ratio between the number of diversity paths and the number of transmitted symbols per block. Since FDE is a very simple detection technique, it is advantageous to implement that in cases where performance can be sacrificed to lower complexity. In Figure 2.17, we once again compare the performance of IFDMA, FH-IFDMA and BS-IFDMA. However, in Figure 2.17, MMSE FDE is used in place of proposed iterative decoder. We plot the performance for different B to illustrate the possible diversity gain from increasing B. From Figure 2.17, we see that BS-IFDMA performs better than IFDMA and FH-IFDMA

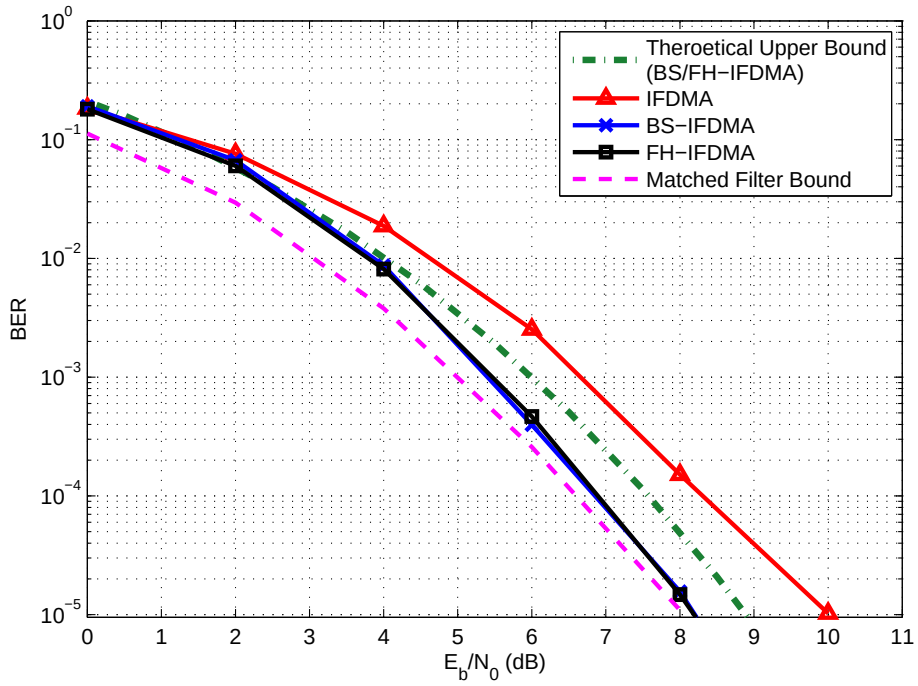

Figure 2.16: Performance Comparison between IFDMA, FH-IFDMA, BS-IFDMA Systems.

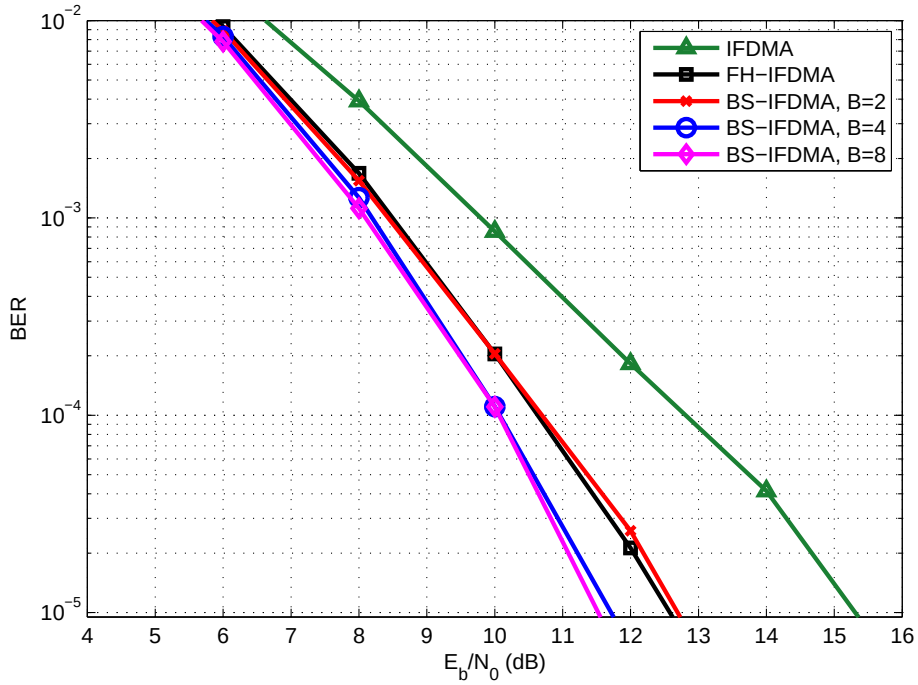

Figure 2.17: FDE Performance Comparison between IFDMA, FH-IFDMA, BS-IFDMA Systems.

when $B > 2$. However, the gain is not significant, with the E_b/N_0 gain saturating at only about 1 dB with increased B. The result does show that with MMSE FDE, BS-IFDMA is the better alternative for increasing the diversity order.

2.7 Chapter Summary

In this chapter, the signal model of a coded MIMO-IFDMA system is formulated in the time domain using matrix form that typifies the signal model of conventional multiple input and multiple output communications. Using this formulation, the coded MIMO-IFDMA system can be viewed as a system with a complex-field code serially concentrated with an outer error-correcting code. Thus, the principles of iterative turbo decoding can be applied to the decoding of coded MIMO-IFDMA system. An iterative detection and decoding algorithm is proposed which incorporates a low-complexity soft decision QRD-M detector in place of the APP detector. Since the proposed algorithm has a generalized form, a common shared hardware platform can be used to enable real-time switching between operation for single transmit antennas and multiple transmit antennas. Simulation results show that the proposed iterative algorithm is able to improves the BER performance significantly in a small number of iterations. Moreover, the iterative algorithm has been shown to be particularly useful in improving the BER performance of the system with larger channel diversity order. The simulated performance also has been shown to match the matched filter lower bound performance at high SNR.

We conduct a performance analysis on the BER performance of IFDMA system using the time domain model, establishing the link between the theoretical performance with the distribution of the channel profile. We also show that it is possible to achieve the maximum channel diversity order either through the use of frequency hopping or block spreading. Frequency hopping is simpler to implementat than block spreading but block spreading has the additional benefit of lower inter-cell interferences and can achieve better performance with the simple FDE.

Chapter 3

Transmit Diversity Technique for IFDMA System

3.1 Introduction

Transmit diversity has became an important MIMO technique for cellular wireless communication system to increase diversity, improve BER performance and boost system coverage [54]. Various transmit diversity schemes have been proposed for SC-FDMA in 3GPP LTE-A [55] including the famous Alamouti coding [56] inspired space time block code (STBC) and space frequency block code (SFBC) [55,57], cyclic delay diversity (CDD) [58] and frequency switched transmit diversity (FSTD) [59].

STBC is the straightforward approach for applying Alamouti coding. Pairs of IFDMA symbols are precoded and sent through two antennas over two successive time intervals. As Alamouti precoding only involves complex conjugation and/or sign changes, the low PAPR feature of IFDMA will not be affected and the signals sent through the different transmit antennas remain as single-carrier signals. However, since the precoding is applied to pairs of IFDMA symbols, there is a constraint on the number of IFDMA symbols transmitted to be even [57]. SFBC is an alternative way to apply Alamouti coding to the IFDMA system to remove the constraint on the number of IFDMA symbols transmitted. Instead of precoding a pair of IFDMA symbols, the Alamouti precoding is applied to a pair of adjacent sub-carriers within a single IFDMA symbol.

The precoding of the sub-carriers changes the frequency structure of the signal and breaks the single-carrier property of the signal, losing the advantage of low PAPR. Unique mapping of the pairs of sub-carriers for the precoding that preserves the single-carrier property has been suggested in [55, 57] for SC-FDMA system using localized distribution of sub-carriers. The assumption required for the application of the unique mapping is that the channel variation between the pair of sub-carriers are minimal or within tolerable limit. This assumption, which is strained even for SC-FDMA system in a frequency-selective channel, is unlikely to hold for IFDMA system as the distance between adjacent sub-carriers are even further. Moreover, STBC and SFBC do not scale well with the increase of transmit antennas as the Hurwitz-Radon theorem shows that the extension of Alamouti codes to more than two antennas with full-diversity and full-rate for the general modulation constellations are not possible [60].

On the other hand, FSTD can be easily scaled for different number of transmit antennas. In FSTD scheme, the transmission of IFDMA symbols are switched between multiple transmit antennas for the duration of a coded data block. Since at any one time only a single transmit antenna is used, the adaption of the scheme to different numerical configurations of transmit antennas are straightforward. However, to make full use of the transmit diversity when the number of transmit antennas increases, the FSTD scheme require a correspondingly large coded data block. Thus the number of transmit antennas that can be used are limited by the number of IFDMA symbols belonging to a single coded data block.

Like the FSTD scheme, the CDD scheme can be easily scaled to different number of transmit antennas. For the CDD scheme using two transmit antennas, the original signal is send on one of the transmit antennas, and a cyclically shifted version of the original signal is sent on the other. When the number of transmit antennas increases, the original signal is simply cyclically-shifted by different delays for each of the transmit antennas [58]. As cyclic delay preserves the single-carrier property, the CDD scheme safeguards the low PAPR property

of IFDMA. At the receiver, the cyclic delayed copies are received as additional multipaths [57]. Moreover, since the CDD scheme applies to individual IFDMA symbol like SFBC, there are no constraints on the number of IFDMA symbols transmitted unlike in FSTD and STBC.

The CDD scheme is flexible in implementation when compared to STBC, SFBC and FSTD but the diversity gain of the CDD scheme are easily limited. In this chapter, we introduce a novel transmit diversity technique for coded IFDMA systems. Like the CDD scheme, the proposed diversity scheme applies to individual IFDMA symbol and preserves low PAPR property of IFDMA. We derive the new transmit diversity scheme named antenna spreading diversity (ASD) from the signal model in Section 2.2.2 using the criteria required for coded MIMO-IFDMA systems to achieve the maximum channel diversity order. We start by introducing the scheme and illustrating the basis for its diversity gain. Then we compare the new scheme with the CDD scheme [58] in terms of their diversity performance. Using the signal model in Section 3.2, we derive the maximum diversity gain for both the ASD and the CDD schemes and show the limitation on the diversity gain of the CDD scheme when compared to the proposed ASD scheme.

The rest of the chapter is organized as follows: In Section 3.2, we modified the signal model in Section 2.2.2 to represent the CDD scheme and the proposed ASD scheme. In Section 3.3, we derive the theoretical performance of the CDD scheme and the proposed ASD scheme and compare their diversity gain. We follow the theoretical analysis with simulation results which are given in Section 3.4 to demonstrate the superiority of the proposed ASD scheme. Then, in Section 3.5, we summarize our observations and contributions.

3.2 System Signal Model

3.2.1 Cyclic Delay Diversity

We consider the case of a single receive antenna system but the extension to multiple receive antennas is straightforward. In cyclic delay diversity (CDD) scheme, the data transmitted from the different transmit antennas are cyclic-shifted version of each other. For example, we consider a two-antenna transmitter employing CDD scheme. The data vector transmitted from the first antenna is written as per (2.1) as:

$$\mathbf{x}_0 = \begin{bmatrix} x_{k,0} & x_{k,1} & \dots & x_{k,S-1} \end{bmatrix}^T \tag{3.1}$$

The transmitted data vector from the second antenna is cyclic-shifted by τ symbols as:

$$\mathbf{x}_1 = \begin{bmatrix} x_{k,S-\tau} & x_{k,S-\tau+1} & \dots & x_{k,S-\tau-1} \end{bmatrix}^T \tag{3.2}$$

Thus, for a system with A_T transmit antennas employing the CDD scheme, the data vector for the a_T^{th} antenna are cyclicly-shifted by $\tau_{a_T}, a_T = 0, \dots, A_T$. Hence, in general, the transmitted data vector from the a_T^{th} antenna is written as:

$$\mathbf{x}_{a_T} = \begin{bmatrix} x_{k,(S-\tau_{a_T})\text{mod}S} & x_{k,(S-\tau_{a_T}+1)\text{mod}S} & \dots & x_{k,(S-\tau_{a_T}-1)\text{mod}S} \end{bmatrix}^T \tag{3.3}$$

Without the loss in generality, we assume that $\tau_0 = 0$ for convention. Recall from (2.25) that the received signal of a particular user at a particular receiver antenna can be written as:

$$\mathbf{r} = \sum_{a_T=0}^{A_T-1} \mathbf{h}_{a_T} \mathbf{x}_{a_T} + \boldsymbol{\eta}' \tag{3.4}$$

For the CDD scheme, the different $\mathbf{x}_{a_T}$ are basically cyclic shifted versions

of each other. Therefore, we can rewrite (3.4) as:

$$\mathbf{r} = \left(\sum_{a_T=0}^{A_T-1} \tilde{\mathbf{h}}_{a_T} \right) \mathbf{x}_0 + \boldsymbol{\eta}' \tag{3.5}$$

where $\tilde{\mathbf{h}}_0 = \mathbf{h}_0$ and $\tilde{\mathbf{h}}_{a_T}$ is column-wise cyclic shifts of $\mathbf{h}_{a_T}$ for $a_T = 1, \ldots, A_T - 1$. Since all $\mathbf{h}_{a_T}$ are circulant matrices, all $\tilde{\mathbf{h}}_{a_T}$ remain as circulant matrices after the cyclic shifts. Therefore, $\sum_{a_T=0}^{A_T-1} \tilde{\mathbf{h}}_{a_T}$ is also a circulant matrix. The CDD scheme works by increasing the number of independent random variables in each column of $\sum_{a_T=0}^{A_T-1} \tilde{\mathbf{h}}_{a_T}$ through appropriate column-wise cyclic shifts of different $\mathbf{h}_{a_T}$. Thus the maximum number of independent random variables is limited to S. In other words, the diversity gain factor from CDD scheme is capped at $\frac{S}{P}$ regardless of the number of transmit antennas available. For example, consider the case where $S = 4$, $P = 2$, $A_T = 2$ and a cyclic shift of 2 is applied to the second transmit antenna relative to the first transmit antenna. Thus,

$$\mathbf{r} = \mathbf{h}_0 \begin{bmatrix} x_0 \\ x_1 \\ x_2 \\ x_3 \end{bmatrix} + \mathbf{h}_1 \begin{bmatrix} x_2 \\ x_3 \\ x_0 \\ x_1 \end{bmatrix} + \boldsymbol{\eta}$$

where

$$\mathbf{h}_0 = \begin{bmatrix} h_{0,0} & 0 & 0 & h_{0,1} \\ h_{0,1} & h_{0,0} & 0 & 0 \\ 0 & h_{0,1} & h_{0,0} & 0 \\ 0 & 0 & h_{0,1} & h_{0,0} \end{bmatrix} \quad \mathbf{h}_1 = \begin{bmatrix} h_{1,0} & 0 & 0 & h_{1,1} \\ h_{1,1} & h_{1,0} & 0 & 0 \\ 0 & h_{1,1} & h_{1,0} & 0 \\ 0 & 0 & h_{1,1} & h_{1,0} \end{bmatrix}$$

and

$$\tilde{\mathbf{h}}_0 = \begin{bmatrix} h_{0,0} & 0 & 0 & h_{0,1} \\ h_{0,1} & h_{0,0} & 0 & 0 \\ 0 & h_{0,1} & h_{0,0} & 0 \\ 0 & 0 & h_{0,1} & h_{0,0} \end{bmatrix} \quad \tilde{\mathbf{h}}_1 = \begin{bmatrix} 0 & h_{1,1} & h_{1,0} & 0 \\ 0 & 0 & h_{1,1} & h_{1,0} \\ h_{1,0} & 0 & 0 & h_{1,1} \\ h_{1,1} & h_{1,0} & 0 & 0 \end{bmatrix}$$

which finally give us:

$$\mathbf{r} = \begin{bmatrix} h_{0,0} & h_{1,1} & h_{1,0} & h_{0,1} \\ h_{0,1} & h_{0,0} & h_{1,1} & h_{1,0} \\ h_{1,0} & h_{0,1} & h_{0,0} & h_{1,1} \\ h_{1,1} & h_{1,0} & h_{0,1} & h_{0,0} \end{bmatrix} \begin{bmatrix} x_0 \\ x_1 \\ x_2 \\ x_3 \end{bmatrix} + \boldsymbol{\eta} \tag{3.6}$$

From (3.6), we see that even if we increase the number of transmit antennas, A_T to more than 2, the number of independent random variables will not change and will be limited to $S = 4$. Moreover, for cases where $P \geq S$, the CDD scheme would not be beneficial at all.

3.2.2 Antenna Spreading Diversity

From Section 2.3.3, we know that the diversity performance is dependent on the number of independent random variables in the $S \times S$ matrix, $\left(\sum_{a_T=0}^{A_T-1} \tilde{\mathbf{h}}_{a_T}\right)$. Hence, the aim is to maximize the number of independent random variables through manipulating the transformation on the different $\mathbf{h}_{a_T}$.

We propose a transmit diversity scheme that is simple to implement at the transmitter for $A_T = 2^q$ transmit antennas, q being a positive integer. We assume that $S \geq A_T$, which holds true for most circumstances. The S symbols are divided into groups of A_T with the remaining symbols grouped together if S is not divisible by A_T. Each symbol in the group is spread across the A_T transmit antennas using a different bipodal spreading code from an orthogonal

spreading code set of size A_T such as the Walsh-Hadamard code. The process is repeated for the different groups of A_T symbols. Since the spreading codes are orthogonal, the corresponding A_T columns of $\sum_{a_T=0}^{A_T-1} \tilde{\mathbf{h}}_{a_T}$ consist of independent random variables as opposed to being merely cyclic shifts of each other. Note that symbols in different groups using the same spreading code will still have columns in $\sum_{a_T=0}^{A_T-1} \tilde{\mathbf{h}}_{a_T}$ that are cyclic shifts of each other.

As a simple illustrative example, we consider the case where $S = 2$, $A_T = 2$ and $A_R = 1$. Hence,

$$\mathbf{h}_0 = \begin{bmatrix} h_{0,0} & h_{0,1} \\ h_{0,1} & h_{0,0} \end{bmatrix} \tag{3.7a}$$

$$\mathbf{h}_1 = \begin{bmatrix} h_{1,0} & h_{1,1} \\ h_{1,1} & h_{1,0} \end{bmatrix} \tag{3.7b}$$

Using the antenna spreading diversity scheme, $\mathbf{h}_0$ is unchanged while the transformed matrix of $\mathbf{h}_1$ is given as:

$$\tilde{\mathbf{h}}_1 = \begin{bmatrix} h_{1,0} & -h_{1,1} \\ h_{1,1} & -h_{1,0} \end{bmatrix} \tag{3.8}$$

Therefore,

$$\begin{aligned} \sum_{a_T=0}^{1} \tilde{\mathbf{h}}_{a_T} &= \begin{bmatrix} h_{0,0} + h_{1,0} & h_{0,1} - h_{1,1} \\ h_{0,1} + h_{1,0} & h_{0,0} - h_{1,0} \end{bmatrix} \\ &= \begin{bmatrix} \tilde{h}_0 & \tilde{h}_2 \\ \tilde{h}_1 & \tilde{h}_3 \end{bmatrix} \end{aligned} \tag{3.9}$$

Assuming that the channels of the two transmit antennas are uncorrelated and $\mathrm{E}\left[h_{0,p}^2\right] = \mathrm{E}\left[h_{1,p}^2\right]$ (i.e. similar channel delay profile for both antennas), $\tilde{h}_i$, $i = 0, 1, 2, 3$, are independent random variables. Since the number of independent random variables is increased by a factor of A_T, the diversity order is also increased by a factor of A_T using the proposed ASD scheme. More importantly,

we can maximize the diversity order by simply having $A_T = S$ antennas as symbols in different groups using the same spreading code will result in cyclic-shifted columns. This may not be practically feasible due to the implementation constraints on the number of antennas at the transmitter especially if S is large. On the other hand, this suggests that the diversity gain of the proposed ASD scheme will unlikely be constrained in practical implementations. Compared to the CDD scheme which has a diversity gain cap of $\frac{S}{P}$, the proposed ASD scheme has a cap of S.

3.2.3 Combining Cyclic Delay Diversity and Antenna Spreading Diversity

From the above discussion, we see that the proposed ASD scheme and the CDD scheme are actually complements of each other. The CDD scheme increases the number of independent random variables in the columns in the combined channel matrix, $\sum_{a_T=0}^{A_T-1} \tilde{\mathbf{h}}_{a_T}$. In contrast, the proposed ASD scheme increases the number of independent columns in the combined channel matrix but not the actual number of independent random variables in a column. Therefore, it is obvious that both scheme can be combined together in various configurations to suit the requirements of practical systems. The CDD scheme is used to maximize the number of independent random variables in a column while the proposed ASD scheme is used on the groups of antennas with the same cyclic shifts to increase the number of independent columns.

For example, consider a transmitter with $A_T = 8$ transmit antennas with $S = 4$ and $P = 2$. The antennas are divided into two groups of four each. Antennas in group one are assigned zero cyclic shift while antennas in group two are assigned cyclic shift of 2. Antenna spreading diversity scheme with spreading factor 4 is applied to the two group individually using the same code set.

The transformed matrices $\tilde{\mathbf{h}}_{a_T}$ are given as:

$$\tilde{\mathbf{h}}_0 = \begin{bmatrix} h_{0,0} & 0 & 0 & h_{0,1} \\ h_{0,1} & h_{0,0} & 0 & 0 \\ 0 & h_{0,1} & h_{0,0} & 0 \\ 0 & 0 & h_{0,1} & h_{0,0} \end{bmatrix} \quad \tilde{\mathbf{h}}_1 = \begin{bmatrix} h_{1,0} & 0 & 0 & -h_{1,1} \\ h_{1,1} & -h_{1,0} & 0 & 0 \\ 0 & -h_{1,1} & h_{1,0} & 0 \\ 0 & 0 & h_{1,1} & -h_{1,0} \end{bmatrix}$$

$$\tilde{\mathbf{h}}_2 = \begin{bmatrix} h_{2,0} & 0 & 0 & -h_{2,1} \\ h_{2,1} & h_{2,0} & 0 & 0 \\ 0 & h_{2,1} & -h_{2,0} & 0 \\ 0 & 0 & -h_{2,1} & -h_{2,0} \end{bmatrix} \quad \tilde{\mathbf{h}}_3 = \begin{bmatrix} h_{3,0} & 0 & 0 & h_{3,1} \\ h_{3,1} & -h_{3,0} & 0 & 0 \\ 0 & -h_{3,1} & -h_{3,0} & 0 \\ 0 & 0 & -h_{3,1} & h_{3,0} \end{bmatrix} \tag{3.10}$$

$$\tilde{\mathbf{h}}_4 = \begin{bmatrix} 0 & h_{4,1} & h_{4,0} & 0 \\ 0 & 0 & h_{4,1} & h_{4,0} \\ h_{4,0} & 0 & 0 & h_{4,1} \\ h_{4,1} & h_{4,0} & 0 & 0 \end{bmatrix} \quad \tilde{\mathbf{h}}_5 = \begin{bmatrix} 0 & -h_{5,1} & h_{5,0} & 0 \\ 0 & 0 & h_{5,1} & -h_{5,0} \\ h_{5,0} & 0 & 0 & -h_{5,1} \\ h_{5,1} & -h_{5,0} & 0 & 0 \end{bmatrix}$$

$$\tilde{\mathbf{h}}_6 = \begin{bmatrix} 0 & h_{6,1} & -h_{6,0} & 0 \\ 0 & 0 & -h_{6,1} & -h_{6,0} \\ h_{6,0} & 0 & 0 & -h_{6,1} \\ h_{6,1} & h_{6,0} & 0 & 0 \end{bmatrix} \quad \tilde{\mathbf{h}}_7 = \begin{bmatrix} 0 & -h_{7,1} & -h_{7,0} & 0 \\ 0 & 0 & -h_{7,1} & h_{7,0} \\ h_{7,0} & 0 & 0 & h_{7,1} \\ h_{7,1} & -h_{7,0} & 0 & 0 \end{bmatrix}$$

Therefore,

$$\sum_{a_T=0}^{A_T-1} \tilde{\mathbf{h}}_{a_T} = \begin{bmatrix} \tilde{h}_{0,0} & \tilde{h}_{1,3} & \tilde{h}_{2,2} & \tilde{h}_{3,1} \\ \tilde{h}_{0,1} & \tilde{h}_{1,0} & \tilde{h}_{2,3} & \tilde{h}_{3,2} \\ \tilde{h}_{0,2} & \tilde{h}_{1,1} & \tilde{h}_{2,0} & \tilde{h}_{3,3} \\ \tilde{h}_{0,3} & \tilde{h}_{1,2} & \tilde{h}_{2,1} & \tilde{h}_{3,0} \end{bmatrix} \tag{3.11}$$

where

$$\tilde{h}_{0,0} = h_{0,0} + h_{1,0} + h_{2,0} + h_{3,0} \tag{3.12a}$$

$$\tilde{h}_{0,1} = h_{0,1} + h_{1,1} + h_{2,1} + h_{3,1} \tag{3.12b}$$

$$\tilde{h}_{0,2} = h_{4,0} + h_{5,0} + h_{6,0} + h_{7,0} \tag{3.12c}$$

$$\tilde{h}_{0,3} = h_{4,1} + h_{5,1} + h_{6,1} + h_{7,1} \tag{3.12d}$$

$$\tilde{h}_{1,0} = h_{0,0} - h_{1,0} + h_{2,0} - h_{3,0} \tag{3.12e}$$

$$\tilde{h}_{1,1} = h_{0,1} - h_{1,1} + h_{2,1} - h_{3,1} \tag{3.12f}$$

$$\tilde{h}_{1,2} = h_{4,0} - h_{5,0} + h_{6,0} - h_{7,0} \tag{3.12g}$$

$$\tilde{h}_{1,3} = h_{4,1} - h_{5,1} + h_{6,1} - h_{7,1} \tag{3.12h}$$

$$\tilde{h}_{2,0} = h_{0,0} + h_{1,0} - h_{2,0} - h_{3,0} \tag{3.12i}$$

$$\tilde{h}_{2,1} = h_{0,1} + h_{1,1} - h_{2,1} - h_{3,1} \tag{3.12j}$$

$$\tilde{h}_{2,2} = h_{4,0} + h_{5,0} - h_{6,0} - h_{7,0} \tag{3.12k}$$

$$\tilde{h}_{2,3} = h_{4,1} + h_{5,1} - h_{6,1} - h_{7,1} \tag{3.12l}$$

$$\tilde{h}_{3,0} = h_{0,0} - h_{1,0} - h_{2,0} + h_{3,0} \tag{3.12m}$$

$$\tilde{h}_{3,1} = h_{0,1} - h_{1,1} - h_{2,1} + h_{3,1} \tag{3.12n}$$

$$\tilde{h}_{3,2} = h_{4,0} - h_{5,0} - h_{6,0} + h_{7,0} \tag{3.12o}$$

$$\tilde{h}_{3,3} = h_{4,1} - h_{5,1} - h_{6,1} + h_{7,1} \tag{3.12p}$$

If the channels of the two transmit antennas are uncorrelated with $h_{i,j}$, $i = 0, \ldots, 7$, $j = 0, 1$ being independent random variables, $\tilde{h}_{i,j}$ $i = 0, \ldots, 3$, $j = 0, \ldots, 3$ are independent random variables. As can be seen from (3.11), the number of independent random variables in each column of the combined channel matrix is four and all the columns are independent. Hence the total number of independent random variables in the combined channel matrix is sixteen. If cyclic delay diversity scheme is used only, the maximum number of independent random variables will only be four. On the other hand, if antenna spreading diversity scheme is used only, the maximum number of independent random variables will only be eight. Thus, in general, the combination of both schemes

brought about greater diversity gain than either scheme could have on its own provided that $S > P$.

3.3 Theoretical Performance Analysis

In this section, we derive the theoretical MLSE upper bound for the CDD scheme and the proposed ASD scheme to compare the diversity order between the two schemes. Following the derivations in Section 2.3, we first need to determine the distribution of the summation of the random variables in the channel matrix for the CDD scheme and the proposed ASD scheme.

For the case of the CDD scheme, the resulting channel matrix in (3.5) is similar to the single antenna case in Section 2.3 in that both channel matrices are $S \times S$ circulant matrices. The main differences lies in the variance of the independent circularly symmetric complex Gaussian random variables in the channel matrix. If we denote the variance of the random variables in the channel matrix, $\mathbf{h}_{a_T}$, which represents the channel of the a^{th} transmit antenna, as $\sigma^2_{a_T,p}, a_T = 0, \ldots, A_T - 1, p = 0, \ldots, S - 1$, where $\sigma^2_{a_T,p} = 0$ for $p \geq P$, the variance of the random variables in the channel matrix, $\sum_{a_T=0}^{A_T-1} \tilde{\mathbf{h}}_{a_T}$, is written as $\sigma^2_p, p = 0, \ldots, S - 1$ where

$$\sigma^2_p = \sum_{a_T=0}^{A_T-1} \sigma^2_{a_T,(p-\tau_{a_T}) \bmod S} \tag{3.13}$$

For the case of channel with uniform power delay profile and $\tau_{a_T} = a_T \cdot P$, $\sigma_p = \frac{1}{A_T P}, p = 0, \ldots, P_C$, where $P_C = \min(S, A_T P)$ and $\sigma_p = 0$ otherwise. Following the derivations in (2.39), the average pairwise error probability is upper bounded by:

$$P_E(d) \leq \frac{1}{2\sqrt{\varepsilon_A}} \binom{2P_A}{P_A} \left(\frac{1 - \varepsilon_A}{4}\right)^{P_A} \tag{3.14}$$

where P_A and ε_A are $A_R P_C$ and $\frac{\delta^2 d}{\delta^2 d + 4P_C N_0}$ respectively. Thus, the upper bound on the BER is rewritten from (2.42) to be:

$$BER \leq \frac{1}{2} \sum_{d=d_{free}}^{\infty} \sum_{i=1}^{L} \frac{i \cdot c_{i,d}}{4^{P_A} L \sqrt{\varepsilon_A}} \binom{2P_A}{P_A} \left(1 + \frac{\delta^2 d}{4P_C N_0}\right)^{-P_A} \tag{3.15}$$

For the case of the proposed ASD scheme, the resulting channel matrix, $\left(\sum_{a_T=0}^{A_T-1} \tilde{\mathbf{h}}_{a_T}\right)$, has A_T columns of independently distributed random variables. If we assume that the error symbol pair in (2.30) is distributed evenly across the symbols within one IFDMA symbol block, we can write the lower bound on the Euclidean distance as $\delta \sqrt{\frac{d}{A_T} \sum_{a_T=0}^{A_T-1} \sum_{p=0}^{P-1} |h_{a_T,p}|^2}$, where $h_{a_T,p}$ denotes the p^{th} entry in the a_T^{th} column in the resulting channel matrix, $\left(\sum_{a_T=0}^{A_T-1} \tilde{\mathbf{h}}_{a_T}\right)$. The variance of the random variables, $h_{a_T,p}$, is denoted as $\sigma^2_{a_T}(p)$ as opposed to $\sigma^2_{a_T,p}$, which represents the variance of the random variables in the channel matrix, $\mathbf{h}_{a_T}$. Given that $h_{a_T,p}$ is the combination of additions or subtractions of the different independent random variables in the channel matrix, $\mathbf{h}_{a_T}$, $\sigma^2_{a_T}(p)$ can be written as the summation of $\sigma^2_{a_T,p}$ as:

$$\sigma^2_{a_T}(p) = \sum_{a_T=0}^{A_T-1} \sigma^2_{a_T,p} \tag{3.16}$$

For the case of channel with uniform power delay profile, the upperbound of the average pairwise error probability for ASD scheme can be simplified accordingly to:

$$P_E(d) \leq \frac{1}{2\sqrt{\varepsilon_B}} \binom{2P_B}{P_B} \left(\frac{1 - \varepsilon_B}{4}\right)^{P_B} \tag{3.17}$$

where $P_B = A_R P D_m$ and $\varepsilon_B = \frac{\delta^2 d}{\delta^2 d + 4P D_m N_0}$ where $D_m = \min(S, A_T)$ and the upper bound on the BER is written as:

$$BER \leq \frac{1}{2} \sum_{d=d_{free}}^{\infty} \sum_{i=1}^{L} \frac{i \cdot c_{i,d}}{4^{P_B} L \sqrt{\varepsilon_B}} \binom{2P_B}{P_B} \left(1 + \frac{\delta^2 d}{4P_C N_0}\right)^{-P_B} \tag{3.18}$$

If the combined diversity scheme in Section 3.2.3 is used, where the total number of transmit antennas employed is $A_T = A_{TASD} \times A_{TCDD}$ with A_{TCDD} representing the number of cyclic shift groups and A_{TASD} representing the number of antenna spreading group, the BER upper bound is given by:

$$BER \leq \frac{1}{2} \sum_{d=d_{free}}^{\infty} \sum_{i=1}^{L} \frac{i \cdot c_{i,d}}{4^{P_2} L \sqrt{\varepsilon_2}} \binom{2P_2}{P_2} \left(1 + \frac{\delta^2 d}{4 P_C D_m N_0}\right)^{-P_2} \tag{3.19}$$

where $P_2 = A_R P'_C D'_m$ and $\varepsilon_2 = \frac{\delta^2 d}{\delta^2 d + 4 P'_C D'_m N_0}$ and $P'_C = \min(S, A_{TCDD} P)$ and $D'_m = \min(S, A_{TASD})$.

From the above discussion, we see that the maximum diversity order of CDD is limited by $A_R S$ while that of ASD is limited by $P A_R S$. In other words, the limit on the diversity order is tighter on the CDD scheme than the ASD scheme. Moreover, for $S > P$, the maximum diversity order of the combined diversity scheme at $A_R S^2$ is greater than that of CDD and ASD scheme.

In Figure 3.1, we compare the theoretical upperbound performance for channels with uniform power delay profile between a system using CDD and a system using ASD with $S = 16$, $P = 8$, $A_R = 1$ and A_T varying from 2 to 16. The theoretical upperbound of a single antenna system is also plotted for reference. Figure 3.1 clearly illustrates the saturation of the diversity gain from the CDD scheme at $S = 16$ regardless of the number of antennas employed while showing how the diversity gain from the ASD scheme is able to follow the increase in the number of transmit antennas employed.

In Figure 3.2, we compare the theoretical upperbound performance between systems using CDD, ASD and the combined diversity scheme. To better illustrate the diversity gain, we consider systems with $S = 8$, $P = 4$, $A_R = 1$ and A_T varying from 2 to 16. As in Figure 3.1, Figure 3.2 illustrates the saturation of the diversity gain from the CDD scheme at $S = 8$. Figure 3.2 also illustrates the saturation of the diversity gain from the ASD scheme at $P \cdot S = 32$ as well as the ability of the combined diversity scheme to surpass that.

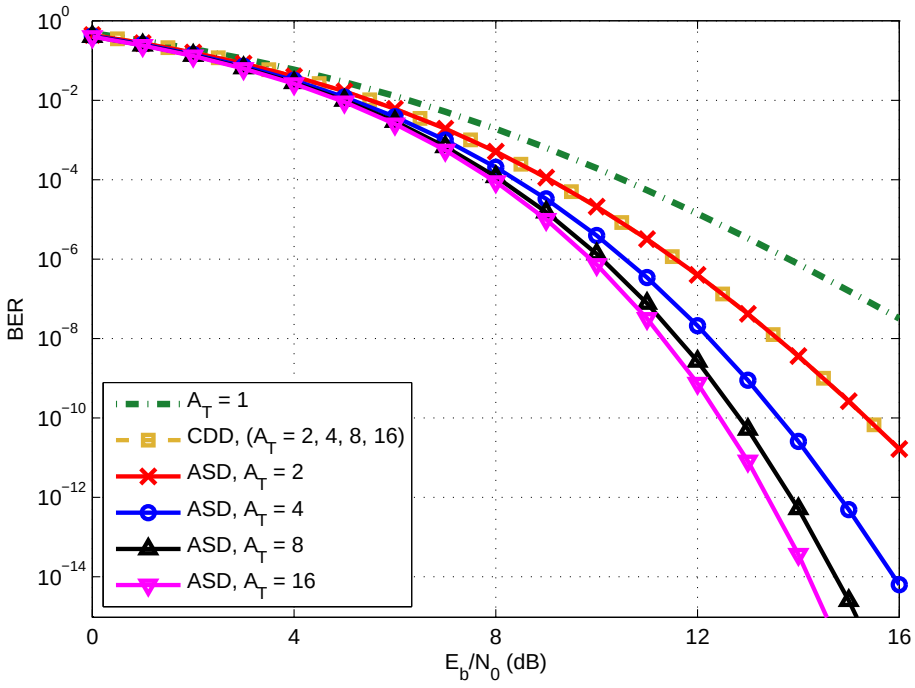

Figure 3.1: Theoretical BER Performance Comparison for proposed ASD and CDD.

3.4 Simulation Results

3.4.1 Simulation System

In this section, we provide the numerical examples and simulation results of the proposed ASD scheme and compare its performance with that of the CDD scheme. We also simulate the performance of the combined diversity scheme which combines the proposed ASD with the CDD scheme to maximize the potential diversity gain. The simulation results will highlight the diversity gain of the proposed ASD scheme over the CDD scheme.

We consider a system with 5 MHz bandwidth and centre frequency of 2.4 GHz with $N = 256$. The designed cyclic prefix length, $N_{CP} = 32$ and all the users' signals are assumed to be synchronized to arrive within N_{CP}. The transmitters use a rate-1/2 terminated convolutional code with generator polynomial [5 7] [53] and QPSK constellation (i.e. $Q = 2$). We consider block transmission using a pseudo-random bit-interleaver with each block containing 254 information bits. Since the constraint length of the convolutional code used is 2, two

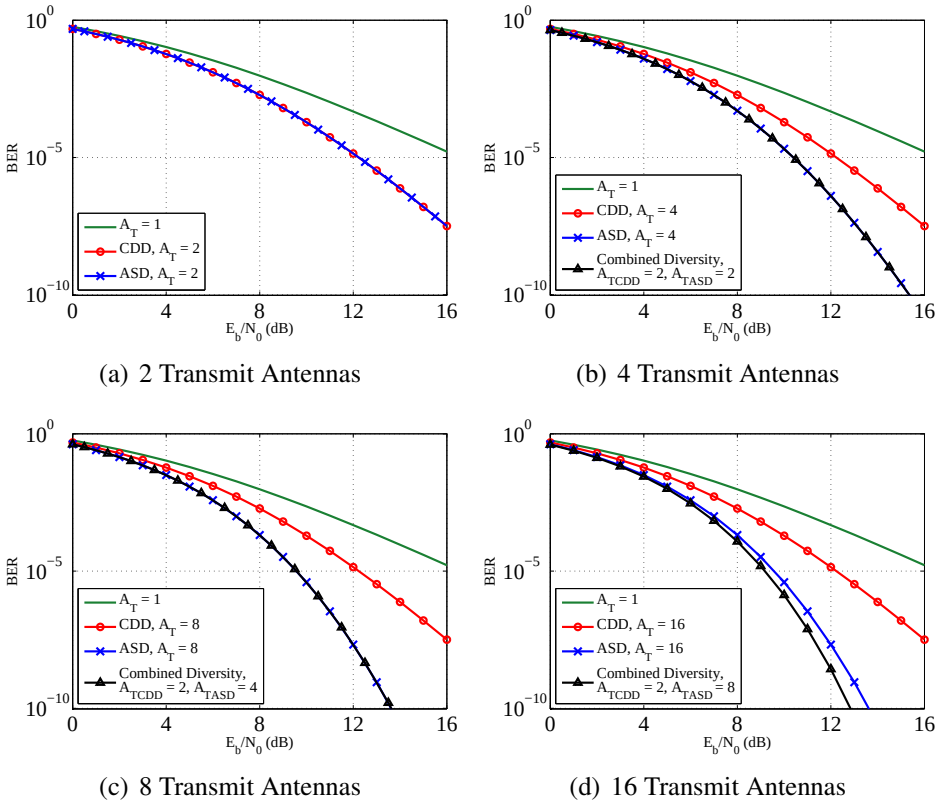

(a) 2 Transmit Antennas (b) 4 Transmit Antennas

(c) 8 Transmit Antennas (d) 16 Transmit Antennas

Figure 3.2: Theoretical BER Performance Comparison for Combined Diversity Scheme.

'0' bits are padded to the information bitstream to terminate the trellis in the all-zeros state.

The channel is assumed to remain unchanged during one transmission block and varies independently for different transmission blocks. We assume each user has independent and identically distributed (i.i.d.) channel profile with independent Rayleigh fading paths and uniform power delay profile [18]. We also assume the channels of the different transmit antennas are uncorrelated. At the receiver, we assume prefect knowledge of the channel and the signals are synchronized in time and frequency at the receiver. For statistical accuracy, we make sure that at least 10000 transmission blocks are simulated and there are at least 50 received blocks with decoding errors. The simulation system configurations are summarized in Table 3.1.

3.4.2 Comparison Between ASD and CDD

We compare the BER performance of our proposed ASD scheme with the CDD scheme for $S = 16$ and $P = 8$ to highlight the ASD scheme's advantage over the CDD scheme. The simulation results for $A_T = 2, 4$ and 8 using ASD and CDD scheme are shown in Figure 3.3. The result for single transmit antenna system without transmit diversity scheme is also plotted for reference. Only the BER performances using the proposed algorithm after the third iteration are plotted for clarity. Comparing the performance for both ASD and CDD for $A_T = 2$ with that of the single antenna system, we see that both schemes have similar diversity gain over the single antenna system as expected from our analysis in Section 3.3. When we compare the CDD performance between $A_T = 2$ and $A_T = 4, 8$, we see that there is no performance gain available. In contrast, the

Table 3.1: Simulation System Configuration for Transmit Diversity.

Centre Frequency		2.4 GHz
System Bandwidth		5 MHz
IFFT Size, N		256
Cyclic Prefix Length, N_{CP}		32
Modulated Symbol Constellation		QPSK
Forward Error Correcting Code	Type	Convolutional Code
	Code Rate	1/2
	Generator Polynomial	[5 7]
Channel Model	Power Delay Profile	Uniform
	Type of Fading Path	Slow Rayleigh Fading
	Antenna Correlation	Uncorrelated
Maximum Number of Iterations in Proposed Algorithm		3
Channel Estimation		Ideal
Minimum Number of Transmitted Packets		10000
Minimum Number of Received Packets with Decoding Error		50
Type of QR Decomposition		MMSE QRD
Number of Paths to Keep in Each Stage, M		8
Number of Receive Antenna, A_R		1
Section 3.4.2	Number of Transmit Antenna, A_T	2, 4, 8
	Number of Users	16
	Number of Sub-carriers per User, S	16
	Number of Channel Path, P	8
Section 3.4.3	Number of Transmit Antenna, A_T	4, 16
	Number of Users	32
	Number of Sub-carriers per User, S	8
	Number of Channel Path, P	4

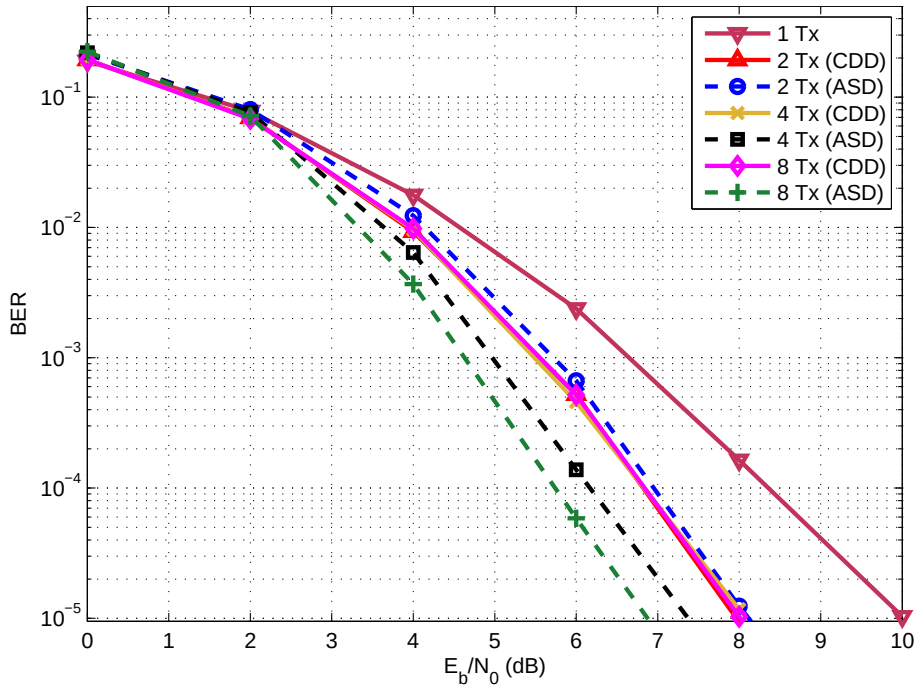

Figure 3.3: BER Performance Comparison for proposed ASD and CDD.

ASD performance for $A_T = 4, 8$ continues to exhibit diversity gain over the ASD performance for $A_T = 2$. Comparing Figure 3.3 with Figure 3.1, we see that the simulation results matches our theoretical analysis of the two transmit diversity schemes in Section 3.3.

3.4.3 Combining ASD and CDD

We also simulate the BER performance for a system with $S = 8$ and $P = 4$ to illustrate the benefits of combining the proposed ASD with CDD. In Figure 3.4, we plot the BER performance for $A_T = 4$ and 16 using the proposed ASD scheme, CDD scheme and the combined diversity scheme. The BER performance for single transmit antenna system without transmit diversity scheme is also plotted for reference. For the case $A_T = 4$, the performance of the CDD scheme is limited by the number of assigned sub-carriers $S = 8$ as shown in Figure 3.4(a) while the performance of the ASD scheme displays a greater diversity order. Similarly, with appropriate configurations of the transmit antennas as recommended in Section 3.2.3, the combined diversity scheme is able to match

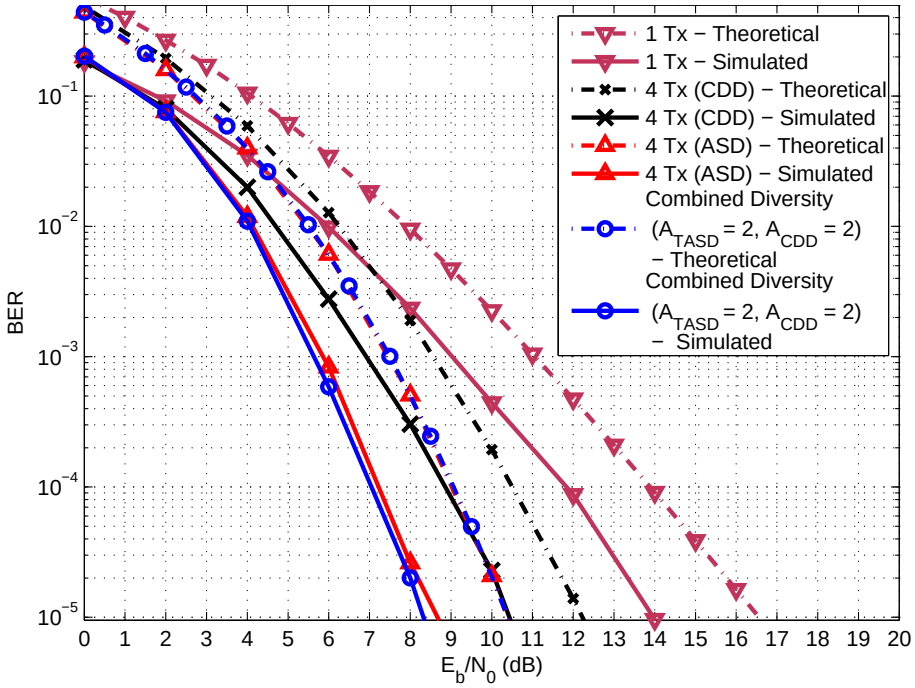

(a) 4 Transmit Antennas

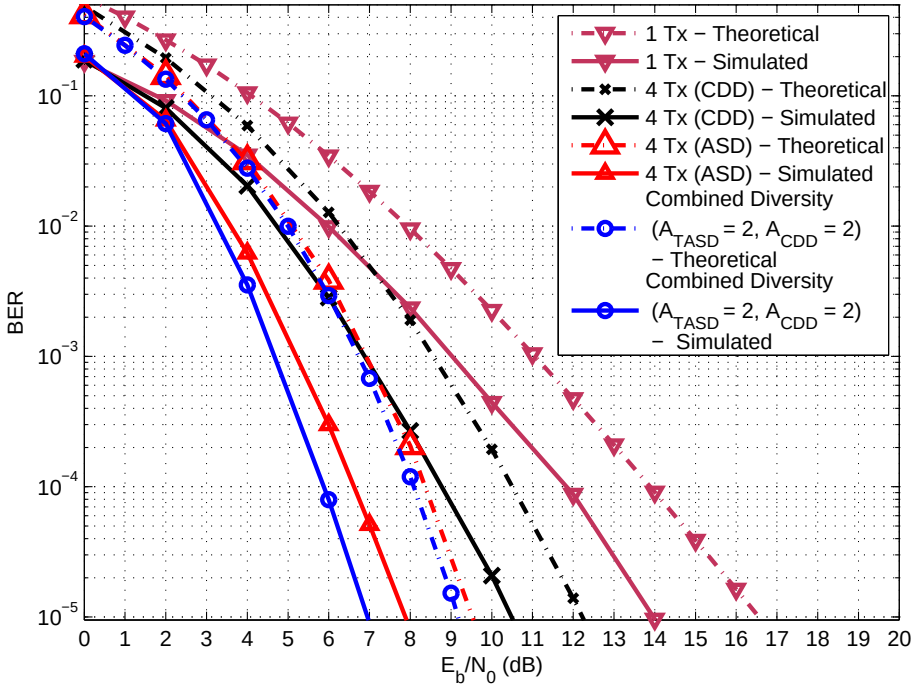

(b) 16 Transmit Antennas

Figure 3.4: BER Performance Comparison for proposed ASD and CDD with Combined Diversity Scheme.

the diversity gain of ASD scheme with the same number of transmit antennas. For the case $A_T = 16$, the simulated performances of both the CDD scheme and ASD scheme are limited by their respective theoretical constraints as derived in Section 3.3. The combined diversity scheme, on the other hand, is able to continue to deliver increasing diversity gain as illustrated in Figure 3.4(b). Moreover, the diversity performance of the simulated BER for all three schemes shown in Figure 3.4 are congruent with the derived theoretical performances shown in Figure 3.2

3.5 Chapter Summary

In this chapter, we introduce a novel transmit diversity scheme for coded IFDMA system which, like the CDD scheme, preserves the low PAPR property of IFDMA signal and can be easily adapted for different numerical configurations of transmit antennas. The proposed ASD scheme guarantees a diversity gain factor equal to the number of transmit antennas. It can also be used in conjunction with the CDD scheme in various configurations to suit the requirements of different systems. Both our theoretical analysis and simulation results show that the proposed ASD scheme outperforms the CDD scheme when the number of transmit antennas increases beyond the diversity gain limit of the CDD scheme. We also demonstrate the benefits of combining the proposed ASD scheme with the CDD scheme through theoretical analysis and simulations, with a design specification for the combination.

Chapter 4

Mobility-Based Interference Cancellation Scheme For BS-IFDMA System with Optimum Code Assignment

4.1 Introduction

The introduction of two-layered code division multiple access (TLS-CDMA) spreading in the uplink of wireless cellular communications has proven to be versatile and performance enhancing in certain operation scenarios [43]. TLS-CDMA combines the usage of chip interleaved block spread (CIBS) CDMA [61, 62] with cyclic prefix CDMA (CP-CDMA) [63–65] to provide the flexibility for the cellular system to adapt to the prevailing cell structure, the channel conditions and the number of active users to support variable data rate transmission among multiple users in emulation of the use of time and frequency domain spreading in orthogonal frequency code division multiplexing (OFCDM) in downlink transmission [20, 21].

Using a similar concept, a block spread (BS)-IFDMA system in [30] was introduced that uses block spreading to suppress ICI while maintaining the intra-cell orthogonality for low mobility users. BS-IFDMA systems also allow more sub-carriers to be assigned to each user for the same number of users in the system. Having more assigned sub-carriers per user will increase the available frequency diversity [19] [66] for each user and hence improve the overall perfor-

mance. However, block spread systems do suffer from multiple access interference (MAI) when high mobility users are introduced into the system. One way to counter the MAI due to the high mobility users is to use tree-structured code generation method of orthogonal variable block spreading factor [67]. However, doing that in a BS-IFDMA system will restrict the number of sub-carriers assigned to each user. Moreover, when there is an asymmetrical number of high mobility users and low mobility users in the system, the use of the variable block spreading factor will not be efficient.

In this thesis, we use an alternative approach to solving the problem of MAI in BS-IFDMA system. We propose a novel mobility-based MAI cancellation scheme to incorporate high mobility users into a BS-IFDMA system without degrading the BER performance [68]. The proposed scheme first distributes the high mobility users evenly across the different frequency groups so that the multiple access interference within each group is limited. By restricting the number of high mobility users within each frequency group, we exploit the characteristic of BS-IFDMA system that separates users in two orthogonal domains: the code and frequency domains to lower the severity of the MAI using the divide and conquer approach. Compared to conventional BS-CDMA or MC-DS-CDMA systems, which separate users only in the code domain and hence require the receiver at the base-station to handle the interference from all the high mobility users collectively, the level of MAI in each frequency group of BS-IFDMA systems due to the reduced number of high mobility users are much less severe. This allows us to use a simple successive MAI cancellation algorithm within each frequency group. Unlike conventional interference cancellation scheme [69] which determine the order of cancellation from the users' received signal strength, the proposed algorithm uses the users' mobility. The conventional interference cancellation scheme operates on the assumption that the channel remains unchanged during the period of a single symbol [69–71] while we consider an operating environment where the different chips of the

same symbol experience varying channel due to the users' high mobility.

We further propose a code assignment algorithm based on the users' Doppler spreads to maximize the number of high mobility users within the system without degrading the system performance. We formulate the total MAI in a system with the proposed interference cancellation scheme as a quadratic assignment problem (QAP) [72] to optimize the spreading code assignments for the users. Based on the characteristics of common spreading codes such as the Walsh-Hadamard and Orthogonal Gold codes, we devise a simplified search procedure in a branch-and-bound algorithm for solving the QAP which lowers the time taken to arrive at the solution by a factor equal to five times the spreading factor used. Numerical evaluations show that the proposed MAI cancellation scheme coupled with the proposed optimized codes assignment enable up to half the total number of users in BS-IFDMA systems to be high mobility users while maintaining the same system performance.

The rest of this chapter is organized as follows: We describe the system model of BS-IFDMA under time-varying channels to describe the system with high mobility users in Section 4.2. We then propose a novel successive MAI cancellation scheme based on user mobility that is uniquely tailored to BS-IFDMA system in Section 4.3. In Section 4.4, we formulate the minimization of the MAI as a QAP and proposed an efficient algorithm to solve the QAP. The theoretical performance of the proposed MAI cancellation scheme is analyzed in Section 4.5 and simulation results are provided in Section 4.6 to illustrate the benefits of the proposed MAI cancellation and code assignment algorithms. Lastly, we summarize our observations and contributions in Section 4.7.

4.2 System Signal Model

In Section 2.4, we have shown that block spreading can be incorporated into IFDMA systems to maximize the channel diversity order. BS-IFDMA scheme

also have the added advantage of lowering inter-cell interference through the despreading process by incorporating a long cell-specific spreading code like in CDMA systems [43]. In a BS-IFDMA system, users are separated into two orthogonal domains: the frequency domain and the code domain. Each user is indexed by $u_{g,b}$, where g is frequency group index and b is the code group index. In addition to the number of orthogonal frequency groups, G, we denote the number of orthogonal code groups, equivalent to the spreading factor, as B. The modulated complex symbols are again transmitted in blocks of S symbols. Blocks of transmitted symbols first undergo IFDMA modulation followed by block spreading. Let the i^{th} block of transmitted symbols sent by the $u_{g,b}$ user be denoted as

$$\mathbf{x}_{u_{g,b}}(i) = \left[\begin{array}{ccc} x_{u_{g,b},0} & \ldots & x_{u_{g,b},S-1} \end{array} \right]^{\mathrm{T}} \tag{4.1}$$

and following (2.2), the i^{th} IFDMA symbol is given by

$$\mathbf{y}_{u_{g,b}}(i) \;\; = \;\; \mathbf{E}_g \tilde{\mathbf{x}}_{u_{g,b}(i)} \tag{4.2}$$

Block spreading is performed on the IFDMA symbol through a Kronecker product operation between $\tilde{\mathbf{y}}_{u_{g,b}}(i)$ and the b^{th} spreading code vector $\mathbf{c}_b$ to give

$$\mathbf{s}_{u_{g,b}}(i) = \mathbf{c}_b \otimes \tilde{\mathbf{y}}^T_{u_{g,b}}(i) = \left(\begin{array}{ccc} c_{b,0}\tilde{y}_{u_{g,b},0}(i) & \cdots & c_{b,0}\tilde{y}_{u_{g,b},N-1}(i) \\ \vdots & \ddots & \vdots \\ c_{b,G-1}\tilde{y}_{u_{g,b},0}(i) & \cdots & c_{b,G-1}\tilde{y}_{u_{g,b},N-1}(i) \end{array} \right) \tag{4.3}$$

where $c_{b,k}$ is the k^{th} entry in the vector $\mathbf{c}_b$ and $\tilde{y}_{u_{g,b},k}(i)$ is the k^{th} entry in the vector $\tilde{\mathbf{y}}_{u_{g,b}}(i)$.

Chips from this matrix will be transmitted row-wise over B sub-block periods with N chips transmitted at each sub-block period. In other words, the transmitted signal for the k^{th} sub-block is given by:

$$\mathbf{s}_{u_{g,b}}(i,k) = c_{b,k}\tilde{\mathbf{y}}_{u_{g,b}}(i) \tag{4.4}$$

At the base-station, the receiver will perform both the frequency group and code group separation to obtain the individual users signals. As both processes are linear, the sequence of these operations is interchangeable. In implementation, the block de-spreading operation (i.e the reversal of the block spreading operation) usually takes precedence to reduce the overall complexity [73]. However, in this thesis, we derive the expression for individual user by considering frequency group separation first to highlight the problem we are interested in (that is, the loss of orthogonality in the code domain due to high mobility) and to create a versatile signal model that can be used for other block-spread system such as in [43].

Following (2.8), the signals in the m^{th} frequency group can be obtained by pre-multiplying the received $\mathbf{r}(i,k)$ with $\mathbf{U}_m$ in (2.7) giving

$$\begin{aligned}
\mathbf{r}_m(i,k) &= \mathbf{U}_m\mathbf{r}(i,k) \\
&= \sum_{b=0}^{B-1}\left(\mathbf{U}_m\tilde{\mathbf{h}}_{u_{m,b}}(i,k)\mathbf{s}_{u_{m,b}}(i,k) + \sum_{\substack{g=0\\g\neq m}}^{G-1}\mathbf{U}_m\tilde{\mathbf{h}}_{u_{g,b}}(i,k)\mathbf{s}_{u_{g,b}}(i,k)\right) \\
&\quad +\mathbf{U}_m\boldsymbol{\eta}(i,k) \\
&= \sum_{b=0}^{B-1} c_{b,k}\mathbf{h}_{u_{m,b}}(i,k)\mathbf{x}_{u_{m,b}}(i) + \boldsymbol{\eta}_m(i,k) \qquad (4.5)
\end{aligned}$$

where $\boldsymbol{\eta}_m(i,k)$ is the AWGN component and $\mathbf{h}_{u_{m,b}}(i,k)$ is the channel circulant matrix as in (2.16). Since there are no interferences between signals within different IFDMA symbols, we shall proceed to drop the index i in subsequent derivation for notation clarity. Furthermore, we assume the frequency offsets including the Doppler shift between the base-station and the mobile devices are estimated at the base-station and feedback to the mobile devices via the downlink channel [74]. The mobile devices will then adjust their oscillators accordingly [74]. In [74], the authors show that the frequency offsets can be usually estimated to within 2% of the sub-carriers spacing at the base-station using the redundancy in the received signals due to the addition of the cyclic

prefix to the transmitted signal. With such estimation accuracy, the signal to interference ratio will be more than 30 dB. Thus we can regard the different frequency groups to be separated from each other at the base-station regardless of the mobiles devices' velocity with negligible interference. Hence we will also drop the frequency group index m and rewrite (4.5) in the general form of a block spread system

$$\mathbf{r}(k) = \sum_{b=0}^{B-1} c_{b,k}\mathbf{h}_b(k)\mathbf{x}_b + \boldsymbol{\eta}(k) \tag{4.6}$$

Applying the de-spreading process [30] to (4.6), we get the signals for the d^{th} user as:

$$\begin{aligned}
\mathbf{r}_d &= \sum_{k=0}^{B-1} \mathbf{r}(k)c_{d,k} \\
&= \sum_{b=0}^{B-1} \left(\sum_{k=0}^{B-1} c_{d,k}c_{b,k}\mathbf{h}_b(k) \right) \mathbf{x}_b + \sum_{k=0}^{B-1} c_{d,k}\boldsymbol{\eta}(k) \\
&= \bar{\mathbf{h}}_{d,d}\mathbf{x}_d + \sum_{\substack{b=0 \\ b\neq d}}^{B-1} \bar{\mathbf{h}}_{d,b}\mathbf{x}_b + \bar{\boldsymbol{\eta}}
\end{aligned} \tag{4.7}$$

where $\bar{\mathbf{h}}_{d,b} = \sum_{k=0}^{B-1} c_{d,k}c_{b,k}\mathbf{h}_b(k)$. Note that since the codes used are orthogonal, if $\mathbf{h}_b(k) \approx \mathbf{h}_b(0)$, $k = 1, \ldots B-1$ (i.e. no significant change in all users' channel within the block spread duration) then $\bar{\mathbf{h}}_{d,b} \approx 0$ for $b \neq d$ implying little or negligible MAI.

More interesting to note is that the MAI that a user experiences is not dependent on the user's Doppler spread but on that of other users within each frequency group. Ironically, if there is only one user with large Doppler spread in the frequency group, this user will experience almost no MAI while the rest of the users will suffer strong MAI from his transmission. This phenomenon provides an opportunity to accommodate high-mobility users with large Doppler spread in the system through MAI cancellation techniques.

4.3 Mobility-Based Successive Interference Cancellation

4.3.1 Multiple Access Interference in BS-IFDMA System

With reference to the signal model presented in Section 4.2, the MAI suffered by individual users in a frequency group are dependent on a number of factors: a) the data transmitted by the other users, b) the channel of other users and c) the cross-correlation between the users' spreading codes. Since in the general case, the knowledge of these variables at the base-station is limited, it is instructive to look at three different measures of the amount of MAI. The first measure, which requires complete knowledge of all the variables at the base-station, is the instantaneous MAI power suffered by the d^{th} user in the frequency group, I_d, can be written as:

$$I_d = \left(\sum_{\substack{b=0 \\ b \neq d}}^{B-1} \bar{\mathbf{h}}_{d,b} \mathbf{x}_b \right)^H \left(\sum_{\substack{b=0 \\ b \neq d}}^{B-1} \bar{\mathbf{h}}_{d,b} \mathbf{x}_b \right) \tag{4.8}$$

As the base-station will typically not have the knowledge on the actual data being transmitted, we can define the average power of MAI (i.e. averaging over different transmitted data) for a particular set of users' channel, $\bar{I}_d$, as a second measure given as:

$$\begin{aligned} \bar{I}_d &= \mathrm{E}\left[\left(\sum_{\substack{b=0 \\ b \neq d}}^{B-1} \bar{\mathbf{h}}_{d,b} \mathbf{x}_b \right)^H \left(\sum_{\substack{b=0 \\ b \neq d}}^{B-1} \bar{\mathbf{h}}_{d,b} \mathbf{x}_b \right) \right] \\ &= \sum_{\substack{b=0 \\ b \neq d}}^{B-1} \mathrm{E}\left[\mathbf{x}_b^H \bar{\mathbf{h}}_{d,b}^H \bar{\mathbf{h}}_{d,b} \mathbf{x}_b \right] \\ &= S \sum_{\substack{b=0 \\ b \neq d}}^{B-1} P_b \sum_{p=0}^{S-1} \bar{h}_{d,b}^2(p) \end{aligned} \tag{4.9}$$

where $P_b = E\left[|x_b|^2\right]$ is the average transmission power per symbol of the b^{th}

user and $\bar{h}^2_{d,b}(p)$ is the p^{th} entry in the first column of $\bar{\mathbf{h}}_{d,b}$.

Similarly, the mean MAI power averaged over different sets of users' channels, $\bar{\bar{I}}_d$ is given as:

$$\begin{aligned}\bar{\bar{I}}_d &= S\sum_{\substack{b=0\\b\neq d}}^{B-1} P_b \mathrm{E}\left[\sum_{p=0}^{S-1}\bar{h}^2_{d,b}(p)\right] \\ &= S\sum_{\substack{b=0\\b\neq d}}^{B-1} P_b \sum_{p=0}^{S-1}\mathrm{E}\left[\bar{h}^2_{d,b}(p)\right] \end{aligned} \tag{4.10}$$

Compared to $\bar{I}_d$, the base-station only requires the knowledge of the ergodic channel conditions to calculate $\bar{\bar{I}}_d$ rather than the knowledge of the specific channels. Assuming block fading,

$$\mathrm{E}\left[\bar{h}^2_{d,b}(p)\right] = R_p\sum_{k=0}^{B-1}\sum_{l=0}^{B-1} z_{d,b}(k,l)J_0\left[2\pi\left(k-l\right)f_D(b)\tau\right] \tag{4.11}$$

where $z_{d,b}(k,l) = c_{d,k}c_{b,k}c_{d,l}c_{b,l}$, R_p is the mean power of the p^{th} path, $f_D(b)$ is the maximum Doppler shift of the b^{th} user, τ is the duration of one BS-IFDMA sub-block and $J_0(x)$ is the Bessel function of the zeroth order. Note that the asymmetrical dependence of $\mathrm{E}\left[\bar{h}^2_{d,b}(p)\right]$ on the user index d and b indicates the interference are not reciprocal. The signals of a user with a higher Doppler spread inflicts a greater interference on the signal of a user with a lower Doppler spread while the signal of the user with lower Doppler spread inflicts a proportionally smaller interference on the signals of a user with higher Doppler spread.

In Figure 4.1, we illustrate the dependence of the power of the generated interference on the maximum Doppler shift of the user by plotting the normalized mean pairwise interference power against the Doppler frequency for Walsh-Hadamard spreading codes with $B = 8$ and $S = 32$. In Figure 4.1, the interference power of all the seven possible cross-correlation pairs arising from the spreading codes are plotted. For all the pairs of codes, the mean pairwise interference power rises sharply and then tapers off to a limiting level. However,

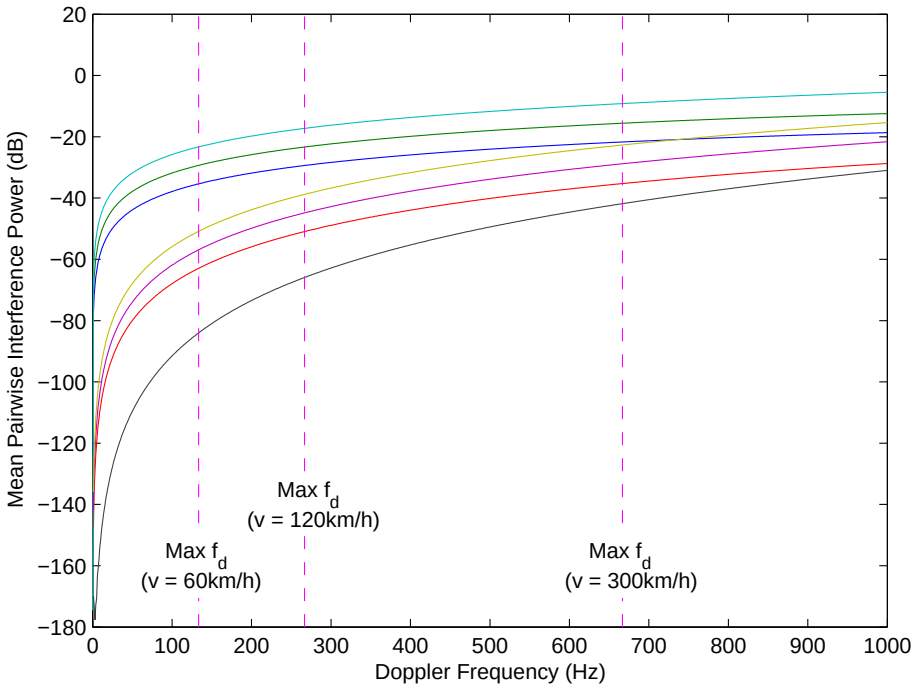

Figure 4.1: Mean pairwise MAI power for S = 32, B = 8

the difference in the interference power for the different pairs can be quite large with the maximum being about 70 dB for Doppler frequencies corresponding to common vehicular velocities. Hence, there are significant benefits in optimizing the assignment of codes to users according to their relative Doppler shift. We will investigate the optimal code assignment in Section 4.4. Here as an illustrative example, we will show the distribution of the mean interference power in the system using random code-to-user assignments in Figure 4.2. The system uses Walsh-Hadamard spreading codes with $B = 8$ and $S = 32$. The mobility of the users are evenly distributed from 0 km/h to 350 km/h. The ensemble average value of the distribution in Figure 4.2 is 7.25 while the minimum value as calculated using the optimal code-to-user assignment, which will be introduced, in Section 4.4 is 3.99.

4.3.2 Successive Interference Cancellation

In view of the significant difference in interference power generated by users with different Doppler spread or equivalently, mobility, we propose a mobility-

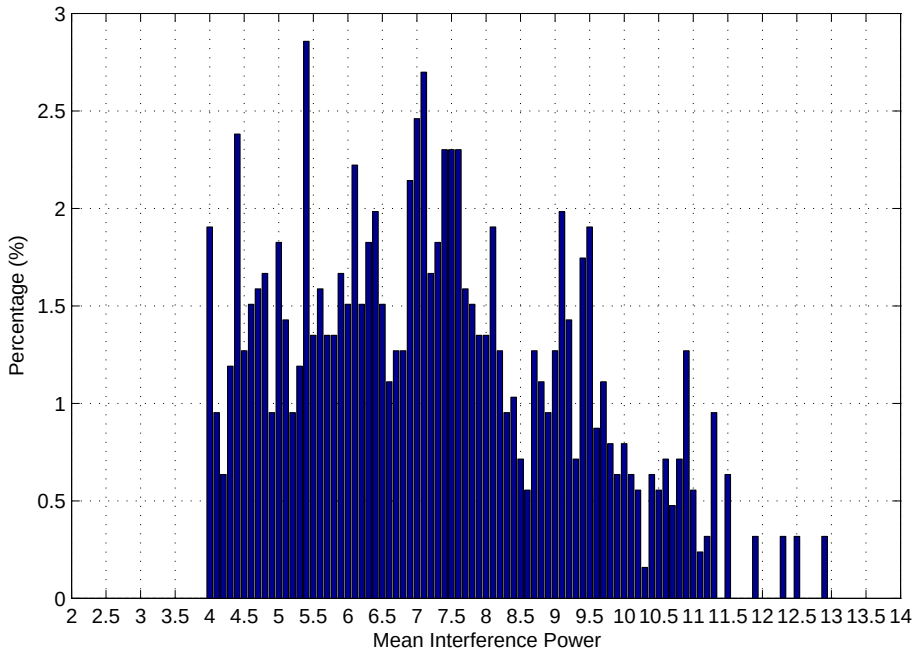

Figure 4.2: Distribution of Mean Interference Power using Random Code Assignment

based successive interference cancellation (SIC) scheme at the base-station receiver. At the receiver, the users are sorted accordingly to their maximum Doppler shift in descending order. The detection of the users' signals are then carried out successively following this order, with the estimated signals from preceding users used to cancel out their interference. The block diagram of the proposed scheme is illustrated in Figure 4.3 for the case of $B = 4$. Note that the complexity of the proposed SIC is similar to the conventional SIC [69], as only the basis for the order of cancellation is changed.

Evidently, the transmitted symbols of the fastest user will, on the average, experience the lowest level of MAI among all the users and will cause the strongest interference on the rest of the users' signals. Hence, by detecting the fastest user's symbols and subsequently cancelling out their interference, we ensure that the system has the most accurate interference detection and that the dominant interference is removed. When the interference from the fastest user is removed, the second fastest user's symbols would experience the least interference and become the dominant interferer. Therefore we repeat the procedure

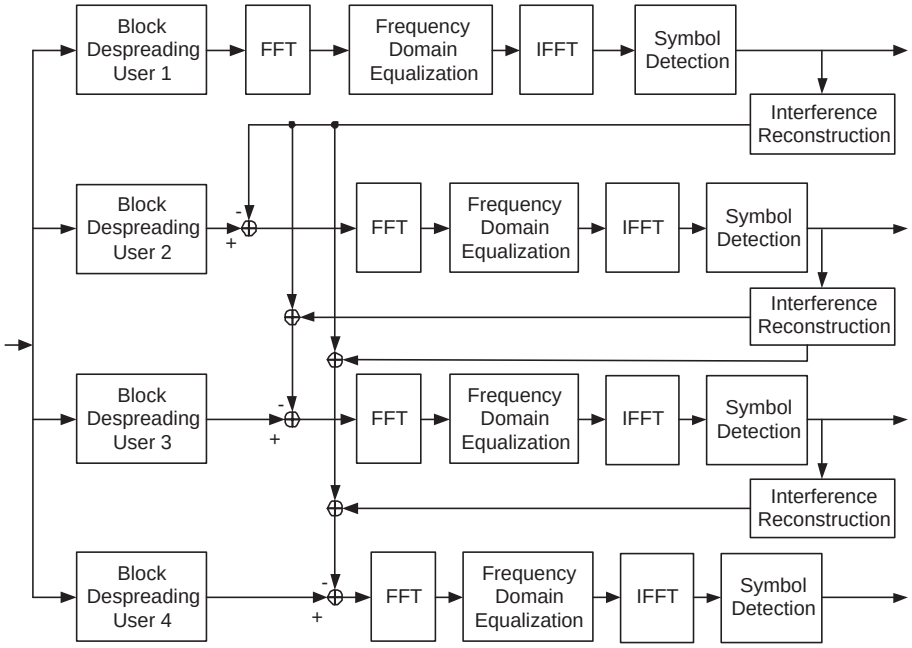

Figure 4.3: Successive MAI Cancellation for BS-IFDMA System for B = 4.

to detect the second fastest user's symbols and then cancel out their interference. The process is repeated until the detection of all users signals are completed.

Alternatively, the users within a frequency group can first be divided into two classifications, interferers and non-interferers based on a heuristic threshold. The threshold will be set at the maximum Doppler spread a user channel can have without causing significant interference to others. Users with Doppler spread greater than the threshold are classified as interferers while the rest are classified as non-interferers. Within the class of interferers, the proposed mobility-based successive interference cancellation described above is first carried out. The interferers' signals are then cancelled from the received signals before the detection of all the non-interferers is carried out in parallel. This will greatly reduce the latency due to successive users detection especially in cases where only a small number of interferers are present.

4.3.3 Multiple Access Interference in Different SIC Stages

Without loss of generality, we index the users according to their Doppler spread in descending order. The number of users separated in the code domain, K is set to be equal to the spreading gain, B. Hence, there are altogether B stages for the proposed SIC scheme. Let $\hat{\mathbf{x}}_k$ represent the detected symbols at the receiver in the k^{th} SIC stage. The instantaneous MAI power at the start of the k^{th} SIC stage is thus:

$$I_{MAI}(k) = \left| \sum_{b=k+1}^{B-1} \bar{\mathbf{h}}_{k,b}\mathbf{x}_b + \sum_{b=0}^{k-1} \bar{\mathbf{h}}_{k,b}\left(\mathbf{x}_b - \hat{\mathbf{x}}_b\right) \right|^2 \tag{4.12}$$

where the first term on the right hand side represents the MAI from users which have not been detected while the second term represents the residue MAI due to detection error from the preceding stages. Similarly, the average MAI power conditioned on the users channel and the mean MAI power averaged over different sets of users channels are given, respectively, by:

$$\bar{I}_{MAI}(k) = S \sum_{b=k+1}^{B-1} P_b \sum_{p=0}^{S-1} \bar{h}_{k,b}^2(p) + S \sum_{b=0}^{k-1} \hat{P}_b \sum_{p=0}^{S-1} \bar{h}_{k,b}^2(p) \tag{4.13}$$

$$\bar{\bar{I}}_{MAI}(k) = S \sum_{b=k+1}^{B-1} P_b \sum_{p=0}^{S-1} \mathrm{E}\left[\bar{h}_{k,b}^2(p)\right] + S \sum_{b=0}^{k-1} \hat{P}_b \sum_{p=0}^{S-1} \mathrm{E}\left[\bar{h}_{k,b}^2(p)\right] \tag{4.14}$$

where $\hat{P}_b = E\left[\left|x_b - \hat{x}_b\right|^2\right]$.

4.3.4 Comparison with Conventional Power based SIC

A common assumption in systems where conventional power based SIC is applied is that the chips belonging to a single spread symbol experience invariant channel condition. Therefore, in these DS-CDMA [69], multi-carriers (MC)-CDMA [70] and MC-DS-CDMA [71] systems, the MAI are the result of the loss in codes' orthogonality due to presence of frequency selective multipaths,

carriers offset due to Doppler shift or asynchronicities of received signals. In these systems, the MAI caused by a user's signals to others are strongly correlated to the received power of the user's signal. Since the power of the signal after a particular code despreading is dominated by the desired signal's received power, the powers of the different despreaded signals provide a good guide to the cancellation order. However, as shown in Section 4.3.1, in BS-IFDMA system when the chips of a single spreaded symbol experience varying channel conditions, the MAI caused by a user's signal are determined not only by the signal's received power but also by the user's mobility. Moreover, the asymmetric levels of interference between a low mobility user and a high mobility user causes the received power of the despreaded signal of the low mobility user to be an unreliable indicator of its own signals' received power in the presence of strong interference power. Thus, a cancellation order based on the conventional power measurement of despreaded signals will not work well in BS-IFDMA system.

4.4 Optimal Code Assignment

In this section, we seek to optimize the performance of the proposed SIC scheme through careful code assignment. In practical wireless communications, there are only a limited number of variables that can be controlled. For example, we can perform power control to adjust the power of different users' transmission but cannot place limitations on the actual data being transmitted. Also the wireless channels are uncontrollable. Since closed-loop power control and real-time adaptation to channel conditions are difficult to achieve in fast-fading channels which are experienced by at least some of the users, we concentrate on the minimization of MAI through conscientious assignment of different spreading codes to users in this thesis.

We assume that the receiver has knowledge of the magnitude of the Doppler

spread of the different transmission devices before the code assignment either through estimation of previous received signals or through reporting by the devices in random access channel during initial access setup. Since the receiver has no knowledge of the transmitted data and will have difficulties in obtaining knowledge of the different users' channels, especially for those with large Doppler spread, the code assignment will be performed by minimizing the sum of the mean MAI power at each stage, $\sum_{k=0}^{B-1} \bar{\bar{I}}_{MAI}(k)$ instead of the instantaneous MAI power or the average MAI power conditioned on the user's channels which requires a reasonably accurate knowledge of all the users' channels.

The MAI minimization code assignment problem resembles a QAP. However, in the conventional formulation of QAPs in [75], the cost matrix is formulated as the Hadamard product of two separable matrices denoted as the flow and distance matrix according to the historical formulation of QAPs as minimization of transportation costs. The MAI presented in Section 4.3.1 cannot be factorized to the conventional form but we can formulate our MAI minimization code assignment into a more general form of QAP as presented in [72]. To do this, the sum of the mean MAI power at each stage, $\sum_{k=0}^{B-1} \bar{\bar{I}}_{MAI}(k)$, is rewritten as a summation of the pairwise interference terms, C_{mdnb} which is indexed by two pairs of users and code index: $\{m, d\}$, $\{n, b\}$, $b, d, m, n = 0, \ldots, B-1$. The pairwise interference, C_{mdnb}, on the m^{th} user using d^{th} spreading code by the n^{th} user using b^{th} spreading code are given as:

$$C_{mdnb} = \begin{cases} P_n \tilde{I}\left(n, d, b\right), & \text{if } m < n. \\ \hat{P}_n \tilde{I}\left(n, d, b\right), & \text{if } m > n. \\ 0, & \text{if } m = n, d = b. \\ \text{N.A.} & \text{otherwise.} \end{cases} \tag{4.15}$$

where $\tilde{I}\left(n, d, b\right) = \sum_{p=0}^{S-1} R_p \sum_{k=0}^{B-1} \sum_{l=0}^{B-1} z_{d,b}(k, l) J_0\left[2\pi \left(k - l\right) f_D(n) \tau\right]$.

Similarly, we can also rewrite (4.12) and (4.13) as:

$$C_{mdnb} = \mathbf{x}_n^H \bar{\mathbf{h}}_{d,b}^H \bar{\mathbf{h}}_{d,b} \mathbf{x}_n \tag{4.16a}$$

$$C_{mdnb} = P_n \sum_{p=0}^{S-1} \bar{h}_{d,b}^2(p) \tag{4.16b}$$

For the sake of brevity, only the mean MAI power will be explicitly used in the rest of the QAP formulation and subsequent derivations as the formulation for all three interferences are identical past this stage.

We denote a code-to-user assignment through a $B \times B$ permutation matrix, $\mathbf{U} = [u_{ij}]$ where the row index, i, indexes the user and the column index, j, indexes the spreading code. We define an assignment matrix, $\mathbf{V} = [v_{mdnb}]$, as the Kronecker product of $\mathbf{U}$ where,

$$\mathbf{V} = \begin{pmatrix} u_{0,0}\mathbf{U} & u_{0,1}\mathbf{U} & \dots & u_{0,B-1}\mathbf{U} \\ u_{1,0}\mathbf{U} & u_{1,1}\mathbf{U} & \dots & u_{1,B-1}\mathbf{U} \\ \vdots & \vdots & \ddots & \vdots \\ u_{B-1,0}\mathbf{U} & u_{B-1,1}\mathbf{U} & \dots & u_{B-1,B-1}\mathbf{U} \end{pmatrix} \tag{4.17}$$

Rewriting the sum of the mean MAI power at each stage, $\sum_{k=0}^{B-1} \bar{\bar{I}}_{MAI}(k)$, as a cost function, $C(\mathbf{V})$, we get,

$$C(\mathbf{V}) = \sum_{m,d,n,b} v_{mdnb} C_{mdnb} \tag{4.18}$$

Correspondingly, we can write the cost matrix $\mathbf{C} = [C_{mdnb}]$ as an amalgamation of submatrices following the pattern of $\mathbf{V}$,

$$\mathbf{C} = \begin{pmatrix} \mathbf{C}_{0,0} & \mathbf{C}_{0,1} & \dots & \mathbf{C}_{0,B-1} \\ \mathbf{C}_{1,0} & \mathbf{C}_{1,1} & \dots & \mathbf{C}_{1,B-1} \\ \vdots & \vdots & \ddots & \vdots \\ \mathbf{C}_{B-1,0} & \mathbf{C}_{B-1,1} & \dots & \mathbf{C}_{B-1,B-1} \end{pmatrix} \tag{4.19}$$

Our aim is to determine a solution matrix from the $B!$ possible assignment matrices which minimize the sum of the MAI power. To do so we need to solve the QAP which is an NP-complete problem [72]. We use a branch-and-bound approach to solve this problem.

4.4.1 Bounding Procedure

A tight lower bound to the cost function is needed for the branch-and-bound procedure [76]. Some of the tightest bounds discovered for solving QAPs are based on eigenvalues of the flow and distance matrix [77, 78] but these bounds cannot be used in our context since our cost matrix cannot be readily factorized into two separable matrices. Instead, we can re-formulate the minimization problem as a dual minimization problem that we can easily solve as linear assignment problems (LAP) to calculate the lower bound. Note that there are two types of action on the cost matrix that allow us to shift the cost by an identical amount.

Type 1: Addition (or subtraction) of a constant to all elements (with an applicable value) of any row or column in the cost matrix.

Type 2: Addition (or subtraction) of a constant to all elements (with an applicable value) of a submatrix row or column and the corresponding subtraction (or addition) of this constant from either another row or column of the submatrix or from the submatrix leader element, defined as the element c_{ij} of the submatrix, $\mathbf{C}_{ij}$.

If the above two operations on the cost matrix are used to decrease the cost by an amount C' with the additional limitation that no element in the cost matrix can become negative in the process, then the following relationship will hold:

$$C' \leq \min_{\mathbf{V}} C\left(\mathbf{V}\right) \tag{4.20}$$

Furthermore, if the equality in (4.20) holds, then the elements within the

adjusted cost matrix that corresponds to the non-zero elements in the optimal assignment matrix $\mathbf{V}$, will necessarily be zero. Therefore, the original minimization problem is transformed into the maximization of the sum of the cost decrease C' using *Type 1* and *Type 2* operations with the constraint that no element in the adjusted cost matrix can be negative. The following algorithm [72] can thus be used to derive a lower bound on the minimum of $C(\mathbf{V})$.

Algorithm 1:

1. Initialize a reduction variable, $R = 0$, and the number of iterations, $count = 0$.

2. Process each of the submatrices, $\mathbf{C}_{ij}$, in the matrix $\mathbf{C}_{ij}$ starting from the top left hand corner, moving sequentially from left to right, top to bottom using the following steps:

   (a) Add the cost of complementary element to the elements in the submatrix which have them and set the value of the complementary elements to zero. A complementary element of the element c_{ijkl} is defined as the element, c_{klij}. Since any assignment involving c_{ijkl} will involve c_{klij}, subtracting a constant from c_{klij} and adding the constant to c_{ijkl} will maintain the cost of all assignment.

   (b) Solve the LAP represented by the submatrix using the Hungarian algorithm [79, 80].

   (c) Add the solution cost for the LAP to the leader element in the solution matrix for the LAP to form $\mathbf{C}'_{ij}$.

   (d) Replace the submatrix $\mathbf{C}_{ij}$ with $\mathbf{C}'_{ij}$ in $\mathbf{C}$.

3. Collect all the leader elements from $\mathbf{C}$ to form the $B \times B$ matrix,

$$\mathbf{L} = \begin{pmatrix} c_{0,0,0,0} & c_{0,1,0,1} & \cdots & c_{0,B-1,0,B-1} \\ c_{1,0,1,0} & c_{1,1,1,1} & \cdots & c_{1,B-1,1,B-1} \\ \vdots & \vdots & \ddots & \vdots \\ c_{B-1,0,B-1,0} & c_{B-1,1,B-1,1} & \cdots & c_{B-1,B-1,B-1,B-1} \end{pmatrix} \quad (4.21)$$

   Apply the Hungarian algorithm to $\mathbf{L}$. Add the solution cost of the algorithm to R. Replace $\mathbf{L}$ with the solution matrix and replace the leader elements in $\mathbf{C}$ with elements from the revised $\mathbf{L}$. Increase the iterations counter by one, or $count = count + 1$.

4. Check if the reduced costs matrix, $\mathbf{C}$, satisfy a QAP assignment.

   (a) If *Yes*, go to Step 10.

   (b) If *No*, and R has increased during Step 3 go to Step 5.

   (c) If *No*, and R was unchanged during Step 3 go to Step 9.

5. Check if the revised leader matrix in Step 3 is an all-zeros matrix.

   (a) If *Yes*, go to Step 9.

   (b) If *No*, go to Step 6.

6. Check if the number of iterations, $count$ exceed the maximum number of allowable iterations.

   (a) If *Yes*, go to Step 9.

   (b) If *No*, go to Step 7.

7. For each non-zero element in the revised leader matrix, $\mathbf{L}$, the corresponding leader elements in $\mathbf{C}$ is reduced to zero and the original value is divided by $B - 1$ and added to the elements in the row of the submatrix of the leader element.

8. Sort the elements in the revised leader matrix, $\mathbf{L}$, in descending order. Repeat the algorithm from Step 2, revising the processing order of the submatrices to follow the sorted order.

9. Return R as the lower bound.

10. Return R as the minimum solution cost and the corresponding solution matrix.

Using the algorithm shown above, we can either get a tight lower bound on the QAP or solve the QAP exactly. However, if $B > 4$, then the algorithm will usually fail to return an exact solution. Therefore, the algorithm is incorporated into a branch-and-bound procedure to effectively solve the minimization problem for $B > 4$.

4.4.2 Branch-and-Bound Strategy

The strategy in the branch-and-bound approach to minimization is to progressively eliminate the different branches of possible solutions. We start off with a feasible solution and calculate the cost of the solution. We assign this the probationary solution $\mathbf{V}_p$ with an associated probationary solution cost C_p. As the first stage of the detection suffers from the most significant amount of MAI, we solve the B LAPs each represented by one of the submatrices, $\mathbf{C}_{0,j}, j = 0, 1, \ldots, B-1$, with the first row and j^{th} column deleted, and choose the one with the lowest solution costs as the initial probationary solution.

Next, we perform a depth-first search seeking the true solution or eliminating a branch from consideration. We do a partial assignment by fixing the code assigned to the user with the highest Doppler spread. Each assignment of a code to a user is considered a branch and we proceed from level to level. At each level, the size of the QAP is reduced compared to the previous level and we try to solve the new QAP using *Algorithm 1* in Section 4.4.1. If we are unable to solve the QAP, we will continue to reduce the size of the QAP by going

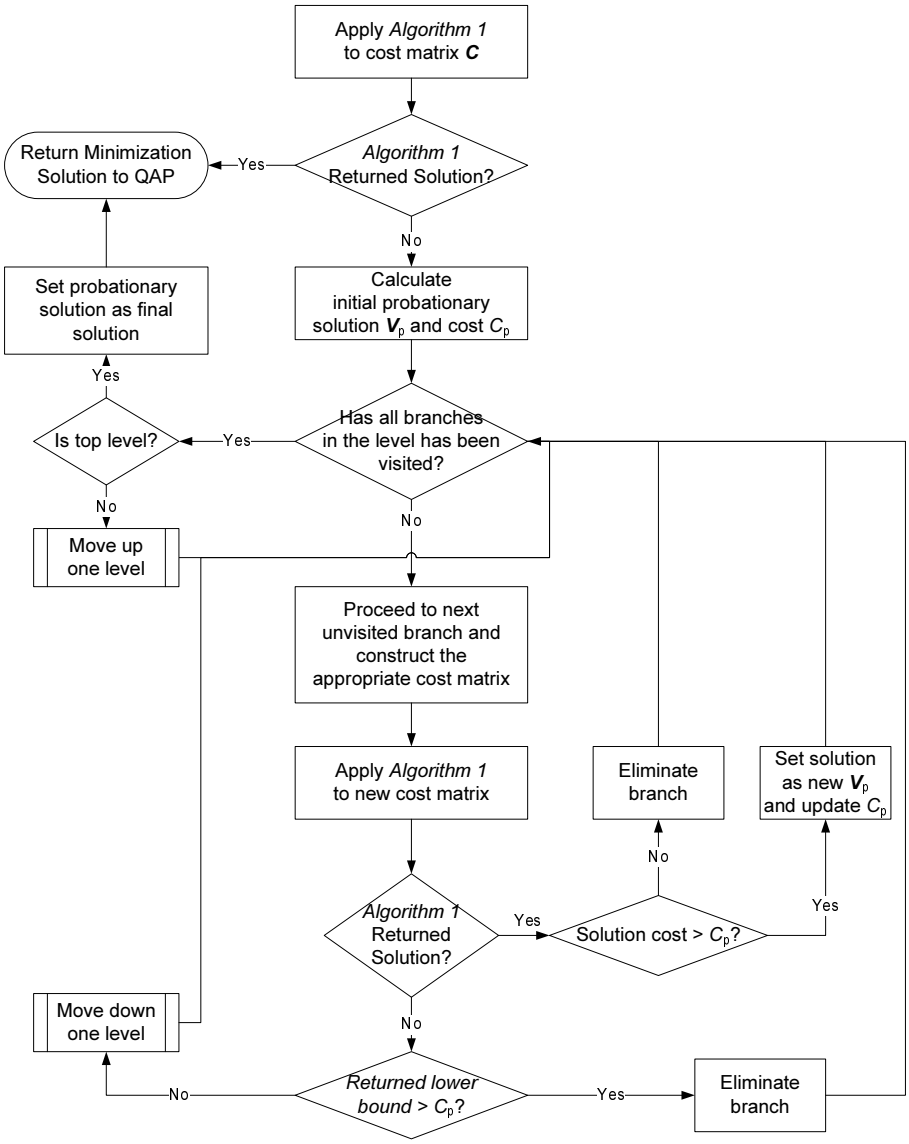

Figure 4.4: Flowchart of Branch-and-Bound Algorithm.

down another level, making another partial assignment by assigning code to the user with the highest Doppler spread among those users which have not been assigned a code. If a solution is found with a lower cost than the probationary solution cost, the new solution will become the new probationary solution. At the same time, we track the lower bound so that whenever the bound exceeds the probationary solution cost C_p, the branch is eliminated as a possible solution, and a new branch can be tested with a new code assigned to the user with the highest Doppler spread. Thus, when we have visited all the possible branches, eliminating all but those which contains the probationary solution $\mathbf{V}_p$,

it naturally will be the solution to the QAP. The branch-and-bound algorithm is summarized as the flowchart shown in Figure 4.4.

The efficiency of the branch-and-bound approach depends on a tight bounding procedure such as *Algorithm 1*. A tight lower bound enables fast elimination of branches not associated with the true solution allowing the visitation of all branches to be completed quickly. Another important factor for efficient performance of the branch-and-bound approach is a good initial probationary solution. A good initial estimate of the solution cost will allow the algorithm to reject the wrong branches faster as the lower bound of the wrong branches will exceed the initial probationary solution cost quickly. The first stage of the detection, where no cancelations has been performed, will contribute the most significant amount of MAI. Hence, we first solve the B LAPs each represented by one of the submatrices, $\mathbf{C}_{0,j}, j = 0, 1, \ldots, B-1$, with the first row and j^{th} column deleted. Next, we compare the solution costs of the different LAPs and choose the one with the lowest solution costs as the initial probationary solution. The tree elaboration strategy, that is the strategy used in the searching of the branches, is another important factor in determining the speed of the optimization computation [81]. We will show in Section 4.4.3 that due to the unique property of our MAI QAP, we can formulate a strategy to lower the computational complexity significantly.

Whenever we do a partial assignment by fixing a code assigned to a user, we need to update the original cost matrix by removing the redundant rows and columns and redistribute the costs due to the partial assignment. We take for an example of $B = 3$ with the costs matrix illustrated in Figure 4.5(a). Assume that as a partial assignment, the first user is assigned the first code. Hence, $c_{0,0,0,0}$ automatically forms part of the solution and will be added to any solution cost that arises from this partial assignment. To redistribute the costs, the remaining elements in the submatrix $\mathbf{C}_{0,0}$ and their complementary costs are replaced by zeros and their combined values are added to the leader elements in the other

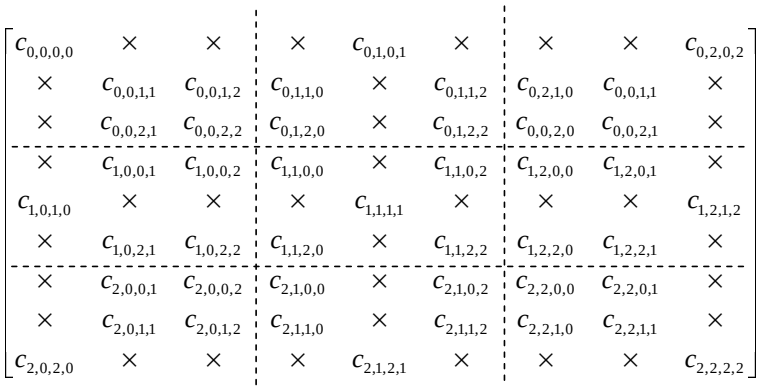

(a) Original Costs Matrix

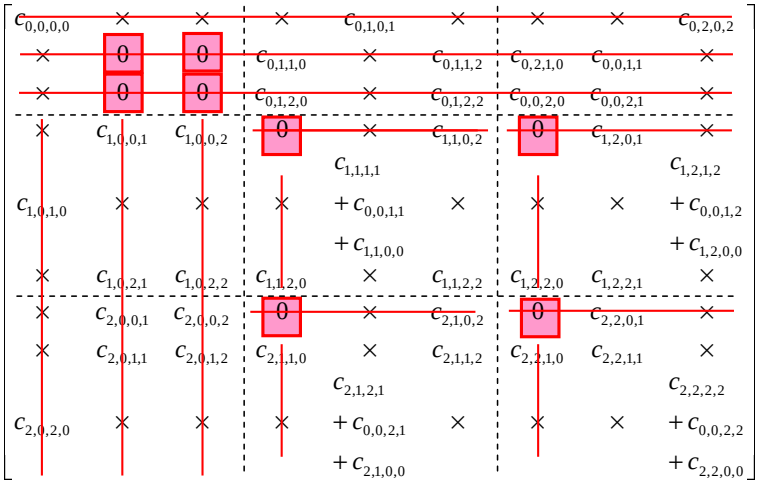

(b) Redistribution of Costs and Cancellations

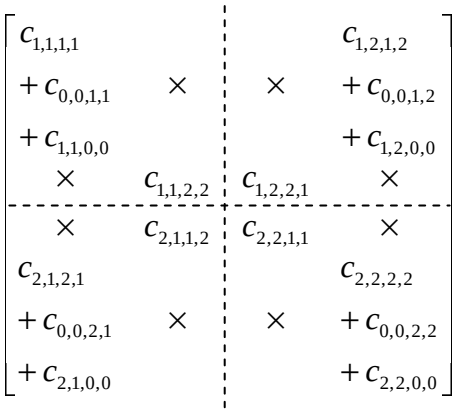

(c) New Costs Matrix

Figure 4.5: Changes to Cost Matrix due to Partial Assignment

submatrices as shown in Figure 4.5(b). The redistribution of costs will ensure that the new cost matrix will reflect the true costs that are inherent in performing the partial assignment. The redundant rows and columns are then cancelled as shown in Figure 4.5(b) to give the new reduced-size costs matrix given in Figure 4.5(c). The new costs matrix is then used to solve the cost minimizations

of the remaining code-to-user assignments.

4.4.3 Equivalent Solutions

We define equivalent solutions of the code assignment QAP as different code-to-user assignments that result in the same minimal cost value. Unlike general QAP, the cost matrix used to minimize the MAI does not have an inherent cost for assigning a particular code to a particular user. In other words, the costs are all due to pairwise interference between different users. Also, the entry-wise or Hadamard product of any pair of code vectors of popular spreading codes like the Walsh-Hadamard codes and orthogonal Gold codes [82] are limited to a set of vectors. Hence, the cost matrix will exhibit a certain degree of periodicity which can be exploited to significantly lower the computational complexity and increase the processing speed of the optimization process. The key lies in that the periodicity of the cost matrix will result in equivalent optimization solutions. By visiting those branches containing equivalent solutions only once instead of repeatedly during the search process, the optimization process will be much faster. We formerly state the theorem:

Theorem 4.4.1 *Consider a set of B bipolar spreading codes of length B where the Hadamard product of any two code vectors, $\boldsymbol{c}_i = [c_{0,i}, c_{1,i}, \ldots, c_{B-1,i}]^T$, $\boldsymbol{c}_j = [c_{0,j},\ c_{1,j}, \ldots, c_{B-1,j}]^T$, $i = 0, 1, \ldots, B-1$, $j = 0, 1, \ldots, B-1$, $i \neq j$, is limited to a set of $B-1$ vectors, X, i.e., $\boldsymbol{c}_i \circ \boldsymbol{c}_j = \boldsymbol{x}_k = [c_{0,i}c_{0,j}, c_{1,i}c_{1,j}, \ldots, c_{B-1,i}c_{B-1,j}]^T$, $\boldsymbol{x}_k \in X$, where $\circ$ represents the Hadamard product, i.e.,*

$$\begin{bmatrix} c_{0,i}c_{0,j} \\ c_{1,i}c_{1,j} \\ \vdots \\ c_{B-1,i}c_{B-1,j} \end{bmatrix} = \begin{bmatrix} x_{0,k} \\ x_{1,k} \\ \vdots \\ x_{B-1,k} \end{bmatrix} \tag{4.22}$$

The corresponding QAP represented by the cost matrix, $\boldsymbol{C}$, will have B dif-

ferent solution assignments with the same minimum cost and each user will be assigned a different code for each of the solution assignments.

To prove Theorem 4.4.1, we make use of the following lemma:

Lemma 4.4.2 *A Hadamard product of any code vector $\boldsymbol{c}_i$, $i = 0, 1, \ldots, B-1$, with vector, $\boldsymbol{x}_k \in X$, $k = 0, 1, \ldots, B-1$, is a one-to-one mapping to another distinct code vector $\boldsymbol{c}_j$, $j \neq i$.*

Proof Consider a particular code vector $\boldsymbol{c}_i$. The Hadamard product of $\boldsymbol{c}_i$ with each of the other $B-1$ code vectors will be a distinct vector. Since there is only $B-1$ vectors in the set X, for any pairs of $\boldsymbol{x}_k$, $k = 0, 1, \ldots, B-2$, and $\boldsymbol{c}_i$, $i = 0, 1, \ldots, B-1$, there is one and only one corresponding $\boldsymbol{c}_j$, $j \neq i$ such that $\boldsymbol{c}_i \circ \boldsymbol{c}_j = \boldsymbol{x}_k$. Hence, $\boldsymbol{x}_k \circ \boldsymbol{c}_i = (\boldsymbol{c}_i \circ \boldsymbol{c}_i) \circ \boldsymbol{c}_j$. Since for any bipolar code, $\boldsymbol{c}_i \circ \boldsymbol{c}_i$ is an all "1"s vector, $\boldsymbol{x}_k \circ \boldsymbol{c}_i = \boldsymbol{c}_j$. ∎

Thus, the proof for Theorem 4.4.1 is as follows:

Proof Consider a solution assignment, $\mathbf{V}$, to the QAP with the minimum cost of $C(\mathbf{V}) = \sum_{m,d,n,b} v_{mdnb} C_{mdnb}$. If we perform a Hadamard product of each of the assigned codes with $\boldsymbol{x}_k$, by Lemma 4.4.2, we will have a valid new assignment, $\mathbf{V}'$. Note that C_{mdnb}, for $m \neq n, b \neq d$, is a function of the Hadamard product of $\boldsymbol{c}_b$ and $\boldsymbol{c}_d$ as seen from (4.15). Since $(\boldsymbol{c}_b \circ \boldsymbol{x}_k) \circ (\boldsymbol{x}_k \circ \boldsymbol{c}_d) = \boldsymbol{c}_b \circ \boldsymbol{c}_d$, C_{mdnb} remain unchanged for the new assignment. Also as $C_{nbnb} = 0$, $C(\mathbf{V}') = C(\mathbf{V})$. Therefore, the new assignment $\mathbf{V}'$ is also a solution to the QAP. Since there are $B-1$ different $\boldsymbol{x}_k$, there are altogether B solution assignments with the same minimum cost. Moreover, each user will be assigned a different code in each of the solution assignments as these assignments are obtained through the Hadamard product with distinct $\boldsymbol{x}_k$. ∎

By Theorem 4.4.1, we can randomly assign the first user any code and arrive at different but equivalent solutions to the minimization problem. This simplifies the initial B QAP to a $B-1$ QAP resulting in a significant reduction in

computational complexity especially for large B as the number of branches to visit drops instantaneously by a factor of B. Moreover, the search for the initial probationary solution can be simplified by assigning the first user the first code in the code matrix as a rule. In other words, the initial probationary solution will be the solution to the linear assignment problem represented by $\mathbf{C}_{0,0}$ with the first row and column removed. Theorem 4.4.1 is also of high practical value since the required property is inherent to popular families of spreading codes such as the Walsh-Hadamard codes and orthogonal Gold codes.

4.4.4 Fast Code Assignment Algorithm

Theorem 4.4.1 is used to speed up the calculation of the optimal code assignment for certain spreading codes. We can reuse the theorem to perform fast code assignment by assuming that the residue interferences from successive interference cancellations are negligible, i.e. $\hat{P}_b = 0$. Given this assumption, each partial assignment results in a new QAP with reduced dimension. If the remaining codes to be assigned after the partial assignments satisfy the requirement in Theorem 4.4.1, which they often do, we can apply the theorem repeatedly to speed up the calculation accordingly as we visit the different branches.

We demonstrate the efficiency of the proposed optimal code assignment algorithms by tracking the number of branches the algorithms need to visit to arrive at the solution at the different levels and comparing them to the number of possible branches at each level. We consider a 64-users BS-IFDMA system with 5 MHz bandwidth and centre frequency of 2.4 GHz. The FFT size is fixed at 256, the spreading factor is, $B = 16$, and the number of frequency groups is, $G = 4$. The number of symbols per block for each user is, $S = 64$, and each user uses QPSK constellation for an identical data rate. The channel model for each user is assumed to be the same. The frequency-selective channel model has 16 independent, equal-power taps with Rayleigh fading and the classical

Table 4.1: Mean Number of Branches Visited.

Level	Total Possible Branches (T)	Proposed Optimal Algorithm ($\rho = 10^{-4}$) Number Visited (A)	Ratio (%) (A/T)	Fast Code Assignment ($\rho = 0$) Number Visited (B)	Ratio (%) (B/T)	(B/A)
1	16	1	6.250	1	6.250	100.0
2	240	13.63	5.679	13.58	5.658	99.63
3	3360	153.68	4.574	34.43	1.025	22.40
4	4.37×10^4	1465.53	3.355	307.05	0.703	20.95
5	5.24×10^5	1.20×10^4	2.290	1800.66	0.344	15.00
6	5.77×10^6	7.90×10^4	1.370	9440.32	0.164	11.95
7	5.77×10^7	3.21×10^5	0.556	2.74×10^4	0.048	8.559
8	5.19×10^8	4.81×10^5	0.093	3.63×10^4	0.007	7.539
9	4.15×10^9	6.10×10^4	0.001	4335.34	0.000	7.108
10	2.91×10^{10}	7747.40	0.000	574.36	0.000	7.414
11	1.74×10^{11}	3000.00	0.000	251.03	0.000	8.368
12	8.72×10^{12}	6029.84	0.000	480.08	0.000	7.962
13	3.49×10^{13}	1.27×10^4	0.000	843.99	0.000	6.620
14	1.05×10^{14}	1.52×10^4	0.000	756.41	0.000	4.970
15	2.09×10^{15}	0	0.000	0	0.000	-
16	2.09×10^{15}	0	0.000	0	0.000	-

Jakes' Doppler spread model [41]. In Table 4.1, we compare the performance of the proposed optimal algorithm in Section 4.4.3, setting the target BER level after cancellation to be $\rho = 10^{-4}$ which in turn determines $\hat{P}_b$, against that of the proposed fast code assignment which assumes $\rho = 0$. We simulate 100 sets of users with random mobility speed and report the mean number of branches visited by each algorithm in Table 4.1. The Walsh-Hadamard code is used as the spreading code. As can be seen from Table 4.1, the fast code assignment algorithm performs much more efficiently than the proposed optimal algorithm. After the second level, the ratio of the number of branches visited by the fast code assignment algorithm to that of the proposed optimal algorithm drops to less than a quarter and after the sixth level, the ratio drops to less than one-tenth. Moreover, the fast code assignment algorithm is able to obtain the same assignment solution as the proposed optimal algorithm 70% of the time as illustrated in Figure 4.6 which shows the histogram of the number of users with different codes assigned by the two algorithms. Even when the code assignments by the two algorithm differs greatly, the solution costs by either algorithms still remain

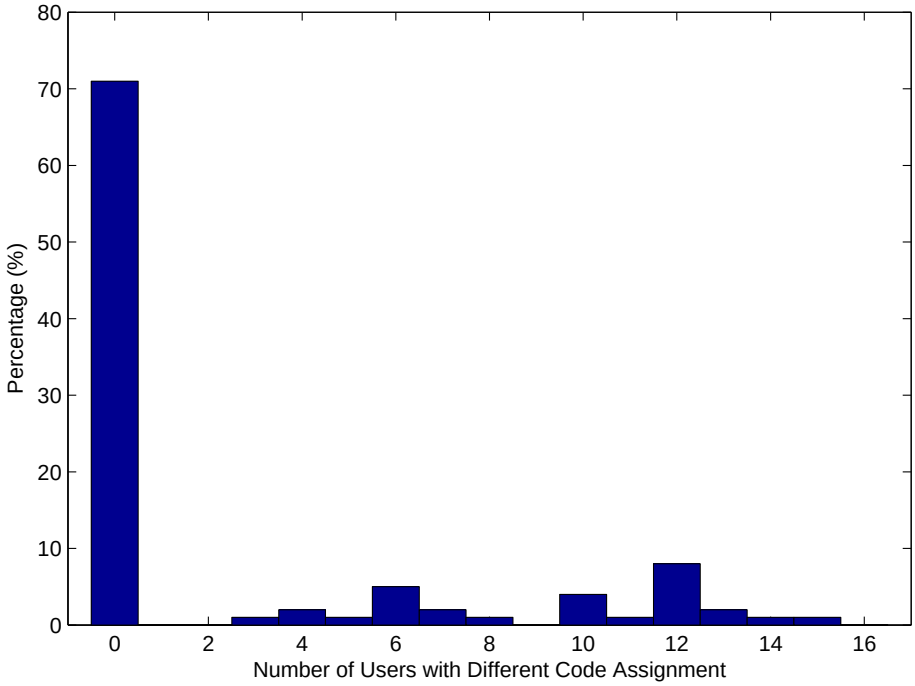

Figure 4.6: Histogram of Number of Users with Different Code Assigned by The Two Algorithms.

nearly identical.

4.5 Theoretical Performance Analysis

In this section, we derive the theoretical BER performance of a system employing the proposed mobility-based SIC scheme and compare it to that of a system that does not. The receiver applies a single-user linear minimum mean squared error (LMMSE) detector to the received signal of each user as given in (4.7). Using matrix notations, the LMMSE detector for the d^{th} user, $\boldsymbol{w}_d$ is given by

$$\mathbf{w}_d = \left(\overline{\mathbf{h}}_{d,d}\overline{\mathbf{h}}_{d,d}^H + \frac{\sigma^2}{P_d}\mathbf{I}\right)^{-1}\overline{\mathbf{h}}_{d,d} \tag{4.23}$$

Hence, $\mathbf{w}_d^H = \overline{\mathbf{h}}_{d,d}^H\left(\overline{\mathbf{h}}_{d,d}^H\overline{\mathbf{h}}_{d,d} + \frac{\sigma^2}{P_d}\mathbf{I}\right)^{-1}$. Let $\mathbf{A}_{d,d} = \left(\overline{\mathbf{h}}_{d,d}^H\overline{\mathbf{h}}_{d,d} + \frac{\sigma^2}{P_d}\mathbf{I}\right)^{-1}$.

Simplifying the expression, we get,

$$\begin{aligned}
\mathbf{A}_{d,d} &= \left[\left(\mathbf{U}^H\mathbf{F}_{d,d}\mathbf{U}\right)^H\left(\mathbf{U}^H\mathbf{F}_{d,d}\mathbf{U}\right)+\frac{\sigma^2}{P_d}\mathbf{I}\right]^{-1} \\
&= \left[\mathbf{U}^H\mathbf{F}_{d,d}^H\mathbf{U}\,\mathbf{U}^H\mathbf{F}_{d,d}\mathbf{U}+\frac{\sigma^2}{P_d}\mathbf{I}\right]^{-1} \\
&= \left[\mathbf{U}^H\mathbf{F}_{d,d}^2\mathbf{U}+\frac{\sigma^2}{P_d}\mathbf{I}\right]^{-1} \\
&= \left[\mathbf{U}^H\mathbf{G}_{d,d}\mathbf{U}\right]^{-1} \\
&= \mathbf{U}^H\mathbf{G}_{d,d}^{-1}\mathbf{U} \qquad (4.24)
\end{aligned}$$

where $\mathbf{U}$ is the discrete Fourier transform (DFT) matrix, $\mathbf{I}$ is the identity matrix, $\mathbf{F}_{d,d} = diag\left\{f_{d,d}(0), f_{d,d}(1), \ldots, f_{d,d}(S-1)\right\}$ is a diagonal matrix with the entries given by the DFT of the first column of $\overline{\mathbf{h}}_{d,d}$ and $\mathbf{F}_{d,d}^2 = \mathbf{F}_{d,d}^H\mathbf{F}_{d,d}$, and $\mathbf{G}_{d,d} = \mathbf{F}_{d,d}^2 + \frac{\sigma^2}{P_d}\mathbf{I}$. Let $\overline{\mathbf{h}}_{d,d}^{\{k\}}$ be the k^{th} column of the matrix $\overline{\mathbf{h}}_{d,d}$ and $\overline{\mathbf{H}}_{d,d}^{\{k\}}$ be formed from the matrix $\overline{\mathbf{h}}_{d,d}$ with the k^{th} column deleted. Considering the 1^{st} symbol of the d^{th} user, the signal-to-interference and noise ratio (SINR) after the detector is given as:

$$\begin{aligned}
\gamma_d &= \frac{\left|\left(\overline{\mathbf{w}}_{d,d}^{\{1\}}\right)^H\overline{\mathbf{h}}_{d,d}^{\{1\}}\right|^2}{\left(\mathbf{w}_{d,d}^{\{1\}}\right)^H\left[\overline{\mathbf{H}}_{d,d}^{\{1\}}\left(\overline{\mathbf{H}}_{d,d}^{\{1\}}\right)^H+\sum_{\substack{b=0\\b\neq d}}^{B-1}\overline{\mathbf{h}}_{d,b}\overline{\mathbf{h}}_{d,b}^H+\frac{\sigma^2}{P_d}\mathbf{I}\right]\mathbf{w}_{d,d}^{\{1\}}} \\
&= \frac{\left|\left(\overline{\mathbf{h}}_{d,d}^{\{1\}}\right)^H\mathbf{A}_{d,d}\overline{\mathbf{h}}_{d,d}^{\{1\}}\right|^2}{\left(\mathbf{w}_{d,d}^{\{1\}}\right)^H\left[\mathbf{A}_{d,d}^{-1}-\overline{\mathbf{h}}_{d,d}^{\{1\}}\left(\overline{\mathbf{h}}_{d,d}^{\{1\}}\right)^H+\sum_{\substack{b=0\\b\neq d}}^{B-1}\overline{\mathbf{h}}_{d,b}\overline{\mathbf{h}}_{d,b}^H\right]\mathbf{w}_{d,d}^{\{1\}}} \qquad (4.25)
\end{aligned}$$

Simplifying the numerator, we get,

$$\begin{aligned}
\left|\left(\overline{\mathbf{h}}_{d,d}^{\{1\}}\right)^H\mathbf{A}_{d,d}\overline{\mathbf{h}}_{d,d}^{\{1\}}\right|^2 &= \left|\left(\overline{\mathbf{h}}_{d,d}^{\{1\}}\right)^H\mathbf{U}^H\mathbf{G}_{d,d}^{-1}\mathbf{U}\overline{\mathbf{h}}_{d,d}^{\{1\}}\right|^2 \\
&= \left|\mathbf{f}_{d,d}^H\mathbf{G}_{d,d}^{-1}\mathbf{f}_{d,d}\right|^2 \\
&= \left(\frac{1}{S}\sum_{k=0}^{S-1}\frac{f_{d,d}^2(k)}{f_{d,d}^2(k)+\frac{\sigma^2}{P_d}}\right)^2 \qquad (4.26)
\end{aligned}$$

where $\mathbf{f}_{d,d} = [f_{d,d}(0), f_{d,d}(1), \ldots, f_{d,d}(S-1)]^T$ is the DFT of the first column of $\overline{\mathbf{h}}_{d,d}$. Simplifying the denominator we get,

$$
\begin{aligned}
& \left(\mathbf{w}_{d,d}^{\{1\}}\right)^H \left[\mathbf{A}_{d,d}^{-1} - \overline{\mathbf{h}}_{d,d}^{\{1\}} \left(\overline{\mathbf{h}}_{d,d}^{\{1\}}\right)^H + \sum_{\substack{b=0 \\ b\neq d}}^{B-1} \overline{\mathbf{h}}_{d,b} \overline{\mathbf{h}}_{d,b}^H\right] \mathbf{w}_{d,d}^{\{1\}} \\
= & \left(\overline{\mathbf{h}}_{d,d}^{\{1\}}\right)^H \mathbf{A}_{d,d} \mathbf{A}_{d,d}^{-1} \mathbf{A}_{d,d} \overline{\mathbf{h}}_{d,d}^{\{1\}} - \left(\mathbf{w}_{d,d}^{\{1\}}\right)^H \overline{\mathbf{h}}_{d,d}^{\{1\}} \left(\overline{\mathbf{h}}_{d,d}^{\{1\}}\right)^H \mathbf{w}_{d,d}^{\{1\}} \\
& + \sum_{\substack{b=0 \\ b\neq d}}^{B-1} \left(\mathbf{w}_{d,d}^{\{1\}}\right)^H \overline{\mathbf{h}}_{d,b} \overline{\mathbf{h}}_{d,b}^H \mathbf{w}_{d,d}^{\{1\}} \\
= & \left(\overline{\mathbf{h}}_{d,d}^{\{1\}}\right)^H \mathbf{A}_{d,d} \overline{\mathbf{h}}_{d,d}^{\{1\}} - \left|\left(\overline{\mathbf{w}}_{d,d}^{\{1\}}\right)^H \overline{\mathbf{h}}_{d,d}^{\{1\}}\right|^2 + \frac{1}{S} \sum_{\substack{b=0 \\ b\neq d}}^{B-1} \mathbf{f}_{d,d}^H \mathbf{G}_{d,d}^{-1} \mathbf{F}_{d,b}^2 \mathbf{G}_{d,d}^{-1} \mathbf{f}_{d,d} \\
= & S\left(\mathbf{f}_{d,d}^H \mathbf{G}_{d,d}^{-1} \mathbf{f}_{d,d}\right) - \left|\mathbf{f}_{d,d}^H \mathbf{G}_{d,d}^{-1} \mathbf{f}_{d,d}\right|^2 + S \sum_{\substack{b=0 \\ b\neq d}}^{B-1} \mathbf{f}_{d,d}^H \mathbf{G}_{d,d}^{-1} \mathbf{F}_{d,b}^2 \mathbf{G}_{d,d}^{-1} \mathbf{f}_{d,d} \\
= & \frac{1}{S^2} \left(\frac{\sigma^2}{P_d} \sum_{k=0}^{S-1} \frac{1}{f_{d,d}^2(k) + \frac{\sigma^2}{P_d}}\right) \left(\sum_{k=0}^{S-1} \frac{f_{d,d}^2(k)}{f_{d,d}^2(k) + \frac{\sigma^2}{P_d}}\right) \\
& + \frac{1}{S} \sum_{\substack{b=0 \\ b\neq d}}^{B-1} \left(\sum_{k=0}^{S-1} \frac{f_{d,d}^2(k) f_{d,b}^2(k)}{\left(f_{d,d}^2(k) + \frac{\sigma^2}{P_d}\right)^2}\right)
\end{aligned}
\tag{4.27}
$$

where $\mathbf{f}_{d,b} = [f_{d,b}(0), f_{d,b}(1), \ldots, f_{d,b}(S-1)]^T$ is the DFT of the first column of $\overline{\mathbf{h}}_{d,b}$.

Since both $\overline{\mathbf{h}}_{d,d}$ and $\mathbf{A}_{d,d}$ are cyclic matrices, the SINR for every symbol of the d^{th} user are equivalent. Hence after applying the LMMSE detector to the received signal of each user, the SINR for the d^{th} user after the detector is given as:

$$
\gamma_d = \frac{\alpha_d}{\beta_d} \left[1 + \frac{S}{\alpha_d \beta_d} \sum_{\substack{b=0 \\ b\neq d}}^{B-1} \chi_{d,b}\right]^{-1} \tag{4.28}
$$

where

$$
\alpha_d = \sum_{k=0}^{S-1} \frac{f_{d,d}^2(k)}{f_{d,d}^2(k) + \frac{\sigma^2}{P_d}} \tag{4.29}
$$

$$\beta_d = \frac{\sigma^2}{P_d} \sum_{k=0}^{S-1} \frac{1}{f_{d,d}^2(k) + \frac{\sigma^2}{P_d}} \tag{4.30}$$

$$\chi_{d,b} = \sum_{k=0}^{S-1} \frac{f_{d,d}^2(k) f_{d,b}^2(k)}{\left(f_{d,d}^2(k) + \frac{\sigma^2}{P_d}\right)^2} \tag{4.31}$$

Note that the SINR for the case of no MAI (i.e. $\chi_{d,b} = 0$ for all b) is given by $\frac{\alpha_d}{\beta_d}$.

Similarly, considering the input signal after each stage of interference cancellation [69], the SINR for the d^{th} user after the LMMSE detector is given as:

$$\gamma_d = \frac{\alpha_d}{\beta_d} \left[1 + \frac{S}{\alpha_d \beta_d} \left(\sum_{b=0}^{d-1} \rho_b \chi_{d,b} + \sum_{b=d+1}^{B-1} \chi_{d,b} \right) \right]^{-1} \tag{4.32}$$

and $\rho_b = \frac{\hat{P}_b}{P_b}$.

The average bit error-rate (BER) for the individual user can then be calculated by averaging the conditional bit error probability over the SINR [83]. Thus, the BER for the d^{th} user can be written as:

$$BER_d = \int_0^\infty P_E(\gamma) p_d(\gamma) d\gamma \tag{4.33}$$

where $P_E(\gamma)$ is the bit error probability conditional on the SINR, γ, and $p_d(\gamma)$ is the probability density function of the SINR for the d^{th} user. Alternatively, by performing the integration in (4.33) by parts [84], the BER can be represented as:

$$BER_d = -\int_0^\infty P'_E(\gamma) F_d(\gamma) d\gamma \tag{4.34}$$

where $P'_E(\gamma) = \frac{d}{d\gamma} P_E(\gamma)$ and $F_d(\gamma)$ is the cumulative distribution function of the SINR or outage probability for the d^{th} user. For QPSK, the conditional error

probability is given by:

$$\begin{aligned} P_E(\gamma) &= Q(\sqrt{\gamma}) \\ &= \frac{1}{\sqrt{\pi}} \int_{\sqrt{\frac{\gamma}{2}}}^{\infty} e^{-t^2} \mathrm{d}t \\ &= \frac{1}{2} \frac{1}{\sqrt{2\pi}} \int_{\gamma}^{\infty} e^{-\frac{t}{2}} t^{-\frac{1}{2}} \mathrm{d}t \\ &= \frac{1}{2} - \frac{1}{2} \frac{1}{\sqrt{2\pi}} \int_{0}^{\gamma} e^{-\frac{t}{2}} t^{-\frac{1}{2}} \mathrm{d}t \end{aligned} \tag{4.35}$$

Hence,

$$P'_E(\gamma) = -\frac{1}{2} \frac{1}{\sqrt{2\pi}} e^{-\frac{\gamma}{2}} \gamma^{-\frac{1}{2}} \tag{4.36}$$

For Rayleigh fading channels, the SINR for the d^{th} user can be easily simplified from (4.28) and (4.32) as:

$$\gamma_d = \frac{X_d}{\sigma^2 + Y_d} \tag{4.37}$$

where $X_d \sim$ Exponential$(\bar{\gamma}_d)$ (i.e. X_d is a random variable with exponential distribution with the mean, $\bar{\gamma}_d$, given by:

$$\bar{\gamma}_d = P_d \left\{ \frac{1}{B} + \frac{2}{B^2} \sum_{k=1}^{B-1} (B-k) J_0 \left[2\pi \left(k \right) f_D(d) \tau \right] \right\} \tag{4.38}$$

and Y_d is a summation of $B-1$ independent random variables, $Y_{d,b}$, where $Y_{d,b} \sim$ Exponential$(\bar{\gamma}_{d,b})$, with $\bar{\gamma}_{d,b}$ given by:

$$\bar{\gamma}_{d,b} = \lambda_{d,b} P_b \sum_{k=0}^{B-1} \sum_{l=0}^{B-1} z_{d,b}(k,l) J_0 \left[2\pi \left(k-l \right) f_D(b) \tau \right] \tag{4.39}$$

where the parameter $\lambda_{d,b}$ is used to effect the change in the mean SINR when interference cancellations are used. Hence, when interference cancellations are not used, $\lambda_{d,b} = 1$ for all d, b. When interference cancellations are used, $\lambda_{d,b} = 1$, for $b > d$ and $\lambda_{d,b} = \rho_b$, for $b < d$.

The outage probability for γ_d is given by

$$\begin{aligned} F_d(\gamma) &= \text{Prob}\left(\gamma_d < \gamma\right) \\ &= \text{Prob}\left(\frac{X_d}{\sigma^2 + Y_d} < \gamma\right) \\ &= \text{Prob}\left[X_d < \gamma\left(\sigma^2 + Y_d\right)\right] \\ &= \int_0^\infty \text{Prob}\left[X_d < \gamma\left(\sigma^2 + Y_d\right)\right]\big|_{Y_d=y} p_y(y)\mathrm{d}y \\ &= \int_0^\infty \left(1 - e^{-\frac{\gamma(y+\sigma^2)}{\bar{\gamma}_d}}\right) p_y(y)\mathrm{d}y \\ &= \int_0^\infty p_y(y)\mathrm{d}y - e^{-\frac{\gamma\sigma^2}{\bar{\gamma}_d}} \int_0^\infty e^{-y\frac{\gamma}{\bar{\gamma}_d}} p_y(y)\mathrm{d}y \\ &= 1 - e^{-\frac{\sigma^2}{\bar{\gamma}_d}\gamma} \Psi_{Y_d}\left(-\frac{\gamma}{\bar{\gamma}_d}\right) \end{aligned} \tag{4.40}$$

where $\Psi_{Y_d}(s)$ is the moment-generating function (MGF) of Y_d. Since, Y_d is a summation of independent exponential random variables, its moment-generating function is simply the product of the MGFs of the constituent random variables. The MGF of an exponential random variable with mean $\bar{\gamma}$ is given as $\Psi(s) = (1 - s\bar{\gamma})^{-1}$. Thus,

$$\begin{aligned} \Psi_{Y_d}\left(-\frac{\gamma}{\bar{\gamma}_d}\right) &= \prod_{\substack{b=0 \\ b\neq d}}^{B-1} \Psi\left(-\frac{\gamma}{\bar{\gamma}_d}\right) \\ &= \prod_{\substack{b=0 \\ b\neq d}}^{B-1} \left(1 + \frac{\bar{\gamma}_{d,b}}{\bar{\gamma}_d}\gamma\right)^{-1} \\ &= \sum_{\substack{b=0 \\ b\neq d}}^{B-1} A_{d,b} \left(1 + \frac{\bar{\gamma}_{d,b}}{\bar{\gamma}_d}\gamma\right)^{-1} \end{aligned} \tag{4.41}$$

where

$$A_{d,b} = \prod_{\substack{i=0 \\ i\neq b,d}}^{B-1} \frac{\bar{\gamma}_{d,b}}{\bar{\gamma}_{d,b} - \bar{\gamma}_{d,i}} \tag{4.42}$$

Note that the simplification using partial fractions in the last line of (4.41) assumes the usual case of distinct $\bar{\gamma}_{d,b}$ with the associated coefficients in (4.42). For non-distinct $\bar{\gamma}_{d,b}$, the coefficients can be generalized as in [85]. Substituting

(4.36), (4.40) and (4.41) into (4.34) and simplifying, we get,

$$BER_d = \frac{1}{2} - \frac{1}{2}\sqrt{\frac{\bar{\gamma}_d}{2\pi}} \sum_{\substack{b=0 \\ b\neq d}}^{B-1} \frac{A_{d,b}}{\sqrt{\bar{\gamma}_{d,b}}} \int_0^\infty e^{-u\left(\frac{\bar{\gamma}_d+2\sigma^2}{2\bar{\gamma}_{d,b}}\right)} u^{-\frac{1}{2}} (1+u)^{-1} \, \mathrm{d}u$$

The integral in (4.43) can be simplified using the hypergeometric function of the second kind (i.e. the Tricomi function), $U_T(a, b, s)$. Thus, for the case where QPSK is used as the modulation scheme and the channels are approximately Rayleigh fading, the BER for the d^{th} user can be simplified as:

$$BER_d = \frac{1}{2} - \frac{1}{2}\sqrt{\frac{\bar{\gamma}_d}{2}} \sum_{\substack{b=0 \\ b\neq d}}^{B-1} \frac{A_{d,b}}{\sqrt{\bar{\gamma}_{d,b}}} U_T\left(\frac{1}{2}, \frac{1}{2}, \frac{\bar{\gamma}_d + 2\sigma^2}{2\bar{\gamma}_{d,b}}\right) \tag{4.43}$$

and $U_T(a, b, s)$ is the Tricomi function defined as:

$$U_T(a, b, s) = \frac{1}{\Gamma(a)} \int_0^\infty e^{-sx} x^{a-1} (1+x)^{b-a-1} \, \mathrm{d}x \tag{4.44}$$

where $\Gamma(a)$ is the gamma function. We can evaluate the BER by using a series representation of the Tricomi function, which converges for our case, or through numerical integration. To illustrate the benefits of the proposed interference cancellation scheme, we consider a scenario where only a single user in the system is moving with the other users having negligible movement. The spreading factor, $B = 16$, is used.

Like other interference limited systems, we are interested in the error floor of the BER when the noise power is insignificant or negligible. In Figure 4.7, we plot the theoretical BER and the BER error floor of the user suffering the greatest level of interference against the mobility speed of the moving user. We compared the case where no interference cancellation scheme is used with the case where interference cancellation scheme is used with two different BER levels of the moving user (i.e. $\rho = 10^{-3}$ and 10^{-5}). As can be expected, the BER error floors for the cases with interference cancellation are lower bounded by

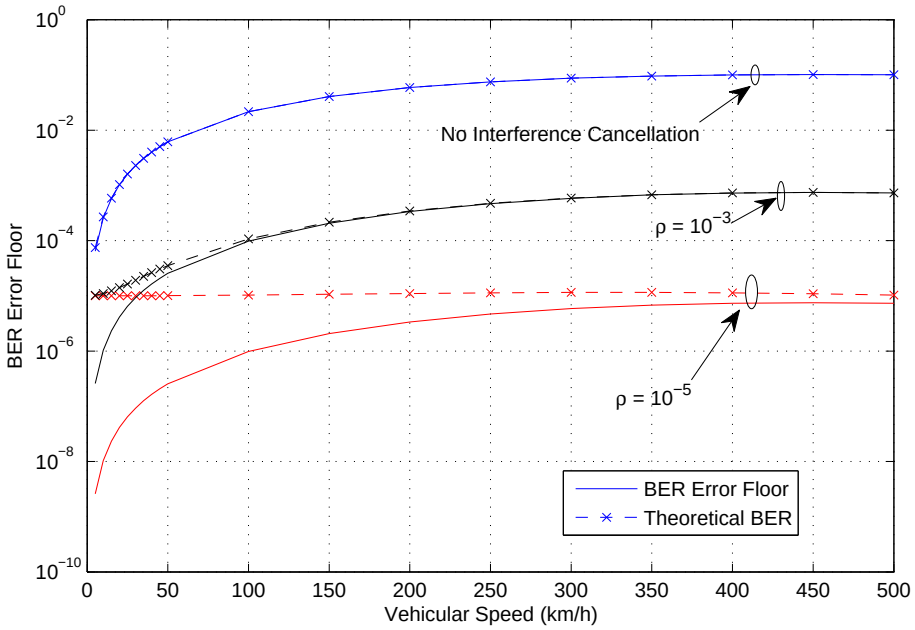

Figure 4.7: Theoretical BER Error Floor.

the BER of the moving user with the bound getting tighter as the mobility of the user increased. Also, the gap between the actual BER and the error floor become wider for lower ρ due to the greater cancellation accuracy. More importantly, the BER error floor are significantly higher when no interference cancellation scheme is used. Furthermore, even relatively low mobility speed of 50 km/h can result in high error floor of 5×10^{-3} if interference cancellation is not used. The theoretical analysis above illustrates the importance of having mobility-based interference cancellation to realize a practical operating BER level.

4.6 Simulation Results

4.6.1 Simulation System

We consider a 64-users BS-IFDMA system with 5 MHz bandwidth and centre frequency of 2.4 GHz. The FFT size is fixed at 256, the spreading factor, $B = 16$, and the number of frequency groups, $G = 4$. The number of symbols per block for each user, $S = 64$, and the typical urban channel model [86] is used.

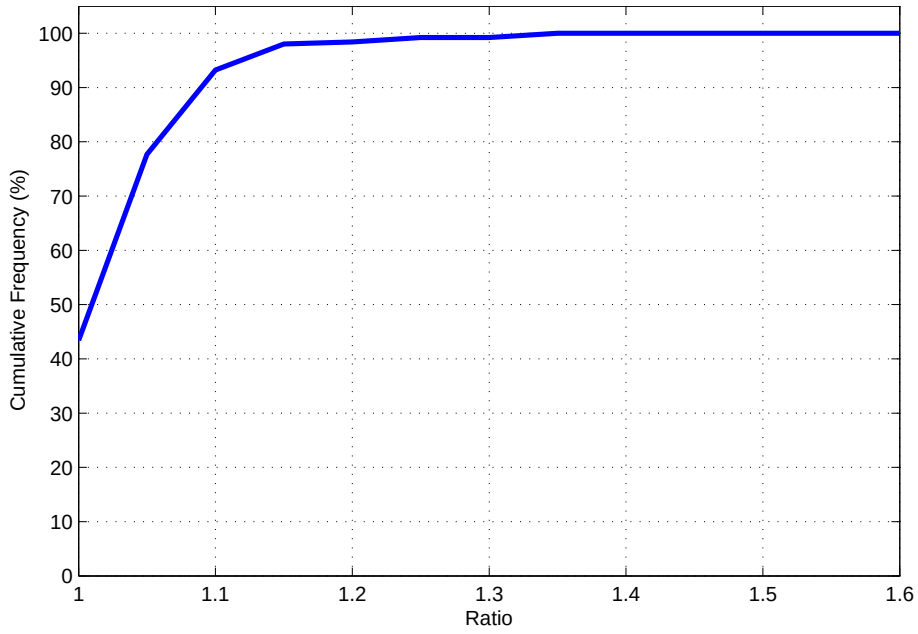

Figure 4.8: Cumulative Frequency of the Ratio (MAI using Code Assignment $\mathbf{V}_M$: MAI using Code Assignment $\mathbf{V}_A$).

4.6.2 Channel Dependent Code Assignment

We have been focusing on code assignment using the channels' statistics instead of the actual transmission channels due to the difficulty of accurately estimating channels with high Doppler spread. In this section, we quantify the difference between the code assignment based on the average MAI power conditioned on the users channel in (4.13) and the code assignment based on the mean MAI power averaged over different sets of users channels in (4.14). We consider the scenario where the speeds of 16 users in a frequency group are evenly distributed from 0 km/h to 375 km/h with 25 km/h separation. The code assignment, $\mathbf{V}_M$, based on the mean MAI power is then determined using the fast code assignment algorithm. We then simulate 250 sets of users channels with the same mobility profile and use the fast code assignment algorithm to determine the code assignment, $\mathbf{V}_A$, based on the average MAI power for each set of channels. We then calculate, for each set of channels, the ratio of the sum of the average MAI power using the code assignment $\mathbf{V}_M$ to the sum of the average MAI power using the code assignment $\mathbf{V}_A$. In Figure 4.8, the cumulative fre-

quency graph of the ratio is plotted. As can be seen from Figure 4.8, the relative difference between the two sums are small with 90% of the ratios falling below 1.1. Therefore, the benefit of using actual channels to perform code assignment is relatively small. In other words, we only need to estimate the users' mobility to assign the spreading codes to the users effectively. Doing so avoids the impracticality of estimating channels of high-mobility users for codes assignment before the actual data transmission.

4.6.3 System BER with High Mobility Users

The aim of the mobility-based interference cancellation scheme is to enable the system to include high-mobility users in it without degrading the overall system BER performance. Hence, we investigate the changes in the system BER as the system is increasingly loaded with high-mobility users. We assume that all the frequency groups in the system share the same user mobility profile and simulate the BER performance for just one of the frequency groups.

We consider three different mobility profiles: moderate-speed profile, high-speed profile and ultra high-speed profile. For each profile, the system will consist of two groups of users: stationary users and high-mobility users. The high-mobility users in the system will be assigned speeds at 5km/h separation in descending order starting from a top speed. The top speed is 95 km/h, 175 km/h and 350 km/h for the moderate-speed, high-speed and ultra high-speed profile respectively. In Figure 4.9, we plot the BER against the number of mobility users in a system using Walsh-Hadamard spreading codes and QPSK constellation with the high-speed profile. We compare the uplink BER performances of five different systems; System 1: BS-IFDMA system without interference cancellation, System 2: BS-IFDMA system with mobility-based interference cancellation and random code assignment, System 3: BS-IFDMA system with mobility-based interference cancellation and code assignment based on

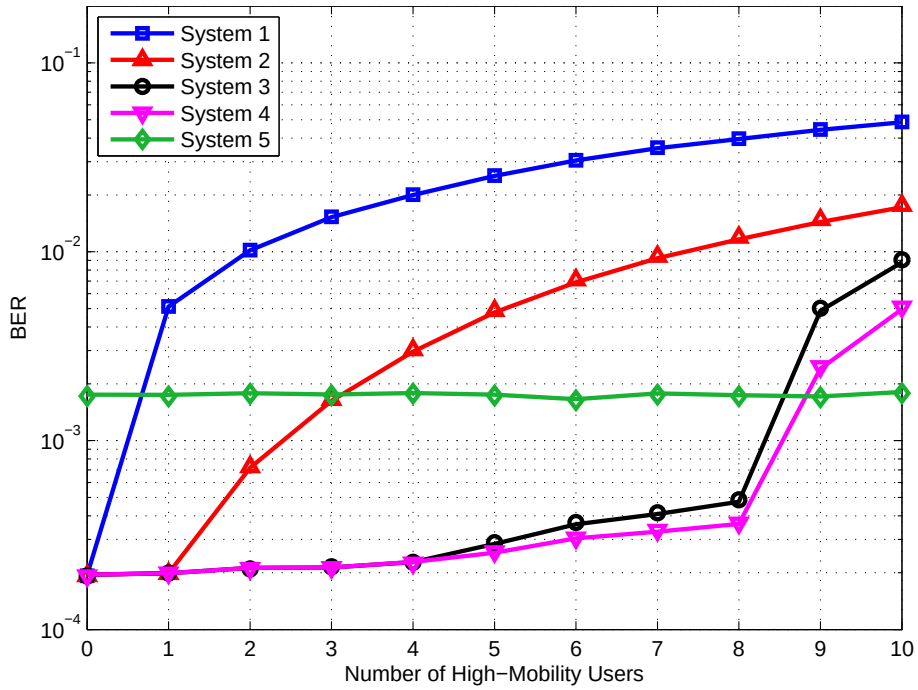

Figure 4.9: BER Comparisons between Different Systems.

the mean MAI power in (4.14), System 4: BS-IFDMA system with mobility-based interference cancellation and code assignment based on the average MAI power in (4.13) and System 5: a baseline IFDMA system used for comparison.

In Figure 4.9, the lines are the theoretical BER and the markers are the simulated BER for $E_b/N_0 = 16dB$. Without mobility-based interference cancellation, the system BER increases significantly with a single high-mobility user in the system. Moreover, the mobility-based interference cancellation scheme though beneficial in improving the system BER, is unable to, by itself, prevent the BER degradation beyond the first high-mobility user. Only when coupled with the proposed code assignment does the mobility-based interference cancellation scheme manage to maintain the BER performance for up to eight high-mobility users, or half the total number of users, as evident from the performance of System 3 and 4. Also, there is no significant difference between the BER performance of System 3 and 4, which reinforces the point that actual channel knowledge is unnecessary in performing code assignment. The IFDMA system, System 5, maintains its performance as the number of high mobility users increases as expected. However, IFDMA performance is worse than that

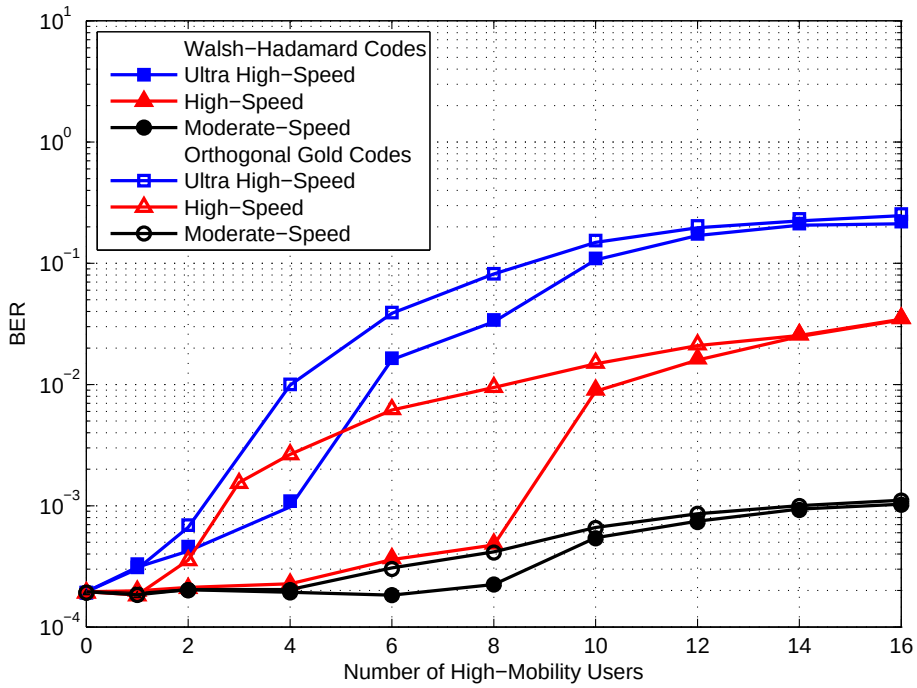

Figure 4.10: BER Comparisons between Different Spreading Codes.

of the BS-IFDMA systems with small number of high mobility users because of the loss of frequency diversity as the same bandwidth is shared among more users in the IFDMA system than compared to the BS-IFDMA systems which allocates some of the users in the code domain, resulting in greater bandwidth for each user.

In Figure 4.10, we compare the BER performances of System 3 for the three different mobility profiles using two different spreading codes: Walsh-Hadamard codes and Orthogonal Gold codes. The Walsh-Hadamard codes outperform the Orthogonal Gold Codes for all three mobility profiles at low number of high-mobility users as shown in Figure 4.10 because the Orthogonal Gold codes have more uniform cross-correlation profiles than the Walsh-Hadamard codes. Nevertheless, the system using Orthogonal Gold codes is able to tolerate at least four users with moderate speed of 80 km/h to 95 km/h without any significant performance degradation.

4.6.4 Operational System BER

Our theoretical analysis and simulation results show that BS-IFDMA system can be designed conscientiously to allow high-mobility users in the system without any significant performance degradation. The key is to distribute the users with ultra-high speed to different frequency groups thus limiting their number within a single frequency group. Using the above system configuration as an example, the number of users with ultra-high speed of above 200 km/h within a frequency group should be limited to two and the number of users with high speed of above 100 km/h should be limited to four while the total number of users with mobility greater than 20 km/h should be kept to eight or below. Using these guidelines, we generate 1000 random users' mobility profiles and simulate the BER performance of a BS-IFDMA using the proposed cancellation scheme. We consider a convolutional coded system using QPSK and 16-QAM constellations. The code rate is 1/2 and the generator polynomial [5 7] is used.

To quantify the effect of mobility and channel estimation on the proposed scheme, we compare the performance for three different sets of assumptions. First, we assume that the receiver has ideal estimates of the users' mobility and channel which provides the ideal performance of the proposed scheme. Second, ideal channel estimation is assumed at the base-station for the decoding of the packet while the estimated mobility of each device used in the code assignment is assumed to be uniformly distributed between $\pm 20\%$ of the true mobility. Third, in addition to the use of estimated mobilities for code assignment as mentioned above, channel estimation is performed at the base-station using the pilot-aided interpolation technique in [38].

In Figure 4.11, we compare the BER performances of a coded BS-IFDMA system with the proposed SIC under the three different sets of assumptions. We also plot the performance of a coded BS-IFDMA system without SIC under the ideal channel estimation assumption for comparison. We also simulate the performances of a coded IFDMA system with the same set of users under

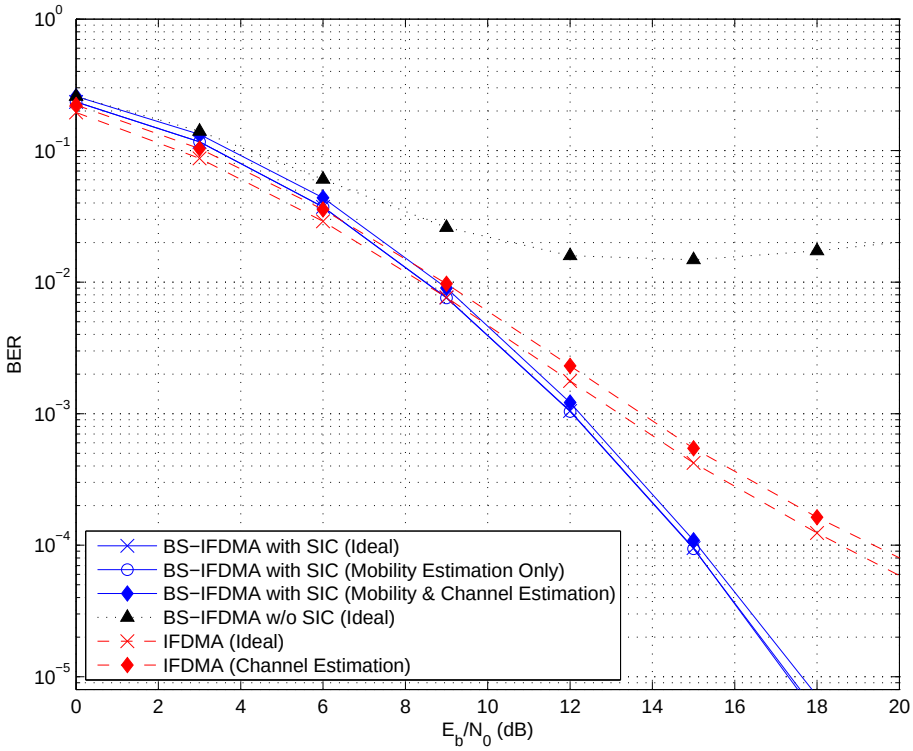

(a) QPSK System

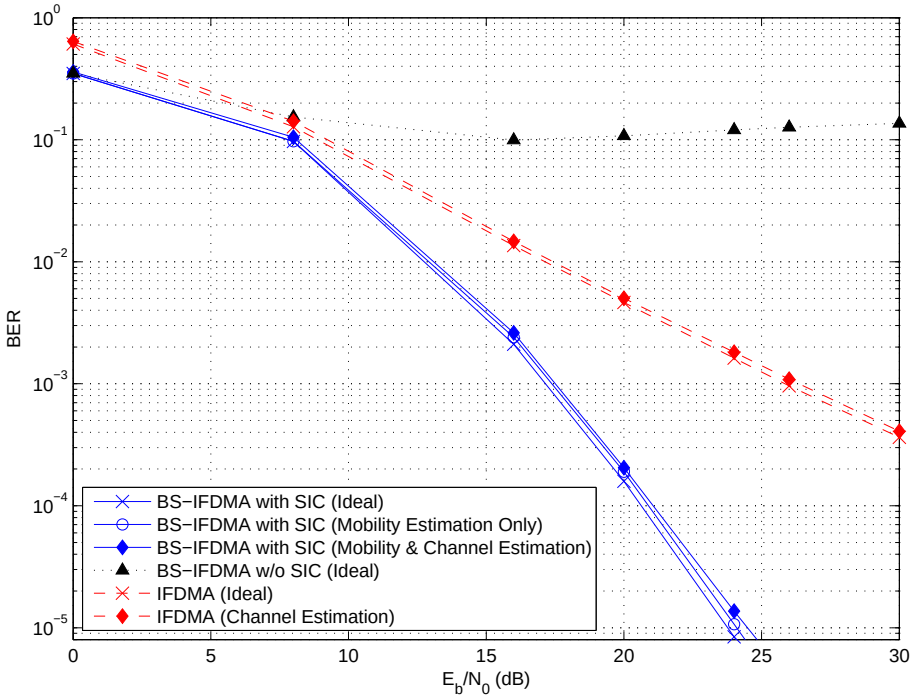

(b) 16-QAM System

Figure 4.11: BER Performance of Coded BS-IFDMA System

ideal and practical channel estimation assumptions for comparison. The BER performances for two different constellations: QPSK and 16-QAM are plotted in Figure 4.11(a) and Figure 4.11(b) respectively. The BER of the BS-IFDMA

system without SIC hits a high error floor as expected from our analysis. The performance degradation of the BS-IFDMA system with the proposed SIC due to non-ideal mobility estimation is minimal for both QPSK and 16-QAM. This is within our expectation as the pairwise interference shown in Figure 4.1 shows distinct limiting upperbound for each pair of codes. The interference is almost constant beyond a certain mobility and hence an accurate estimation in the region of high mobility is not required. On the other hand, at low mobility, the difference in the interference are small enough that a non-ideal assignment does not degrade the overall performance significantly. Also, the performance degradation due to channel estimation is within 0.5dB for both QPSK and 16-QAM systems. The BS-IFDMA system with SIC also outperforms the IFDMA system due to the gain in frequency diversity as mentioned above and the ability of the proposed cancellation scheme to limit the MAI in the system.

4.7 Chapter Summary

In this chapter, a BS-IFDMA system using the principle of TLS-CDMA is considered to achieve a frequency reuse factor of 1 by using cell-specific spreading code to efficiently suppress OCI in a multi-cells environment. We introduced a novel multiple access interference cancellation scheme based on users' mobility and demonstrated, through theoretical analysis and simulations, the ability of the proposed scheme to incorporate high mobility users with speed up to 375 km/h in BS-IFDMA system with no performance degradation. To maximize the benefits of the proposed mobility-based interference cancellation scheme, we optimize the spreading codes assignment to the users in the system. The optimization problem is formulated as a quadratic assignment problem for minimizing the interference in the system through an optimal code-to-user assignment. We proposed a computationally efficient algorithm that solves the NP-hard assignment problem faster by a factor equal to five times the number of users in the

system. With proper codes assignment, half of the users in BS-IFDMA system can have high mobility without causing any system performance degradation. The proposed scheme can be used for any block spread systems with or without an additional layer of frequency division multiple access but the use of IFDMA does allow for the distribution of users with very high mobility to different frequency groups and thus limits the severe interference caused by them within any single frequency group.

Chapter 5

Summary

In this chapter, we provide a summary of the contributions in the thesis along with suggestions of some possible future works on the topics covered in the thesis. We have analyzed the performance of the coded MIMO-IFDMA system and proposed an iterative soft QRD-M algorithm to maximize the diversity performance of coded MIMO-IFDMA system with various numerical configurations of transmit and receive antennas. Going forward, it will be worthwhile to investigate the trade-off between computational complexity and performance of the proposed algorithm by limiting the number of channel variables considered in each stage of the LLR calculations. We have also proposed a novel transmit diversity scheme for coded MIMO-IFDMA system which achieves the same order of diversity gain as the number of transmit antennas used. Channel estimation for the different antennas can be performed by using orthogonal pilots. However, given the limited number of sequences with good cross-correlation properties, future research effort can be directed to investigate the joint estimation for the channels of different antennas. Our proposed successive MAI cancellation scheme for BS-IFDMA system has been shown to be effective in maintaining performance when the system is loaded with high mobility users through the proposed optimal code assignment. Further research can be in the direction of using more sophisticated cancellation schemes like parallel cancellations or iterative cancellations with corresponding optimal code assignments to enhance the performance.

5.1 Summary of Thesis Contributions

In Chapter 2, the signal model of a coded MIMO-IFDMA system is formulated in the time domain using matrix form that typifies the signal model of conventional multiple input and multiple output communications. Using this formulation, the coded MIMO-IFDMA system can be viewed as a system with a complex-field code serially concentrated with an outer error-correcting code. Thus, the principles of iterative turbo decoding is applied, resulting in a proposed iterative detection and decoding algorithm for coded MIMO-IFDMA systems. The proposed algorithm incorporates a low-complexity soft decision QRD-M detector in place of the APP detector. Since it has a generalized form, a common shared hardware platform can be used to enable real-time switching between operation for single transmit antenna and multiple transmit antennas operations. We also conducted a performance analysis on the BER performance of IFDMA system using the time domain model, establishing the link between the theoretical performance with the distribution of the channel profile. We show that it is possible to achieve the maximum channel diversity order either through the use of frequency hopping or block spreading. Frequency hopping is simpler to implement than block spreading but block spreading has the additional benefit of lower inter-cell interferences and can achieve better performance with the simple FDE. Through simulations, we show that the proposed iterative algorithm is able to improve the BER performance significantly using a small number of iterations. Moreover, the iterative algorithm has been shown to be particularly useful in improving the BER performance of the system with larger channel diversity order. The simulated performance has also been shown to match the matched filter lower bound performance at high SNR.

In Chapter 3, we introduce a novel transmit diversity scheme for coded IFDMA system which, like the CDD scheme, preserves the low PAPR property of IFDMA signal and can be easily adapted for different numerical configurations of transmit antennas. The proposed ASD scheme has a guaranteed

diversity gain factor equal to the number of transmit antennas and can be used in conjunction with the CDD scheme in various configurations to suit the requirements of different systems. Both our theoretical analysis and simulation results show that the proposed ASD scheme outperforms the CDD scheme when the number of transmit antennas increases beyond the diversity gain limit of the CDD scheme. We also demonstrate the benefits of combining the proposed ASD scheme with the CDD scheme through theoretical analysis and simulations, with a design specification for the combination.

In Chapter 4, a BS-IFDMA system using the principle of TLS-CDMA is considered to achieve a frequency reuse factor of 1 by using cell-specific spreading code to efficiently suppress OCI in a multi-cells environment. We derive the multiple access interference (MAI) in BS-IFDMA system under time-varying channel and introduce a novel MAI cancellation scheme based on the users' mobilities. The proposed scheme first distribute the high mobility users evenly across the different frequency groups so that the multiple access interference within each group is limited. A simple successive MAI cancellation algorithm is then applied within each frequency group. We demonstrate, through theoretical analysis and simulations, the ability of the proposed scheme to incorporate high mobility users with speed of up to 375 km/h in BS-IFDMA system with no performance degradation. To maximize the benefits of the proposed mobility-based interference cancellation scheme, we optimize the spreading codes assignment to the users in the system. The optimization problem is formulated as a quadratic assignment problem for minimizing the interference in the system through an optimal code-to-user assignment. We proposed a computationally efficient algorithm that solves the NP-hard assignment problem faster by a factor of five times the number of users in the system. With proper codes assignment, half of the users in BS-IFDMA system can have high mobility without causing any system performance degradation.

5.2 Future Works

In Chapter 2, we introduced a low-complexity soft decision QRD-M detector as an implementable alternative to the computationally complex APP detector. We also show that the $\mathbf{R}$ matrix after the QR decomposition is based on the auto-correlation of the channel impulse response. Thus, it is possible to design a real-time adaptation of the soft decision QRD-M detector so that the LLR computation is limited to the strongest few contributors in the $\mathbf{R}$ matrix. This will reduce the computation requirement significantly. However, the theoretical optimum rules to minimize the computational complexity without sacrificing too much of the diversity performance are not straight forward. Considerable future research effort is needed to achieve the optimal trade-off between complexity and performance.

In Chapter 3, we proposed the ASD scheme for coded MIMO-IFDMA system. Compared to existing transmit diversity scheme for IFDMA system such as STBC, SFBC and FSTD, the proposed ASD scheme retains the low PAPR property of IFDMA signals and can be easily extended to more than two transmit antennas with no constraints on the number of IFDMA symbols transmitted. However, like all the existing schemes mentioned above, explicit channel estimation for the ASD scheme need to be performed at the receiver. This is unlike the CDD scheme which is transparent to the receiver. The channel estimation can be performed by transmitting orthogonal pilots for the different antennas. However, there are limited number of sequences with good cross-correlation properties available. Therefore, future research effort can be directed to investigate the joint estimation of the channels for different antennas for the proposed ASD scheme.

In Chapter 4, a MAI cancellation scheme is proposed where high mobility users are evenly distribute across the different frequency groups to limit the MAI within each group and a simple successive MAI cancellation algorithm is applied within each group. There are limits to the performance of the proposed

scheme in terms of the total tolerable number of high mobility users within the system and the distribution of mobility profile of those users. More sophisticated cancellation schemes such as parallel cancellations or iterative cancellations with correspondingly optimal code assignments can be investigated for future research to enhance the performance while balancing the required signal processing complexity at the receiver.

Bibliography

[1] T. S. Rappaport, *Wireless Communications: Principles and Practice*, 2nd ed. Prentice Hall, 2002.

[2] M. L. Roberts, M. A. Temple, R. F. Mills, and R. A. Raines, "Evolution of the Air Interface of Cellular Communications Systems toward 4G Realization," *IEEE Communications Surveys & Tutorials*, vol. 8, no. 1, pp. 2–23, 1st Quarter 2006.

[3] M. A. A. El-Ata, "Evolution of Mobile Cellular Communication Systems: The Journey to UMTS," in *Proc. of Radio Science Conference*.

[4] P. Jung, P. W. Baier, and A. Steil, "Advantages of CDMA and Spread Spectrum Techniques over FDMA and TDMA in Cellular Mobile Radio Applications," *IEEE Trans. Veh. Technol.*, vol. 42, no. 3, pp. 357–364, 1993.

[5] F. Adachi, M. Sawahashi, and H. Suda, "Wideband DS-CDMA for Next-Generation Mobile Communications Systems," *IEEE Commun. Mag.*, vol. 36, no. 9, pp. 56–69, Sep 1998.

[6] C. Berrou, A. Glavieux, and P. Thitimajshima, "Near Shannon Limit Error-Correcting Coding and Decoding:Turbo-Codes," in *Proc. of IEEE ICC*, vol. 2, May 1993, pp. 1064–1070.

[7] C. Berrou and A. Glavieux, "Near Shannon Limit Error-Correcting Coding and Decoding:Turbo-Codes," *IEEE Trans. Commun.*, vol. 44, no. 10, pp. 1261–1271, Oct 1996.

[8] "3GPP: Technical Specification Group Radio Access Network; Physical Layer Aspects for Evolved Universal Terrestrial Radio Access (UTRA) (Release 7)," *3GPP TR 25.814 V7.1.0*, Sep 2006.

[9] H. G. Myung, J. Lim, and D. J. Goodman, "Single Carrier FDMA for Uplink Wireless Transmission," *IEEE Veh. Technol. Mag.*, vol. 1, no. 3, pp. 30–38, Sep 2006.

[10] T. Svensson, T. Frank, D. Falconer, M. Sternad, E. Costa, and A. Klein, "B-IFDMA - A Power Efficient Multiple Access Scheme for Non-frequency-adaptive Transmission," in *Proc. of Mobile and Wireless Communications Summit*, Jul 2007, pp. 1–5.

[11] J. Karout, L. S. Muppirisetty, and T. Svensson, "Performance Trade-Off Investigation of B-IFDMA," in *Proc. of IEEE VTC-Fall*, Sep 2009, pp. 1–5.

[12] X. Mao, A. Maaref, and K. H. Teo, "Adaptive Soft Frequency Reuse for Inter-Cell Interference Coordination in SC-FDMA Based 3GPP LTE Uplinks," in *Proc. of IEEE GLOBECOM*, Dec 2008, pp. 1–6.

[13] M. Porjazoski and B. Popovski, "Impact of Fractional Frequency Reuse on LTE Performances in Uplink," in *Proc. of IEEEI*, Nov 2011, pp. 1–5.

[14] J. Lafuente-Martnez, ngela Hernndez-Solana, I. Guo, and A. Valdovinos, "Inter-Cell Interference Management in SC-FDMA Cellular Systems," in *Proc. of IEEE VTC-Spring*, May 2011, pp. 1–5.

[15] Y. Kazama, A. Yamasaki, K. Adachi, and M. Nakagawa, "Impact of Frequency Diversity and Multi-User Diversity in IFDMA," in *Proc. of IEEE VTC-Spring*, May 2010, pp. 1–5.

[16] M. Schell and I. DeBroeck, "Interleaved FDMA: Equalization and Coded Performance in Mobile Radio Applications," in *Proc. of IEEE ICC*, vol. 3, Jun 1999, pp. 1939–1944.

[17] P. Xia, S. Zhou, and G. B. Giannakis, "Bandwidth- and Power-Efficient Multi-Carrier Multiple Access," *IEEE Trans. Commun.*, vol. 51, no. 11, pp. 1828 –1837, Nov 2003.

[18] Y. Goto, T. Kawamura, H. Atarashi, and M. Sawahashi, "Variable spreading and chip repetition factor (VSCRF) - CDMA in reverse link for broadband wireless access," in *Proc. of IEEE PIMRC*, vol. 1, Sept 2003, pp. 254–259.

[19] A. Tajer and A. Nosratinia, "Diversity Order of MMSE Single-Carrier Frequency Domain Linear Equalization," in *Proc. of IEEE GLOBECOM*, Nov 2007, pp. 1524–1528.

[20] H. Atarashi, S. Abeta, and M. Sawahashi, "Variable Spreading Factor-Othogonal Frequency and Code Division Multiplexing (VSF-OFCDM) for Broadband Packet Wireless Access," *IEICE Trans. Commun.*, vol. E86-B, no. 1, pp. 291–299, Jan 2003.

[21] N. Maeda, Y. Kishiyama, H. Atarashi, and M. Sawahashi, "Variable Spreading Factor-OFCDM with Two Dimensional Spreading that Prioritizes Time Domain Spreading for Forward Link Broadband Packet Wireless Access," in *Proc. of IEEE VTC-Spring*, vol. 1, Apr 2003, pp. 127–132.

[22] U. Sorger, I. DeBroeck, and M. Schell, "Interleaved FDMA - A New Spread-Spectrum Multiple-Access Scheme," in *Proc. of IEEE ICC*, vol. 2, Jun 1998, pp. 1013–1017.

[23] F. Horlin, A. Bourdoux, E. Lopez-Estraviz, and L. V. der Perre, "Single-Carrier FDMA or Cyclic-Prefix CDMA with Optimized Spreading Se-

quences?" *IEEE Trans. Veh. Technol.*, vol. 57, no. 5, pp. 3230–3234, Feb 2008.

[24] R. Dinis, D. Falconer, C. T. Lam, and M. Sabbaghian, "A Multiple Access Scheme for the Uplink of Broadband Wireless Systems," in *Proc. of IEEE GLOBECOM*, vol. 6, Nov 2004, pp. 3808–3812.

[25] T. Frank, A. Klein, and E. Costa, "IFDMA: A Scheme Combining the Advantages of OFDMA and CDMA," *IEEE Wireless Commun. Mag.*, vol. 14, no. 3, pp. 9–17, Jun 2007.

[26] I. Koffman and V. Roman, "Broadband Wireless Access Solutions based on OFDM Access in IEEE 802.16," *IEEE Commun. Mag.*, vol. 40, no. 4, pp. 96–103, Apr 2002.

[27] D. Galda and H. Rohling, "A Multiple Access Scheme for the Uplink of Broadband Wireless Systems," in *Proc. of IEEE VTC-Spring*, vol. 4, May 2002, pp. 1737– 1741.

[28] C.-M. Chang and K.-C. Chen, "Frequency-Domain Approach to Multiuser Detection in DS-CDMA Communications," *IEEE Commun. Lett.*, vol. 4, no. 11, pp. 331–333, Nov 2000.

[29] H. Cheng, M. Ma, and B. Jiao, "On the Design of Comb Spectrum Code for Multiple Access Scheme," *IEEE Trans. Commun.*, vol. 57, no. 3, pp. 754–763, Mar 2009.

[30] X. Peng, K.-B. Png, Z. Lei, F. Chin, and C. C. Ko, "Block Spread IFDMA: An Improved Uplink Transmission Scheme," in *Proc. of IEEE PIMRC*, Sep 2007, pp. 1–4.

[31] Y. Pei and Y.-C. Liang, "Subcarrier-Based Block-Iterative GDFE (BI-GDFE) Receivers for MIMO Interleaved FDMA," in *Proc. of IEEE VTC-Spring*, Apr 2007, pp. 2033–2037.

[32] R. Dinis, P. Montezuma, N. Souto, and J. Silva, "Iterative Frequency-Domain Equalization for General Constellations," in *Proc. of IEEE Sarnoff Symposium*, Apr 2010, pp. 1–5.

[33] K.-B. Png, X. Peng, F. Chin, and C. C. Ko, "Soft QRD-M Decoding for Coded IFDMA Systems," in *Proc. of IEEE PIMRC*, Sep 2009, pp. 1–5.

[34] ——, "Iterative Soft QRD-M Decoding of Coded IFDMA Systems," in *Proc. of IEEE WCNC*, Apr 2010, pp. 1–5.

[35] T. Kawamura, H. Atarashi, and M. Sawahashi, "Adaptive transmission timing control using reservation packet in reverse link for broadband ds-cdma wireless access," in *Proc. of IEEE VTC-Fall*, vol. 2, Oct 2003, pp. 877–881.

[36] R. Morrison, L. J. C. (Jr), and S. K. Wilson, "On the use of a cyclic extension in ofdm," in *Proc. of IEEE VTC-Fall*, vol. 2, Oct 2003, pp. 664–668.

[37] C.-M. Chang and K.-C. Chen, "Frequency-Domain Approach to DS-CDMA Multiuser Detection over Frequency-Selective Slowly Fading Channels," in *Proc. of IEEE PIMRC*, vol. 3, Sept 2002, pp. 1280–1284.

[38] S. Coleri, M. Ergen, A. Puri, and A. Bahai, "Channel Estimation Techniques based on Pilot Arrangement in OFDM Systems," *IEEE Trans. Broadcast.*, vol. 48, no. 3, pp. 223 – 229, Sep 2002.

[39] S. V. Amari and R. B. Misra, "Closed-Form Expressions for Distribution of Sum of Exponential Random Variables," *IEEE Trans. Rel.*, vol. 46, no. 4, pp. 519–522, Dec 1997.

[40] D. Hammarwall, M. Bengtsson, and B. Ottersten, "Acquiring Partial CSI for Spatially Selective Transmission by Instantaneous Channel Norm Feedback," *IEEE Trans. Signal Processing*, vol. 56, no. 3, pp. 1188–1204, Mar 2008.

[41] J. G. Proakis, *Digital Communications*, 4th ed. McGraw Hill, 2001.

[42] H. Moon and D. C. Cox, "Improved Performance Upper Bounds for Terminated Convolutional Codes," *IEEE Commun. Lett.*, vol. 11, no. 6, pp. 519–521, Jun 2007.

[43] X. Peng, K.-B. Png, Z. Lei, F. Chin, and C. C. Ko, "Two-layer Spreading CDMA: An Improved Method For Broadband Uplink Transmission," *IEEE Trans. Veh. Technol.*, vol. 57, no. 6, pp. 3563–3577, Nov 2008.

[44] D. L. Ruyet, T. Bertozzi, and B. Ozbek, "Breadth First Algorithms for APP Detectors over mimo channels," in *Proc. of IEEE ICC*, vol. 2, Jun 2004, pp. 926–930.

[45] K. J. Kim, T. Reid, and R. A. Iltis, "Iterative Soft-QRD-M for Turbo Coded MIMO-OFDM Systems," *IEEE Trans. Commun.*, vol. 56, no. 7, pp. 1043–1046, July 2008.

[46] S. Lin and D. J. Costello, *Error Control Coding*, 2nd ed. Prentice Hall, 2004.

[47] F. Jelinek and J. Anderson, "Instrumentable Tree Encoding of Information Sources (Corresp.)," *IEEE Trans. Inform. Theory*, vol. 17, no. 1, pp. 118–119, Jan 1971.

[48] D. R. Sweet, "Fast Toeplitz Orthogonalization," *Numerische Mathematik*, vol. 43, pp. 1–21, 1984.

[49] B. Hassibi, "An Efficient Square-Root Algorithm for BLAST," in *Proc. of IEEE ICASSP*, vol. 2, Jun 2000, pp. 737–740.

[50] D. Wubben, R. Bohnke, V. Kuhn, and K.-D. Kammeyer, "MMSE Extension of V-BLAST based on Sorted QR Decomposition," in *Proc. of IEEE VTC-Fall*, vol. 1, May 2003, pp. 508–512.

[51] S. Sun, Y. Dai, Z. Lei, H. Kenichi, and H. Kawait, "Pseudo-Inverse MMSE Based QRD-M Algorithm for MIMO OFDM," in *Proc. of IEEE VTC-Spring*, vol. 3, May 2006, pp. 1545–1549.

[52] H. Kawai, K. Higuchi, N. Maeda, and M. Sawahashi, "Adaptive Control of Surviving Symbol Replica Candidates in QRM-MLD for OFDM MIMO Multiplexing," *IEEE J. Select. Areas Commun.*, vol. 24, no. 6, pp. 1130–1140, 2006.

[53] P. Frenger, P. Orten, and T. Ottosson, "Convolutional Codes with Optimum Distance Spectrum," *IEEE Commun. Lett.*, vol. 3, no. 11, pp. 317–319, Nov 1999.

[54] D. Tse and P. Viswanath, *Fundamentals of Wireless Communications*. Cambridge University Press, 2005.

[55] Y. Meng, M. You, J. Liu, and H. Luo, "A Novel Space-Frequency Block Coding Scheme for SC-FDMA," in *Proc. of IEEE VTC-Fall*, Sep 2009, pp. 1 – 5.

[56] S. M. Alamouti, "A Simple Transmit Diversity Technique for Wireless Communications," *IEEE J. Select. Areas Commun.*, vol. 16, no. 8, pp. 1451 – 1458, Oct 1998.

[57] C. Ciochina, D. Castelain, D. Mottier, and H. Sari, "Single-Carrier Space-Frequency Block Coding: Performance Evaluation," in *Proc. of IEEE VTC-Fall*, Oct 2007, pp. 715–719.

[58] J. Xiang, Y. Cai, Y.-C. Liang, K. H. Li, and K. C. Teh, "Low-Complexity Iterative Receiver for Interleaved FDMA (IFDMA) with Cyclic Delay Diversity," Oct 2006, pp. 1 – 5.

[59] A. F. Molisch and M. Win, "MIMO Systems with Antenna Selection An Overview," in *Proc. of IEEE Radio and Wireless Symposium*, Aug 2003, pp. 167–170.

[60] V. Tarokh, H. Jafarkhani, and A. R. Calderbank, "SpaceTime Block Codes from Orthogonal Designs," *IEEE Trans. Inform. Theory*, vol. 45, no. 5, pp. 1456–1467, Jul 1999.

[61] S. Zhou, , G. B. Giannakis, and C. L. Martret, "Chip-interleaved Block-spread Code Division Multiple Accesss," *IEEE Trans. Commun.*, vol. 50, no. 2, pp. 235–248, Feb 2002.

[62] S. Zhou, P. Xia, G. Leus, and G. B. Giannakis, "Chip-interleaved Block-spread Code Division Multiple Accesss versus DS-CDMA for Cellular Downlink: A Comparative Study," *IEEE Trans. Wireless Commun.*, vol. 3, no. 1, pp. 176–190, Jan 2004.

[63] K. L. Baum, T. A. Thomas, F. W. Vook, and V. Nangia, "Cyclic Prefix CDMA: An Improved Transmission Method for Broadband DS-CDMA Cellular Systems," in *Proc. of IEEE WCNC*, vol. 2, Mar 2002, pp. 183–188.

[64] A. Madhukumar, F. Chin, Y.-C. Liang, and K. Yang, "Single Carrier Cyclic Prefix-Assisted CDMA System with Frequency Domain Equalization for High Data Rate Transmission," *EURASIP J. Wireless Commun., Networking*, pp. 149–160, Mar 2004.

[65] W. S. Leon and Y.-C. Liang, "Blind Chip-level Equalizer for the Downlink of Cyclic-Prefix CDMA Systems," *IEEE Trans. Veh. Technol.*, vol. 55, no. 444, pp. 1208–1214, Jul 2006.

[66] K.-B. Png, X. Peng, F. Chin, and C. C. Ko, "Performance Analysis of Coded IFDMA Systems: Maximizing Channel Diversity Order," in *Proc. of IEEE WCNC*, Apr 2010, pp. 1–5.

[67] F. Adachi, M. Sawahashi, and K. Okawa, "Tree-structured Generation of Orthogonal Spreading Codes with Different Lengths for Forward Link of

DS-CDMA Mobile Radio," *IEE Electron. Lett.*, vol. 3, no. 1, pp. 27–28, Jan 1997.

[68] K.-B. Png, X. Peng, F. Chin, and C. C. Ko, "Mobility-Based Interference Cancellation Scheme for BS-IFDMA Systems with Optimum Code Assignment," *Accepted for Publiation in IEEE Trans. Veh. Technol.*

[69] P. Patel and J. Holtzman, "Analysis of a simple successive interfernce cancellation scheme in a ds/cdma system," *IEEE J. Select. Areas Commun.*, vol. 12, no. 5, pp. 796–807, Jun 1994.

[70] J.-P. M. G. Linnartz, "Performance Analysis of Synchronous MC-CDMA in Mobile Rayleigh Channel with both Delay and Doppler Spreads," *IEEE Trans. Veh. Technol.*, vol. 50, no. 6, pp. 1375–1387, Nov 2001.

[71] L. Fang and L. B. Milstein, "Successive Interference Cancellation in Multicarrier DS/CDMA," *IEEE Trans. Commun.*, vol. 48, no. 9, pp. 1530–1540, Sep 2000.

[72] P. Hahn and T. Grant, "Lower Bounds for the Quadratic Assignment Problem Based upon a Dual Formaulation," *Operational Research*, vol. 46, no. 6, pp. 912–922, Jun 1998.

[73] X. Peng, F. Chin, T. T. Tjhung, and A. Madhukumar, "A Simplified Transceiver Structure for Cyclic Extended CDMA System with Frequency Domain Equalization," in *Proc. of IEEE VTC-Spring*, vol. 3, May 2005, pp. 1753–1757.

[74] J.-J. van de Beek, P. O. Borjesson, M.-L. Boucheret, D. Landstrom, J. M. Arenas, P. Odling, C. Ostberg, M. Wahlqvist, and S. K. Wilson, "A Time and Frequency Synchronization Scheme for Multiuser OFDM," *IEEE J. Select. Areas Commun.*, vol. 17, no. 11, pp. 1900–1914, Nov 1999.

[75] T. C. Koopmans and M. Beckmann, "Assignment Problems and the Location of Economic Activities," *Econometrica*, vol. 25, pp. 53–76, 1957.

[76] P. Hahn, T. Grant, and N. Hall, "A Branch-and-Bound Algorithm for the Quadratic Assignment Problem Based on the Hungarian Method," *European Journal of Operational Research*, vol. 108, no. 3, pp. 629–640, Aug 1998.

[77] G. Finke, R. E. Burkard, and F. Rendl, "Quadratic Assignment Problems," *Annals of Discrete Mathematics*, vol. 31, pp. 61–72, 1987.

[78] F. Rendl and H. Wolkowicz, "Applications of Parametric Programming and Eigenvalue Maximization to the Quadratic Assignment Problem," *Mathematical Programming*, vol. 53, pp. 63–78, Jun 1992.

[79] H. W. Kuhn, "The Hungarian Method for The Assignment Problem," *Naval Research Logistics Quarterly*, vol. 2, pp. 83–97, 1955.

[80] J. Munkres, "Algorithms for the Assignment and Transportation Problems," *Journal of the Society for Industrial and Applied Mathematics*, vol. 5, no. 1, pp. 32–38, Mar 1957.

[81] P. Hahn, W. Hightower, T. A. Johnson, M. Guignard-Spielberg, and C. Roucairol, "Tree Elaboration Strategies in Branch and Bound Algorithms for Solving the Quadratic Assignment Problem," *Yugoslav Journal of Operational Research*, vol. 11, no. 1, pp. 1–25, 2001.

[82] H. Donelan and T. O'Farrell, "Method for generating sets of orthogonal sequences," *Electronics Letters*, vol. 35, no. 18, pp. 1537–1538, Sep 1999.

[83] J. M. Romero-Jerez, J. P. Pena-Martin, and A. J. Goldsmith, "Bit Error Rate Analysis in MIMO Channels with Fading and Interference," in *Proc. of IEEE VTC-Spring*, Jun 2009, pp. 1 – 5.

[84] Y. Chen and C. Tellambura, "Distribution Functions of Selection Combiner Output in Equally Correlated Rayleigh, Rician, and Nakagami-*m* Fading Channels," *IEEE Trans. Commun.*, vol. 52, no. 11, pp. 1948 – 1956, Nov 2004.

[85] J. M. Romero-Jerez, J. P. Pena-Martin, G. Aguilera, and A. J. Goldsmith, "Performance of MIMO MRC Systems with Co-Channel Interference," in *Proc. of IEEE ICC*, Jun 2006, pp. 1343 – 1349.

[86] "3GPP: Technical Specification Group GSM/EDGE Radio Access Network; Radio transmission and reception (Release 1999)," *3GPP TS 05.05 V8.20.0*, Nov 2005.